Design Manual Development for a Hybrid, FRP Double-Web Beam and Characterization of Shear Stiffness in FRP Composite Beams

By
Timothy John Schniepp

Thesis submitted to the Faculty of the
Virginia Polytechnic and State University
in partial fulfillment of the requirements for the degree of

Master of Science
in
Engineering Science and Mechanics

Approvals

John J. Lesko, Chair — Committee Chairman

Scott W. Case — Committee Member

Carin L. Roberts-Wollmann

Committee Member

Friday, August 2, 2002
Blacksburg, Virginia

Keywords: Composite materials, FRP, hybrid composite beam, pultruded structural shapes, shear stiffness, kGA, shear deformation, shear lag

Design Manual Development for a Hybrid, FRP Double-Web Beam and Characterization of Shear Stiffness in Composite Beams

Timothy J. Schniepp

(ABSTRACT)

Fiber-reinforced polymeric (FRP) composites are being considered for structural members in bridge construction as lighter, more durable alternatives to steel and concrete. Extensive testing and analysis of a pultruded, hybrid double web beam (DWB) developed for use in bridge construction has been conducted at Virginia Tech. A primary purpose of this testing is the development of a structural design guide for the DWB, which includes stiffness and strength data. The design manual also includes design allowables determined through a statistical analysis of test data.

Static testing of the beams, including failure tests, has been conducted in order to determine such beam properties as bending modulus, shear stiffness, failure mode, and ultimate capacity. Measuring and calculating the shear stiffness has proven to be an area of particular interest and difficulty. Shear stiffness is calculated using Timoshenko beam theory which combines the shear stiffness and shear area together along with a shear correction factor, k, which accounts for the nonuniform distribution of shear stress/strain through the cross-section of a structure. There are several methods for determining shear stiffness, kGA, in the laboratory, including a direct method and a multi-span slope method. Herein lays the difficulty as it has been found that varying methods produces significantly different results. One of the objectives of current research is to determine reasons for the differences in results, to identify which method is most accurate in determining kGA, and also to examine other parameters affecting the determination of kGA that may further aid the understanding of this property.

This document will outline the development of the design guide, the philosophy for the selection of allowables and review and discuss the challenges of interpreting laboratory data to develop a complete understanding of shear effects in large FRP structural members.

Acknowledgments

The author would like to acknowledge the following for their contribution and support in this work:

- **Dr. Jack Lesko**, for serving as my advisor during my time here at Virginia Tech. My main reason for coming to Tech was to work under your guidance and along with you, and I have not been disappointed. Your constant enthusiasm, optimism, and encouraging words were always appreciated and made every task more enjoyable. Your willingness to go out of your way to help in any and every way possible is something for which I have the utmost respect. Thank you again for all your help.

- **Dr. Thomas Cousins**, for serving on my graduate committee and answering countless questions during my time spent out at the structures lab.

- **Dr. Scott Case**, for serving on my graduate committee and always being available and willing to help, regardless of what the topic was.

- **Dr. Roberts-Wollmann**, for serving on my graduate committee in the end when Dr. Cousins wasn't available. Your help in getting me finished up here in a timely manner really is appreciated.

- **Michael Hayes**, a.k.a. The Great and All-Knowing Michael Hayes, for ALL of your help. For answering the 2 billion questions I asked along the way and for always taking the time to help and explain things despite how busy you were yourself. Especially the last few weeks, it would have been a much more difficult road without your help and guidance.

- **Dr. Samuel Easterling**, for providing us access to the structures lab testing facilities.

- **Brett Farmer and Dennis Huffman**, for all of your help out at the lab getting me setup and moving beams all over the place.

- **Beverly Williams, Sheila Collins, and Loretta Tickle**, as well as all the staff of the MRG and ESM department. I've enjoyed getting to know you and appreciate all of your help.

- **Bob Simonds and George Lough**, for helping me out in the busting lab.

- **Dan Witcher and Glenn Barefoot of Strongwell Inc.**, for providing the many beams that I had the opportunity to then destroy. And for all of your help and participation in this project.

- **John Bausano**, my roommate and very good friend, for something I guess. You must have helped me out in some way! Of course I'm joking. You know all you've done to help me out along the way and keep me entertained—I've appreciated and enjoyed it all!

- **Vanessa Walters and Tracy Carroll**, I would like to thank you both for being such good friends during my time here, providing the encouragement and support I needed to finish everything up without losing my mind!

And of course, thank you to my parents and family, for everything—support, encouragement, and love.

Table of Contents

List of Tables

List of Figures

Chapter 1 Introduction and Literature Review

1.1 Introduction

Fiber-reinforced polymeric (FRP) composites are being considered for structural members in civil infrastructure applications as lighter, more durable alternatives to steel and concrete. The interest in these materials can be attributed to the ability of FRP to better meet the performance and durability needs of current construction. Existing structural shapes include wide-flange beams, box beams, sandwich beams, and multi-cellular panels. The constituent materials of these structural components tend to be E-glass fibers and low cost resin systems (polyester, vinyl ester, etc.). Occasionally, carbon fiber is utilized in flanges or face sheets in order to increase bending stiffness. Construction typically utilizes off-the-shelf pultruded sections or structural members may be manufactured using vacuum-assisted resin transfer molding. A few of the benefits of FRP for use in infrastructure compared to conventional materials are high strength to weight ratios, high corrosion resistance, lightweight, electromagnetic transparency, and excellent fatigue performance.

The claim of FRP composites to have excellent long-term durability makes them well-suited for infrastructure applications. The problem is that there are few documented cases in literature to validate these claims. Some data from short-term laboratory projects is available. However, it is difficult to make long-term generalizations since these studies typically involve specific materials and conditions (environmental, loading, etc.). Some evidence of success can be seen from marine and chemical storage applications, but data from these areas is difficult to obtain as little actual documentation exists. The majority of information on the performance of composite materials comes from the aerospace industry, an area where cost and long-term durability are often of secondary importance. Additionally, the high performance applications of the aerospace industry demand such materials as carbon fiber and epoxy resins. Construction and civil infrastructure applications require the more cost competitive glass fibers and polyester or vinyl ester resins, materials with less existing data available on performance.

The lack of long-term durability data has led to the slow acceptance of FRP composites in the civil infrastructure community. There are also additional factors inhibiting widespread

use. Composites tend to have considerably higher initial costs than conventional engineering materials (i.e. steel, concrete, wood, etc.). It is believed by advocates that composites will have lower life-cycle costs due to their increased durability, but again the lack of long-term data has left this claim not fully substantiated. Since composites are relatively new to the industry, the lack of experience designing with these materials tends to drive initial costs higher yet. And although the high stiffness-to-weight ratio of FRP composites makes them appealing for many applications, the relatively low absolute stiffness of these materials causes difficulties in fully utilizing their strength since most infrastructure design is deflection controlled. Additionally, few standards for design and repair with composites are available. Some of the larger manufacturers of composite structures are creating design manuals for their own products independently, occasionally in conjunction with academic and government research groups.

Overall, composites continue to gain acceptance and find new roles in infrastructure applications due to their numerous advantages. Along with the aforementioned benefits, the lighter structures that are produced utilizing composites allow for increased live load capacities on abutments and easier implementation in previously less accessible locations. In order to continue to enhance approval in the infrastructure community, more long-term durability information is required, the costs of constituent materials (especially carbon fiber) must continue to decrease, and more field trials must be conducted. Demonstration and low-risk, small-scale projects utilizing composites is perhaps the key to widespread acceptance. One such project demonstrating the use of FRP composites in bridge applications is the replacement of the steel stringer, timber deck bridge on Route 601 in Smyth County, Virginia.

1.2 The Route 601 Bridge

The former Route 601 Bridge (Figure 1-1) spanned 30 ft (9.1 m) across Dickey Creek in rural, southwest Virginia (Marion, VA) and consisted of eight, 8 to 10 in. (203 to 254 mm) deep steel girders. The Virginia Department of Transportation (VDOT)-owned structure was built in 1932 and was found to be in need of rehabilitation after a 1998 inspection due to excessive corrosion. The site provided an excellent opportunity for a demonstration of an innovative composite material superstructure.

The replacement bridge (Figure 1-2) was designed through collaboration by Virginia Tech, Strongwell, Corp., the Virginia Transportation Research Council (VTRC) and VDOT. The new structure spans 39 ft (11.8 m) from center-of-bearing to center-of-bearing and consists of eight 36 in. (914 mm) double-web composite beams with a 42 in. (1.1 m) transverse beam spacing. The span of the bridge was increased to account for the greater depth of the composite beams to prevent any restriction of drainage. Ten, 4 ft long by 30 ft wide by 5 1/8 in. thick (1.2 m x 9.1 m x 130 mm) glue laminated timber panels make up the deck and the structure is topped off with an asphalt wearing surface. Prior to the rehabilitation of the Route 601 Bridge, the beams to be implemented in the new structure were tested quasi-statically to obtain stiffness data and one beam was tested to failure. Since the completion of the rehabilitation, failure testing of additional beams (19 beams in all) has also been completed. For further details on the design of and girder proof testing for the Route 601 Bridge refer to the Virginia Tech Master of Science Thesis by Waldron [23].

1.3 The 36 in. Hybrid FRP, Double-Web Beam (DWB)

The 36 in. (914 mm) FRP DWB (Figure 1-3) is manufactured by Strongwell, Corp. in Bristol, Virginia by means of the pultrusion process. The hybrid beam is comprised of both glass and carbon fibers in a vinyl ester resin matrix (Dow Chemical's Derakane 411-350). Glass roving, 0/90° and ±45° fabric, and continuous strand mat (CSM) are located throughout the section and unidirectional carbon fiber tows are utilized in the flanges to increase the bending modulus and to move the failure plane of the DWB away from the web-flange interface and into the top flange. A fiber volume fraction of approximately 45% is targeted. The actual fiber lay-up is proprietary, though the webs and flanges are basically quasi-isotropic with the flanges also utilizing the unidirectional carbon fiber laminae. The unique shape of the beam was designed to utilize the properties of composites. The double-webs and sub-flanges work to increase the shear stiffness of the structure as well as increase resistance to lateral-torsional buckling. This increase in shear stiffness is of great significance since shear deformation in composite materials cannot be ignored as it can in steel and concrete structures. Shear deflection in these composite

structures can contribute as much as 15- and even 20% of the total beam deflection at spans that are common to the type of bridges these beams were designed for.

During the development of the 36 in. DWB, an 8 in. (203 mm) (Figure 1-4) deep subscale prototype was studied and implemented in the Tom's Creek Bridge rehabilitation in 1997 [1]. The results of extensive testing of this section including stiffness and strength data have been published in a structural design guide, published in 2000 [2]. As tested in three- and four-point bending, the 8 in. DWB consistently fails by delamination within the compressive flange at the interface between carbon and glass fibers. The critical stress in this case is thought to be the normal, out-of-plane stress at the free edges. Furthermore, the delamination appears to initiate at the load points, suggesting that load concentrations have a significant effect on the critical stress. The failure mechanisms of the 36 in. DWB will be addressed in Chapter 4.

1.4 The 36 in. DWB Structural Design Guide

As it was previously stated, failure and stiffness testing has been conducted on a number of 36 in. DWBs. The primary purpose of this testing is the development of a structural design guide for the DWB, which will contain strength and stiffness data obtained during testing. The design guide is presented as a material specification where the material system and the manufacturing process are well defined and controlled. Knowing the tolerances of this system and process, guidelines are defined for the use of the structural member. As a basis for defining operating limits, a modified Load Resistance Factor Design (LRFD) approach is considered [3]. For this approach the probability distribution of loads/stress (Loads, Q) is compared to the probability of failure strength of the material (Resistance, R), typically represented as illustrated in Figure 1-5. The region of overlap is *related* to the risk associated with the situation designed. Specifically in the design guide, the resistance portion of the design problem is presented by employment of Weibull statistics [2, 25, 26] on test data. Weibull statistics help capture the variability of materials by describing the probability of failure and tend to describe the distribution of data for composite materials more accurately than a normal distribution. A reliability based selection approach is used, from the recorded variability of girder test data, to define A- and B-basis allowable levels of resistance. The Weibull statistics equations that are

used to calculate the A and B allowables can be found in Appendix A. An A-basis allowable means that there is a 99% probability that the calculated value is within a 95% confidence interval. Similarly, a B-basis allowable suggests that there is a 95% probability that the calculated value falls within a 95% confidence interval. These values define for users of the design guide the level of risk allowed in operating the structure based on a determined design load. The difference between the selected design loads and the resistance (defined as a probability of failure load/stress) defines the level of risk (or inversely the margin of safety) for the design (Figure 1-5). The probability and confidence levels that are set for the A and B allowables are determined by the Mil-17 Specification on composite materials [27].

The purpose of the design guide is to assist potential users of the DWB in specifying the component in various structural applications. The content includes the specification of bending stiffness, shear stiffness, shear capacity, moment capacity, lateral-torsional stability, bearing capacity, and bolted connection specifications. An overview of the testing and results follows in subsequent chapters.

1.5 Literature Review

A review of the literature has been conducted on the use of composite materials in infrastructure, the status of infrastructure in the United States, and some issues that are restricting the general acceptance of composites in the industry and this information is presented in the following sections. In addition to this, a survey of literature on the characterization of shear effects in composite structures, in particular shear stiffness, has also been conducted in order to get a better understanding of this material property.

1.5.1 Status of U.S. Infrastructure

The deteriorating condition of the transportation infrastructure of the U.S. has become a severe problem, especially considering the economic impact that the industry as on the national economy. The value of the transportation infrastructure is said to be worth more than $2.5

trillion. In addition to this, about $900 billion annually or about 20% of the gross domestic product comes from transportation related activities. Construction, maintenance, and operation of the transportation network requires $120 billion in funding per year, with maintenance alone drawing up nearly $100 billion [4]. One source estimated that by the year 2000, $50 billion per year would be required for the maintenance of bridges [5]. This high requirement for bridge maintenance costs is due to indications that approximately 4 to 10% of the Country's 550,000+ bridges are considered to be in an advanced state of deterioration and over 30% are said to be "structurally deficient" or "functionally obsolete". As many as 200,000 bridges may need to be rehabilitated over the course of this and the next decade [5]. Anywhere from $10 to $50 billion or more annually will be required to keep up with this state of degeneration in U.S. infrastructure, however only about $5 billion is budgeted for infrastructure improvement [6].

Since it is not always possible to build new roadways to avert the increasing demand of traffic and to relieve congestion, the only remaining option is to make improvements to existing structures. Small investments into ideas that promote research and education such as RIPE (research, implementation, promotion, and education) can result in huge cost and efficiency gains [4]. One source indicated that improving the durability of pavement by only 1% could save $10 billion or much more in the next 20 years [4]. U.S. bridges are typically designed for a life of 70 years and require rehabilitation at some time around mid-life due to deterioration. Since the majority of bridges in the U.S. were built after 1945, it is inevitable that a large number of replacements structures will have to be built in the next 10 to 20 years. And since the majority of deterioration to existing bridge structures can be attributed to the corrosive environment created by de-icing salts, there is additional motivation to invest time and resources into researching and implementing new systems and materials more resistant to such environments [5].

1.5.2 Composites in Infrastructure

The nearly routine use of FRP composites for such applications as aircraft structures and even space shuttle components suggest that the composites industry has made great advancements in design considerations. It should come as no surprise then that the success

attained in the aforementioned applications along with the advantageous features of these materials is allowing them to carve out a niche in the infrastructure industry as well. And although acceptance may be occurring at a rather slow rate, FRP composites are currently being implemented in a number of civil and military infrastructure applications as experimental projects and demonstrations [4].

There are additional motivations for civil engineers to explore new alternatives for bridge design and materials as well. There has been some investment of effort into trying such things as coatings and binders with traditional materials, but the majority of new interest is in exploring composite materials as alternatives to steel, concrete, and timber. The concern for the state of bridges in the near future combined with financial restraints has fueled this interest as there is a need for new technologies [6].

There are numerous reasons why FRP composites are being utilized in civil and military infrastructure. There obviously is also a rationale for why their adoption has been somewhat slow. The lack of long-term durability data has already been mentioned as one of the primary hindrances to FRP usage. The long-term degradation of FRP composites due to moisture, freeze-thaw cycling, UV radiation, chemical state changes, etc. has been studied at various levels in laboratories and in some field applications, but due to the limited use of most current composite structures in civil applications, the long-term effects of these types of degradation are not yet known. Moreover, most bridge designs are deflection controlled and the low stiffness of FRP composites compared to steel can also limit their use. The large deformations that occur can cause problems with concrete overlay and deck connections as well [6]. The addition of carbon fiber as a means for stiffening glass-fiber composites can alleviate some of these problems, but the high cost of the resulting hybrid structure is another obstacle.

Despite the limitations of FRP composites, engineers are finding ways to overcome these factors and utilize their many advantages. For instance, although the relatively low absolute stiffness of FRP composites is a limitation, the high strength- and stiffness-to-weight ratios make them ideal for applications where the location is less accessible. A composite structure can significantly reduce a bridge's dead load allowing for an increased live load without abutment strengthening and may also give the structure a larger load carrying capacity. One of the primary advantages of FRP composites is they tend to be more corrosion resistant than metals. This increased resistance can be attributed to the chemical stability and resistance to fatigue crack

growth that composites exhibit. Due to the light weight and durability of these materials, a properly designed FRP bridge structure can weigh less, last as long or longer, reduce maintenance costs, and have increased strength when compared to a steel or concrete bridge.

1.5.3 Issues and Characteristics of FRP Composites

As FRP composites continue to gain acceptance in the infrastructure community, they are finding additional roles in new applications as both secondary and primary load bearing members. Some of the applications currently utilizing composites include guard rails, diaphragms, column wrapping, reinforcement of concrete beams, reinforcement and repair of steel members and splice plates, and as a method of protecting joints and bridge bearings from various environmental factors [5]. The potential also exists for use as bridge beams and decks as a means for improving durability, but to this point the majority of instances for this type of role has been as demonstration projects and experimental cases. The FRP composites that are typically being utilized tend to be the more cost-effective glass-fiber, polyester resin or glass-fiber, vinyl ester resin combinations. In some instances, carbon fiber is also being utilized when the need for increased mechanical properties (e.g., bending stiffness) can offset some of the deterring higher costs. One of the more popular methods for manufacturing these composite structures, especially in large-scale applications and production, is the pultrusion process. The relatively simple, cost-effective, flexible, continuous nature of this process makes it ideal for manufacturing infrastructure components. As constituent materials, pultrusion generally utilizes a combination of fiber rovings, stitched fabrics, and continuous and chopped strand mats resulting in relatively low fiber volume fractions of about 40 to 55% [6]. Resin infusion and resin transfer molding are also occasionally used to produce infrastructure components, but these processes are more common in cases where customization is needed or prototype structures are required [7].

There continues to be an increasing demand for guidelines and standards to follow in the design and implementation of FRP composite structures. The American Society for Testing and Materials (ASTM) and such organizations as the American Concrete Institute (ACI) and the American Association of State Highway Transportation Officials (AASHTO) are a few of the

institutions addressing these needs. In addition to these groups, as it was mentioned previously, various component suppliers and manufacturers, including Strongwell Corp., Hardcore Composites, and Creative Pultrusions, are also independently developing design guides for their own products to assist users in the proper use of those products. Clearly defined and easily accessible guidelines are necessary to assist those utilizing composite components that have limited experience with FRP composites. It is also important that these guidelines include methods for reducing structural properties over time and deal with the possibility that the failure mode of the structure may change in time as well [8].

As it was mentioned, there are a few cases where independent product manufacturers have developed design guides for their own products. Not only is Strongwell Corp. in the process of developing such a manual for the 36 in. DWB as this document is outlining, they also have already published a guide for the 8 in. DWB, as mentioned, and provide another such publication for their EXTREN family of structures, which includes a variety of pultruded structural shapes [9]. Hardcore Composites of New Castle Delaware provides a design guide for composite tubular piles. This guide (available over the internet) contains explanations for use and typical applications of the piles, as well as such design properties as bending stiffness (EI) and ultimate bending moment, including the computational methods utilized [10]. Another pultruder of structural shapes, Creative Pultrusions, also has an online design guide for their structural shape product line, Pultex. This guide provides physical and mechanical properties, load tables, environmental considerations, fabrication and quality assurance information, as well as additional information regarding the use of their product [11].

In addition to the abovementioned design manuals provided by independent companies, there are also a number of guides provided by governmental organizations. The EUROCOMP design code and handbook for design with polymer composites exists to provide specifications for structural design of composites in European countries [28]. The Japan Society of Civil Engineers (JSCE) has published a comprehensive guide for the proper design and construction of concrete structures reinforced using composite materials. This 300+ page document provides guidelines for such things as design basics, material specifications, and load tables to ultimate conditions, serviceability conditions, and fatigue information, as well as other information [12]. The previously mentioned ACI has developed a design manual for designing concrete structures using FRP rebar [13].

1.5.4 Shear Effects in FRP Structures

There is not an abundance of literature available on shear effects in FRP structures. And very little of what is available specifically involves the study of shear stiffness (kGA), the importance of which will be discussed for the 36 in. DWB in later chapters. Some information is available on shear deformable beam theories, the shear correction factor (k) (primarily for beams with rectangular cross-sections), the influences of shear in sandwich composites, and the effects of shear lag and warping.

For sandwich composites, the determination of shear stiffness is explained using the potential energy of applied loads and balancing that with the strain energy of the system. And this theory is extended for cases where typical sandwich conditions do not apply (modulus of the core << modulus of the flanges, which is the weak core assumption, thin face assumption, etc.) [14]. The influence of shear effects in isotropic beams was first proposed by Timoshenko in 1921 in order to correct his first order beam theory to account for the shear effects. He rederived the results a year later using an approach based on elasticity. In this second paper, the shear correction factor, k, was introduced to take into account the non-uniform distribution of shear across a structure's cross-section. The first accepted definition for k was the ratio of the average shear strain through the cross section to that at the centroid, but this definition proved to give poor results and the definition was revised. A possible, more accurate definition for k is given by one source as the ratio of shear area to the cross-sectional area of the beam [15].

In 1966, Cowper [16] derived the shear coefficient using three-dimensional elasticity equations. This approach was extended to thin-walled sections consisting of orthotropic composite laminates in the late 1980's [17]. In this last approach, the effect of out-of-plane Poisson's ratio is neglected and only the in-plane mechanical properties of the lamina that make up the beam are utilized. There are a handful of other sources that derive and extend the relationship for the shear correction factor for such cases as nonsymmetric, orthotropic laminates [18]; rectangular beams with arbitrary lay-ups [19]; cases where the Poisson's ratio effect is important [15], and similar cases in Bank, Pai et al., and Barbero et al. [20, 21, 22].

As far as the characterization of shear stiffness in FRP composite beams goes, fewer references are available. However, one source did present a similar study to that contained in Chapter 5 of this document. The objectives of the study were to examine the response of FRP sections to various static loading, specifically looking at shear influences, warping, shear lag, and so forth. Three- and four-point bending tests were performed on a variety of wide flange (WF) beam sections. For this particular study, an "approximate" Classical Laminate Theory (CLT) was used to first predict the flexural and shear rigidity of the structures involved. Then, experimentally the flexural rigidity was determined using both deflection and strain data. In the case of using deflection data, Timoshenko shear deformable beam theory was utilized to account for shear deflections (i.e. the calculated shear deflection was subtracted from the total experimental deflection to obtain the deflection due to bending alone. This allows for the determination of flexural rigidity using Bernoulli/Euler beam theory equations, which do not account for shear deformation.) [15].

Once the flexural rigidity was known, an expression for shear rigidity (kGA) was simplified based on an approach for determining the shear correction factor by Barbero [22]. This simplified expression states that kGA is approximately equal to GA, neglecting the effect of a non-uniform shear strain distribution through the depth of a section or assuming that k is approximately equal to one for a WF beam, which according to other sources [17] is not the case. However, the theoretical calculations agreed well with experimental results (within 5%). To determine the shear rigidity experimentally, the Timoshenko beam equation for three-point bending was used (seen below, without the shear correction factor).

$$\Delta_T = \frac{PL^3}{48EI} + \frac{PL}{4GA} \tag{1-1}$$

In Equation (1-1), the flexural rigidity (EI) was determined experimentally, as mentioned, from the four-point bending tests and the total deflection was determined using the three-point bend setup. The only remaining unknown is the shear rigidity (GA), which was then calculated [15].

1.5.5 Summary

The status of the transportation infrastructure in the United States reveals that there is a need for technological changes in the industry in order to correct for the deteriorating conditions of bridges and roadways. The potential for composite materials to help reverse this trend has been shown. Their advantages over traditional materials, in particular their high stiffness- and strength-to-weight ratios, long-term durability, and corrosion resistance has enabled them to begin creating a niche in the civil infrastructure community, although there acceptance is still slowed by some of the uncertainties and disadvantages previously mentioned. The need for design guides and standards was noted as one factor in particular that needs to be addressed and it is the purpose of this research to address that concern.

1.6 Problem Statement

To date, there are few guidelines and standards available to assist users with the proper design of FRP structures for civil infrastructure applications. The need for such has been discussed and the need for structures, materials, and technology that will aide in the rehabilitation of the transportation infrastructure of the United States has also been established. Additionally, there is limited information available on the influence of shear effects on FRP girders, with very little of what is available dealing specifically with shear stiffness. It is the intent of this research to add to what is available regarding the characterization of shear effects in FRP composite structures, as well as assist in the development of a structural design guide for the 36 in. DWB. It is believed that this hybrid composite structure has the ability to provide a durable, corrosion resistant alternative to steel and concrete for the efficient rehabilitation of relatively short span bridges across the country.

There were two primary goals for this research. The first goal was to characterize the properties of the 36 in. DWB for specification in a structural design guide. This was done by conducting stiffness and strength testing of the girder to determine such attributes as bending stiffness, shear stiffness, and ultimate load limits at a number of spans. The A and B basis allowables were determined for each of these properties for the design manual. Failure modes

were investigated. The second goad was to investigate shear effects in the DWB and in other FRP structures as it is believed these effects are not fully understood. In order to better understand shear effects, a model study was conducted on additional, smaller FRP structures to supplement the data obtained for the DWB and to further examine some of the factors thought to contribute to the variation seen in shear stiffness.

1.7 Tables and Figures

Figure 1-1. Former Route 601 Bridge

Figure 1-2. New Route 601 Bridge with 36 in. DWBs

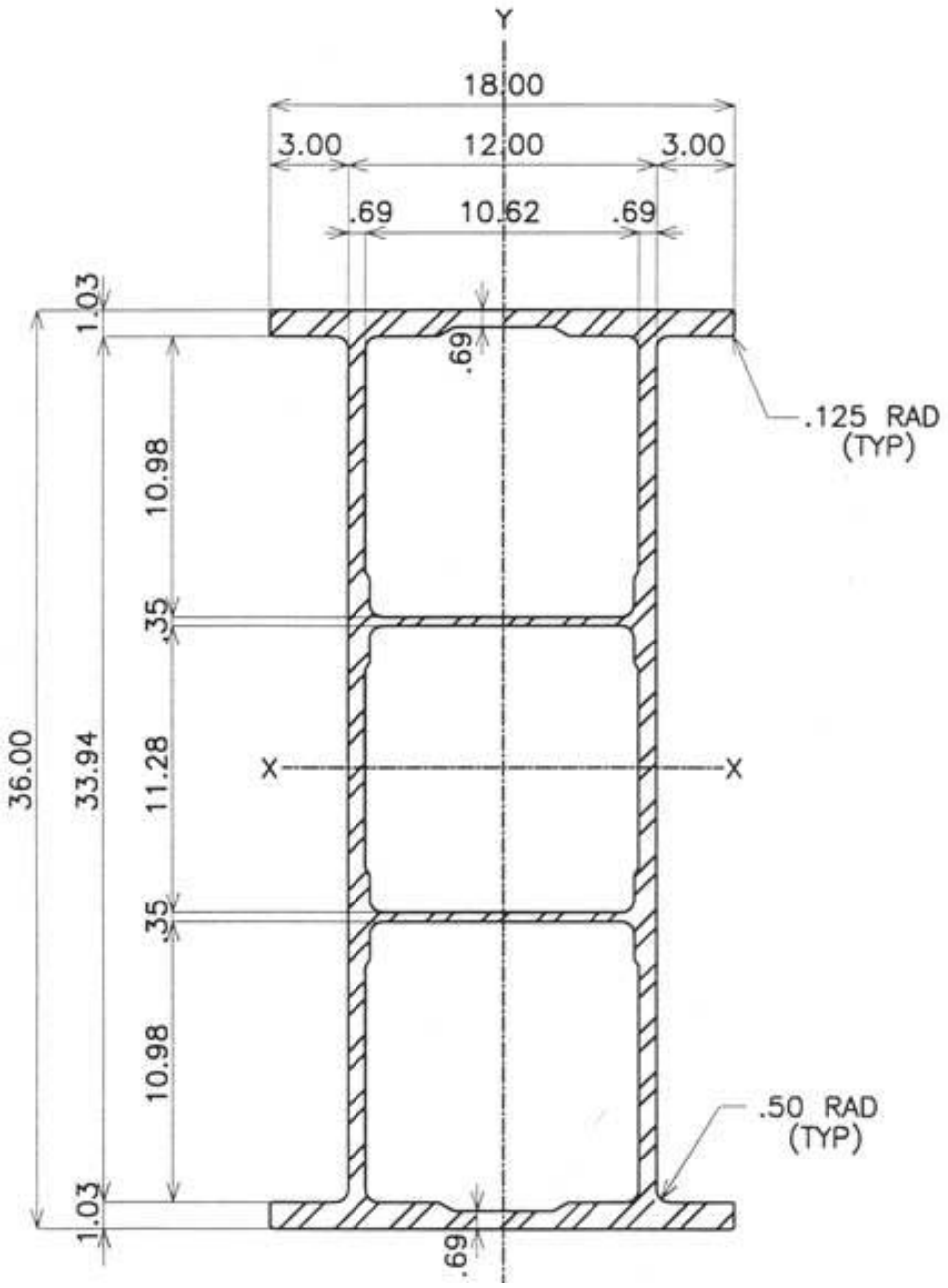

Figure 1-3. 36 in. DWB cross section (all dimensions in inches)

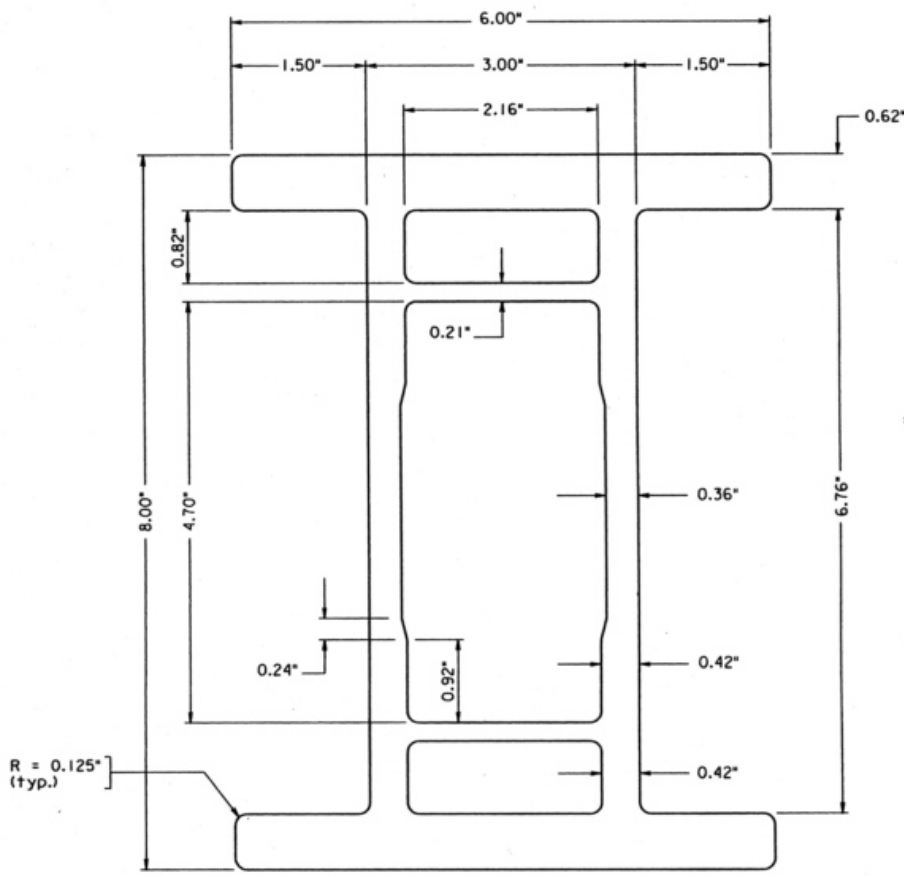

Figure 1-4. 8 in. DWB cross-section (all dimensions in inches)

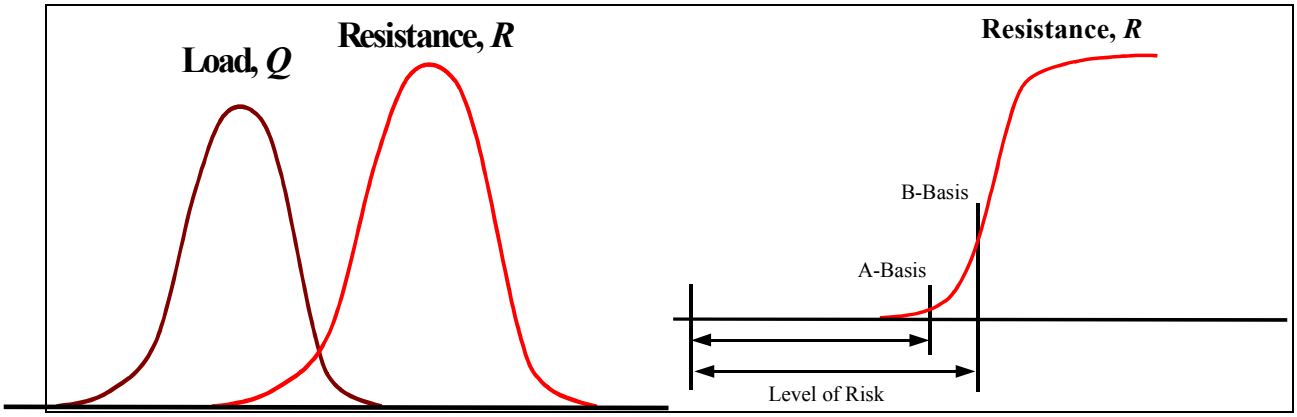

Figure 1-5. LRFD conceptual representation for design; A- and B-basis allowable levels of resistance

Chapter 2 Experimental Testing Procedures

2.1 Material System: Double-Web Composite Beams

As it was previously mentioned, the testing of two double-web beams (i.e. the 8 in. and 36 in. DWBs) has led to the development of a structural design guide for the 36 in. (914 mm) DWB (Figure 1-3). During the development of the 36 in. DWB, an 8 in. (203 mm) deep subscale prototype (Figure 1-4) was studied and implemented in the Tom's Creek Bridge rehabilitation in 1997 [1]. The results of extensive testing of this section including stiffness and strength data have been published in a structural design guide, published in 2000 [2]. The 8 in. DWB, like the 36 in. girder, is a combination of glass roving, 0/90° and ±45° fabric, and CSM with unidirectional carbon fiber laminae in top and bottom flanges embedded in Dow Chemical's Derakane 411-350 vinyl ester resin.

2.2 8 in. DWB Short Span Testing

An explanation of the testing conducted on the 8 in. DWB follows. Select results will also be presented in this section as they were utilized to establish a plan for testing the 36 in. DWB. *Values in tables and figures are presented in U.S. Customary units as they will appear in the structural design manual.*

As a precursor to the aforementioned strength testing of the 36 in. DWB, a number of tests were performed on the 8 in. DWB. Preliminary results from strength testing the 8 in. DWB indicated that the moment to failure varied with span. In order to further examine the contribution of span (and therefore shear) to the failure of the 8 in. DWB, a number of three-point, short-span failure tests were performed. Spans of 16, 32 and 60 inches (406, 813, and1524 mm), corresponding to 2, 3 and 7.5 times the depth of the beam, were chosen. Data at longer spans of 8, 14 and 17.5 feet (2.4, 4.3, and 5.3 m), length-to-depth ratios of 12, 21 and 26,

respectively, had been previously collected. For the short beam tests, three beams of each length were loaded to failure in a three-point bend test geometry (Figure 2-1). A 6 in. (152 mm) square, 1 in. (25 mm) thick elastomeric bearing pad was used at the load point (and similar, thinner pads at the end supports) to distribute the load evenly; and a 1 in. (25 mm) thick steel plate under the actuator was also utilized. The ends were restrained to prevent any lateral translation. Deflection was measured at mid-span using a wire potentiometer. Shear strain in the web near the loading point was measured in one test at each span with strain gages placed at a ±45° orientation along the neutral axis of the beam in order to examine the effect of a concentrated load on the local stress field, i.e. the degree to which cross-sectional warping affects the flange stresses. Beginning underneath the load patch at mid-span, shear gauges were placed every 1.5 in. (38 mm) extending out at least one pad's width from the beam center after which every 3 to 6 in. (76 to 152 mm) of spacing was utilized until the beam end was reached. The gauge plan and set-up can be seen in Figure 2-2.

One area of interest in the short span testing of the 8 in. DWB was to establish the distance from the load patch that was required for shear strain in the beam web to become a constant value, i.e., the shear lag. As a result of prior testing, it was thought that this distance was equal to one width of the load pad. To further evaluate these results, a 6 in. (152 mm) load pad was used. A plot of shear strain versus position (Figure 2-3) shows that at a distance of 6 inches (152 mm) from mid-span (the center of the load pad), the shear strain in the beam web appears to reach a constant value. This particular plot is for a load of 30 kips (133 kN), but the relationship remained the same at all loads. The arrows on the plot indicate the edge of the load pad and the distance required for shear strain to become constant (one pad width), respectively.

The primary purpose of this short span testing was to establish the dependence on span of the shear capacity of the 8 in. DWB and use that information to predict the capacity of the 36 in. DWB. The shear capacity of the 8 in. beam versus the length-to-depth ratio, as well as the original projection for the 36 in. beam can be seen in Figure 2-4. This projection was made using a ratio of the capacity for the 8 in. DWB to the one experimentally determined strength of the 36 in. DWB (i.e. the capacity of the 39-ft (11.9 m) girder failed prior to the rehabilitation of the Route 601 Bridge) and then extending this relationship for the other known values of the 8 in. DWB. The purpose of developing the projection was to determine the spans at which to conduct stiffness and failure tests of the 36 in. DWB.

The final point of interest in the testing of the 8 in. DWB was an analysis of the failure mechanism. As tested in three- and four-point bending (the four-point bending tests were conducted during the development of the aforementioned structural design guide), the 8 in. DWB consistently fails by delamination within the compressive flange at the interface between carbon and glass fibers. The critical stress in this case is thought to be the normal, out-of-plane stress at the free edges. Furthermore, the delamination appears to initiate at the load points, suggesting that load concentrations have a significant effect on the critical stress. A picture of a typical failure obtained during testing can be seen in Figure 2-5.

2.3 36 in. DWB Stiffness and Strength Testing

As it was explained in the previous section, short span failure testing of the 8 in. DWB was conducted, among other reasons, to determine at which spans the 36 in. DWB would be evaluated for the purpose of obtaining material properties for a structural design guide. After considering the capacity of the test set-up available and the projection seen in Figure 2-4, spans of roughly 20, 40, and 60 ft. (6.1, 12.2, and 18.3 m) were selected as it was thought that these spans would provide sufficient data to determine the relationship between shear capacity and span. Due to various factors on the laboratory floor (e.g. available space, bolt hole locations, reaction floor length, etc.), the spans at which the girders were actually initially tested were 18, 39, and 58 ft. (5.5, 11.9, and 17.7 m), which correspond to length-to-depth ratios (L/d) of 6, 13, and 19 1/3, respectively. Seventeen girders (five to six beams at each span from three different manufacturing batches) were initially scheduled to be tested and failed. After testing girders at the aforementioned spans, additional beams at a span of 30 ft (9.1 m), an L/d of 10, were also tested for reasons that are discussed in Chapter 4.

For the stiffness and failure testing of the 36 in. DWB, a four-point bending setup was utilized. The test setup involves two hydraulically driven 400 kip (1779 kN) actuators located at the third points with two 9- by 14-in. (229 by 356 mm) long elastomeric bearing pads (used to mimic bridge applications) at both the supports and the loading points (Figure 2-6). Also at the load points, in an attempt to more evenly distribute the load across the entire width of the beam, the load is delivered onto 2 in. (51 mm) thick steel plates welded to small, reinforced steel I-

beams (Figure 2-7). The boundary conditions provided by the elastomeric bearing pads are considered to be the same as or very similar to that of a simply supported beam since the pads allow both rotation and lateral translation through axial compression and shear deformation of the pads. Additionally, displacement was measured at the midspan of each beam and at the quarter points for the 60-foot span using wire potentiomers and, for stiffness tests, the more precise ±1 in. (±25 mm) Linear Variable Displacement Transformer (LVDT). The end deflections (which occur due to the use of the elastomeric bearing pads) at the supports were also measured using LVDTs and subsequently subtracted from midspan deflections to find the net deflection of the girder.

A variety of different strain gauging plans were implemented on the different beams of each span. On every beam, three gauges were evenly spaced across the top and bottom flange at midspan to measure bending strain and axial gauges were placed on the web along the neutral axis to monitor for any warping in the beam. As with the 8 in. DWB, shear strain in the web was also measured in the proximity of the load points and supports for beams at each span to examine the effect of a concentrated load on the local stress field. On various beams, strain gauges were positioned at different locations on the girders in an attempt to measure a variety of different beam characteristics. For instance, bending strains were measured a distance of 1 in. (25 mm) from the load point to further examine the effects of a concentrated load, gauges were placed vertically in a grid-like pattern on the web under a load point to look into the presence of any web compression or warping, and other similar attempts were made to better understand the complexities of a double-webbed composite beam. On a number of beams crack gauges were also used in an attempt to better characterize the failure mode of the 36 in. DWB. An instrumentation diagram can be seen in Figure 2-8.

Testing of each beam began with low load stiffness testing. The magnitude of the load for this testing was limited by the stroke (approximately 1.25 in. (32 mm)) of the LVDT located at midspan. This was necessary in order to obtain the most accurate deflection data possible. Once stiffness testing was completed, the centrally located LVDT was removed and the beams were loaded and unloaded to progressively higher loads until failure occurred. For safety reasons, lateral restraints were placed on the beam on each side of both load points, all test equipment was secured in some manner to the test frame, a Plexiglas shield was placed between the beam and test engineer (i.e. the author), and the lab was evacuated. Due to the large amount

of energy released by the beams at the moment of failure and the high loads involved, these precautions were deemed necessary and if nothing else gave some peace of mind to the test engineer loading the beam (the author).

Once failure testing was completed, a post-failure inspection was conducted to examine the method of failure (to be discussed later in Chapter 4), examine residual deflection and deformation, conduct post-failure loading (one beam), and document cracks and delaminations.

2.4 Figures

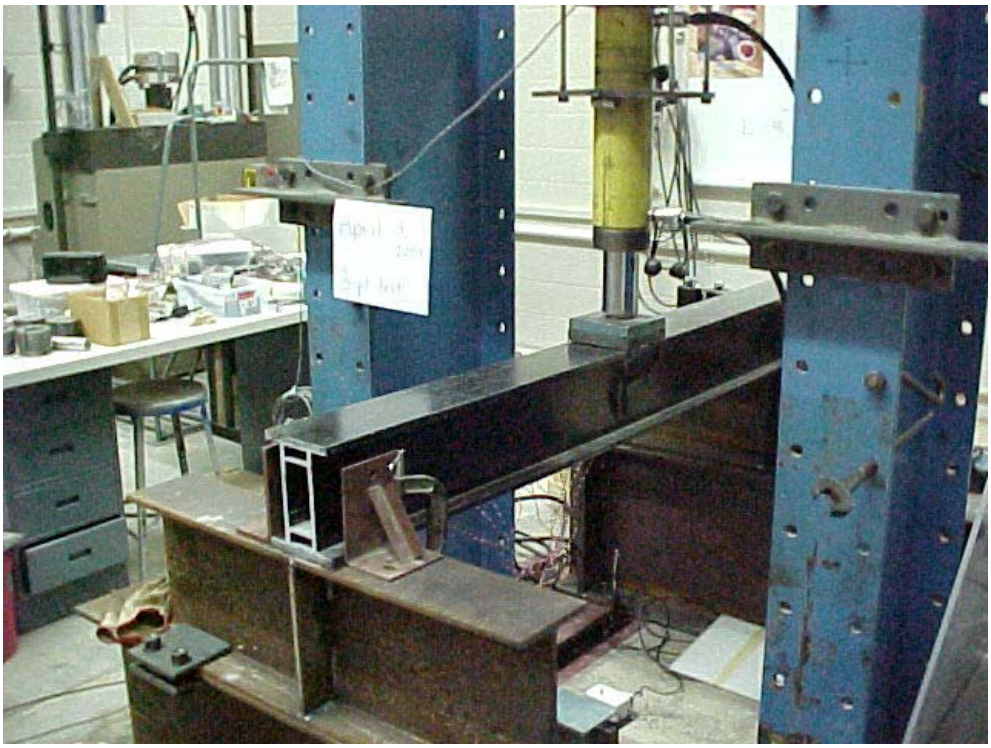

Figure 2-1. 3-Point bend test setup for short span 8 in. DWB testing

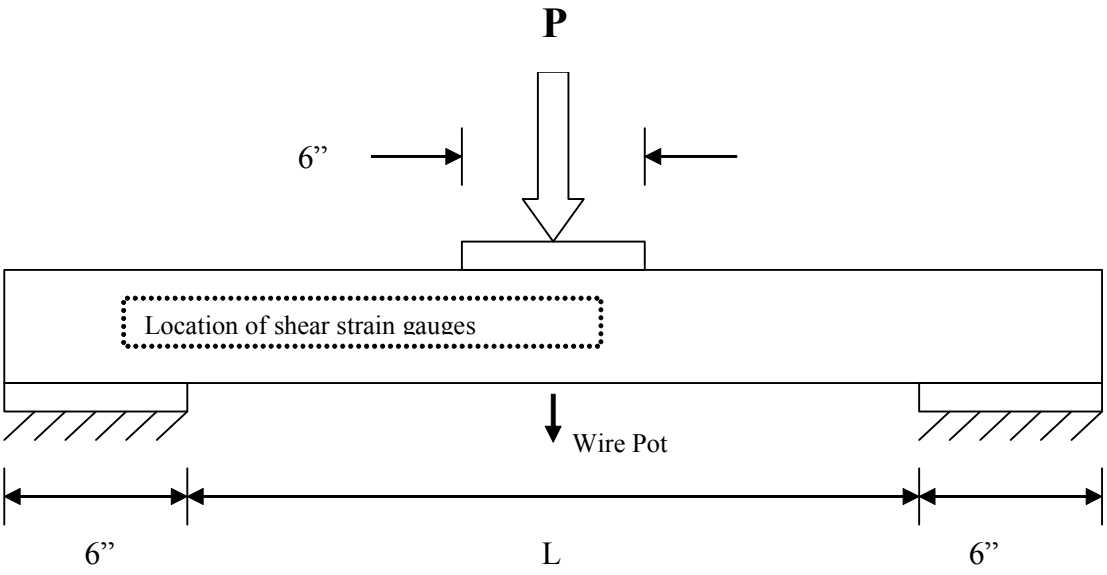

Figure 2-2. 8 in. DWB short span testing instrumentation plan

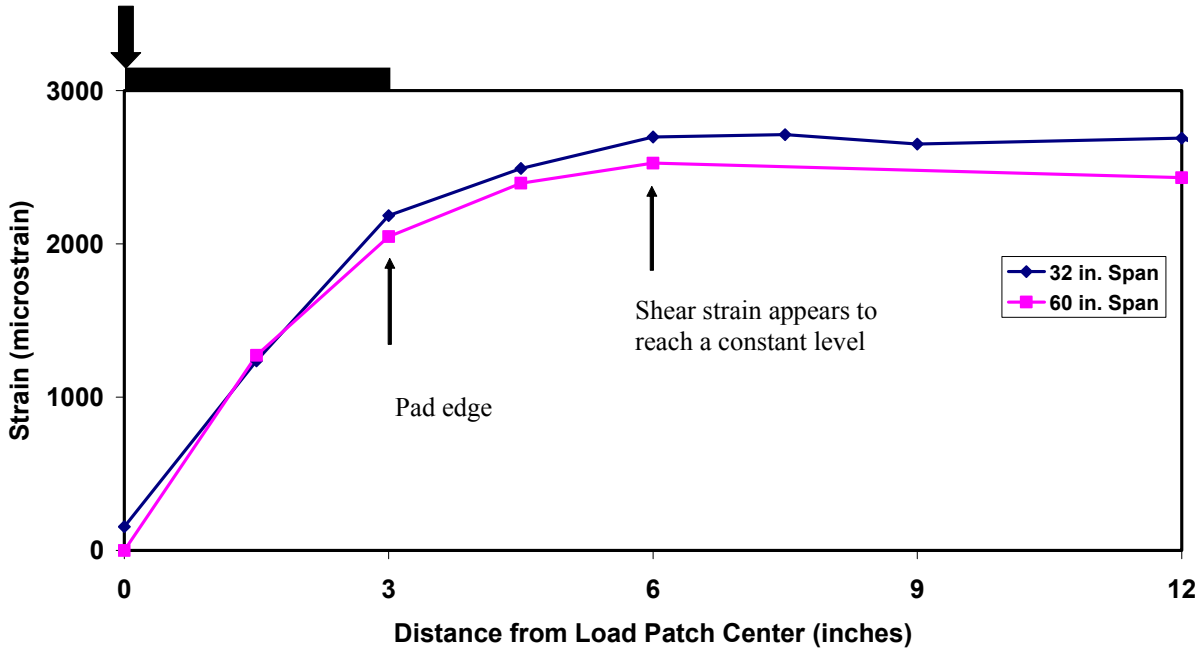

Figure 2-3. Shear strain distribution in the web, at the neutral axis, of 8 in. DWB (P = 30 kips)

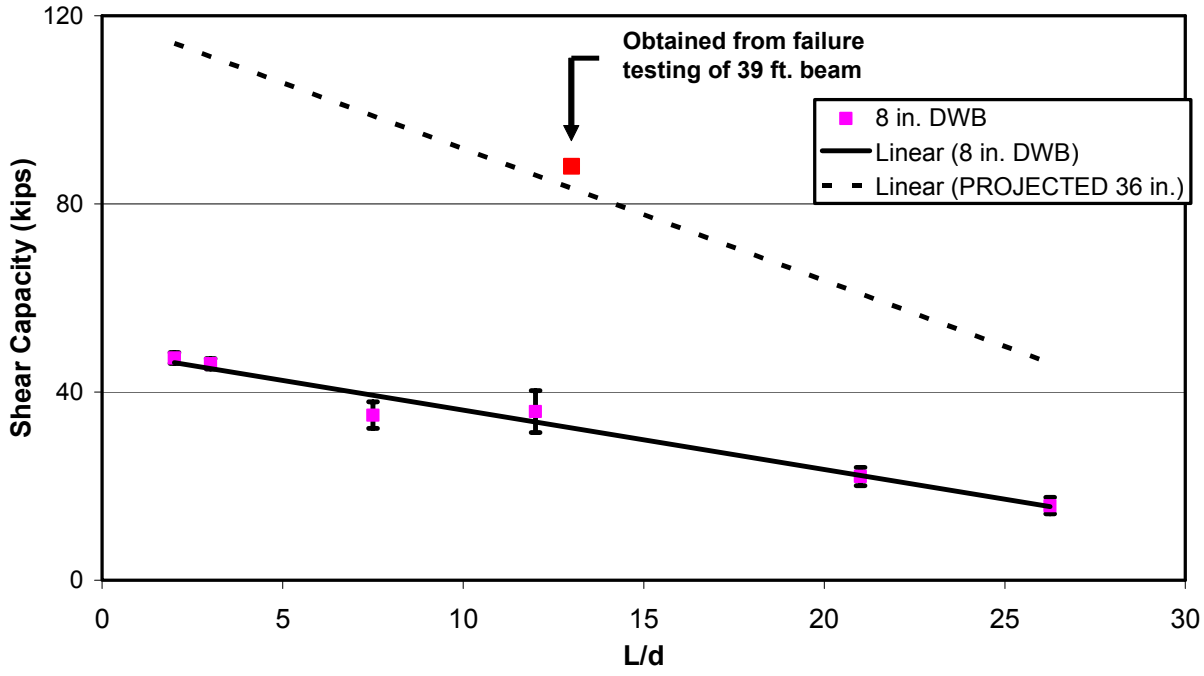

Figure 2-4. Shear capacity vs. L/d for 8 in. DWB and *initial* prediction for the 36 in. DWB

Figure 2-5. Typical delamination failure of 8 in. DWB obtained during short span testing

Figure 2-6. Four-point bend setup for stiffness and strength testing of 36 in. DWB

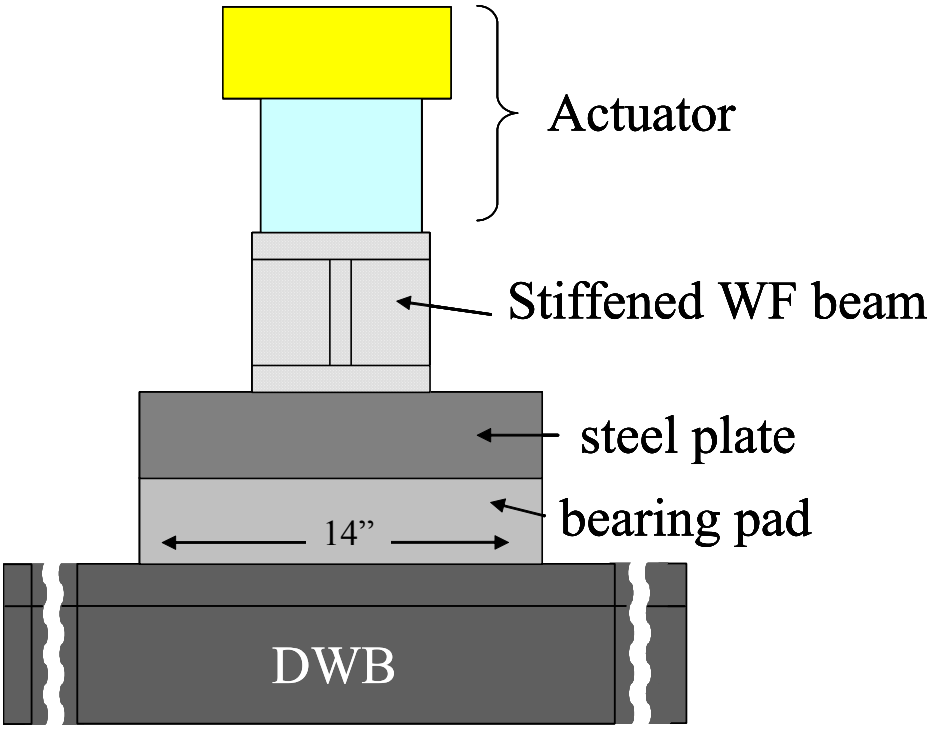

Figure 2-7. Schematic of load patch for 36 in. DWB testing

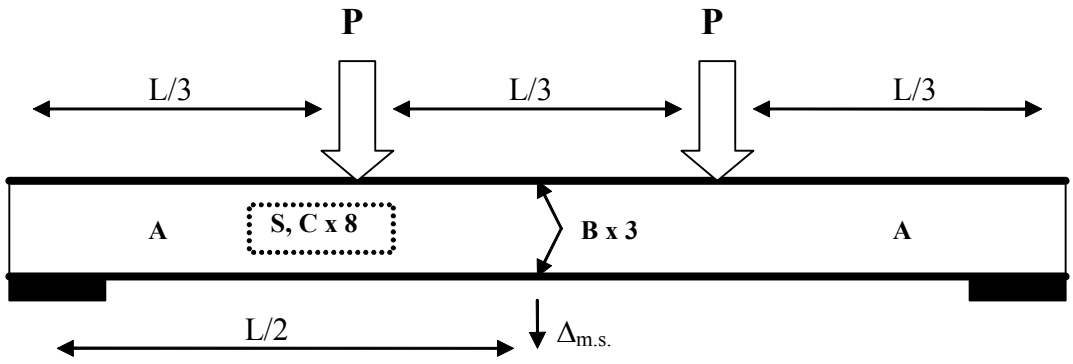

P-Load, L-Span, A-Axial Gauge, B-Bending Gage, S-Shear Bridge, C-Compression Gauge

Figure 2-8. Instrumentation plan for testing of 36 in. DWB

Chapter 3 Analysis Procedures

After testing of the 36 in. (914 mm) DWB was complete, the next step was to perform an analysis of the collected data. Nineteen beams were tested, according to the methods discussed in the previous chapter, in order to determine the strengths and stiffnesses that will assist future users of this structure by helping to form the structural design guide for this member. The results of analyzed data are presented in Chapter 4. The methods used to determine those results are presented here in the sections to follow.

3.1 Beam Stiffness Characterization

Each of the nineteen beams tested were done so in order to first determine their bending modulus (E) and shear stiffness (kGA). Bending stiffness (EI) is the property more commonly used by civil engineers. In this case, since the moment of inertia (I) was known, the two terms will be separated. For a typical bridge type structure with conventional materials, the deflection of a beam under transverse loads can be accurately characterized using only EI. For materials like steel and concrete in typical infrastructure applications, Bernoulli/Euler beam theory, which does not account for shear deformation, is used for analysis since deformation due to bending controls the response of the structure and shear deformations are negligible [23].

In Bernoulli/Euler beam theory, beam cross-sections that are plane and normal to the longitudinal axis prior to bending remain plane and normal during bending. The following equation (Equation 3-1) is the midspan deflection of a simply supported beam loaded at a distance “a” from one end:

$$\Delta_{m.s.} = \frac{Pa(3L^2 - 4a^2)}{48EI} \text{ (in)}, \qquad (3\text{-}1)$$

P = Load (kips)

E = Bending Modulus (Msi)

I = Moment of Inertia (in^4)

L = Beam Length (in)

a = Distance from beam end to load point (in).

The problem with using this theory for composites is that shear deformation in composites is not a negligible quantity and can in fact contribute a considerable amount to the total deformation of the structure (the extent of which will be discussed further in the next chapter), especially when considering the use of these beams in short span applications. Therefore, when using Bernoulli/Euler beam theory in conjunction with measured deflections, it is not a true bending stiffness (EI) that is experimentally determined, but rather some combination of bending and shear stiffness, i.e. the quantity measured is an effective bending stiffness ($E_{eff}I$).

In order to account for the contribution of shear deformation in FRP composite structures, Timoshenko's shear deformable theory is utilized. In this theory, plane sections of the cross-section still remain plane after bending, but in order to account for shear, they are no longer required to remain normal to the longitudinal axis. For a simply supported, three-point bending case, the total deflection is given by:

$$\Delta_{m.s.} = \frac{PL^3}{48EI} + \frac{PL}{4kGA} \text{ (in)}, \qquad (3\text{-}2)$$

P = Load (kips)

E = Bending Modulus (Msi)

kGA = Effective Shear Stiffness (Msi-in²)

I = Moment of Inertia (in^4)

L = Beam Length (in).

The deflection for the case of a four-point bending setup with load applied at a distance "a" from one end can then be derived, and the resulting equation is [6]:

$$\Delta_{m.s.} = \frac{Pa(3L^2 - 4a^2)}{48EI} + \frac{Pa}{2kGA} \text{ (in).} \qquad (3\text{-}3)$$

The total deflection is now a summation of the deformation due to bending (the first term), which it can be seen is the Bernoulli/Euler deflection term (Equation 3-1), and shear (represented by the second term).

The shear stiffness in this equation is represented by the term kGA. For this term, G is the shear modulus, A is the shear area, and the k term, as it was discussed in Chapter 1, is known as the shear correction factor. Again, k is used to account for a non-uniform shear distribution and is dependent upon both the geometry of the structure and its material properties. The shear correction factor may be calculated using a method determined by Cowper [16] and the application of this method to thin-walled composite structures is applied by Bank [17] and is utilized and discussed for another composite structure in Chapter 5. The reason that the stiffness term (kGA) is determined as a single, combined quantity, or an effective stiffness, is that G for this structure is difficult to determine experimentally, without which k cannot be determined experimentally, and both terms are difficult to estimate for a composite section, especially one as complex as the DWB. An estimation of the shear correction factor for both the 8 in. (203 mm) and 36 in. DWBs found it to be approximately equal to one, which would be expected due to the double-web geometry [6].

3.2 Determination of E and kGA

In preparation for the rehabilitation of the Route 601 Bridge (Chapter 1), EI and kGA for each girder were determined using two different methods. The first method used was to directly calculate the two properties, E and kGA, using midspan bending strain data and midspan deflection, respectively. The second technique (only utilized for two of the girders) involved using a multi-span slope-intercept method. For this method, Equation (3-2) is divided through by PL^3 and $\Delta_{m.s.}/PL^3$ is plotted versus $1/L^2$ for each span length. The resulting slope of the line is then related to the shear stiffness (kGA) and the y-intercept is related to the bending stiffness

(EI). For the design guide beams (i.e. the beams tested in this study), only the method of calculating E and kGA from strain and deflection data was utilized. The values of bending and shear stiffness calculated from the slope-intercept method did not agree well with those values calculated directly from strain and deflection data in the Route 601 Bridge girder study so the method was temporarily abandoned for the design guide beams. A study where the multi-span slope-intercept method is reinvestigated is presented in Chapter 5.

3.2.1 Determination of Bending Modulus (E)

The bending modulus for the 36 in. DWB was calculated directly from top and bottom flange axial bending strain data collected at the midspan of each beam. A four-point bending setup was utilized so that a constant moment region would exist, i.e. the region between the loading points. Theoretically, no shear strain exists in this region so the measured strain is a result of pure bending. Solving the well-known relationship for stress and strain then gives the equation used to calculate E:

$$E = \frac{Mc}{I\varepsilon} \text{ (Msi)}, \qquad (3\text{-}4)$$

M = Moment (kip-in)

c = Centroidal Distance (in)

I = Moment of Inertia (in^4)

ε = Average of Flange Strains (in/in).

3.2.2 Determination of Shear Stiffness (kGA)

After obtaining the bending modulus, shear stiffness (kGA) could then be calculated using the midspan deflection data. For the testing of the 36 in. DWB, the load is applied at the third points of the beam. Thus, substituting L/3 for "a" into the Timoshenko beam deflection equation (Equation (3-3)) of a simply supported beam loaded in four-point bending and superimposing the results for the two loads gives the resulting midspan deflection seen below:

$$\Delta_{m.s.} = \frac{23PL^3}{648EI} + \frac{PL}{3kGA} \text{ (in).} \qquad (3\text{-}5)$$

The only unknown in the equation is now kGA so Equation (3-5) can now be solved for the shear stiffness.

$$kGA = \frac{PL}{3\left(\Delta_{m.x.} - \frac{23PL^3}{648EI}\right)} \text{ (ksi-in²)} \qquad (3\text{-}6)$$

At this point, equations for kGA for each test geometry (i.e. the four different spans tested) were derived. Rearranging and substituting in for each span gives the following equations:

L = 704 in. (17.9 m)
a = 232.5 in. (5.91 m): $$kGA = \frac{3720EIP}{16EI\Delta_{m.s.} - 196946565P} \text{ (ksi-in²),} \qquad (3\text{-}7)$$

L = 477 in. (12.1 m)
a = 160.5 in. (4.08 m): $$kGA = \frac{1284EIP}{8EI\Delta_{m.s.} - 31005711P} \text{ (ksi-in²),} \qquad (3\text{-}8)$$

L = 360 in. (9.14 m)
a = 120 in. (3.05 m): $$kGA = \frac{120EIP}{EI\Delta_{m.s.} - 1656000P} \text{ (ksi-in²),} \qquad (3\text{-}9)$$

L = 225 in. (5.72 m)
a = 76.5 in. (1.94 m): $$kGA = \frac{612EIP}{8EI\Delta_{m.s.} - 3275883P} \text{ (ksi-in²).} \qquad (3\text{-}10)$$

The lengths that are used above to derive Equations (3-7) through (3-10) are the spans at which the 36 in. DWB was tested. The span is defined for analysis purposes as the distance between the centers-of-bearing of the beam. For example, a beam with a clear span of 39 ft. (11.9 m) or 468 in. with a 9 in. (229 mm) long bearing pad relative to the length of the beam would have a resulting span of 468 in. plus two times 4.5 in. (114 mm), or 477 in. (12.1 m).

3.3 Determination of E and kGA for the Structural Design Guide

To date, the method being implemented to determine and select the values of bending modulus (E) and shear stiffness (kGA) for the structural design guide of the 36 in. DWB is as follows. From the data collected during stiffness testing, the instantaneous E and kGA are calculated for each sampled point of load, bending strain, and midspan deflection (sampling rate is approximately 10 samples/second). The values over a set range of deflections were then selected and the average of E and kGA at those points is taken. The deflections that were chosen correspond to eleven evenly spaced values between the L/600 and L/800 deflection criteria, i.e. the deflections at L/600, L/620, L/640,…, L/780, and L/800 (beam lengths must be in inches). The L/800 criterion was selected as it is specified for bridge design by AASHTO [3]. The method of taking the average of these eleven points versus the average of the entire range between the end points was chosen because it was found that it was as accurate as and considerably more efficient than the latter method.

The L/600 and L/800 criteria were chosen for two reasons. It was decided that consistency was most important in selecting E and kGA, so a range of deflections had to be chosen that could be reached at each span. Therefore, the controlling factors became the stroke of the midspan LVDT responsible for measuring deflection and the length of the longest span. At the 704 in. (17.9 m) span, the resulting deflection at the L/600 criteria is approximately 1.2 in. (30 mm), which is roughly the upper limit of the linear range of the LVDT used to measure deflection. Since it is necessary to calculate kGA using the more accurate LVDT deflection data (versus that of a wire potentiometer), the deflection of the beam at the L/600 criteria became the upper limit of the range. Though bending modulus does not depend upon deflection, this property was also taken from the same range for consistency. The reason that both properties

had to be selected from any range at all and not just averaged over the course of the entire test can easily be seen from a plot of E and kGA versus load (Figure 3-1). As the plot demonstrates, E and kGA do not reach a constant value instantaneously so a range must be selected in order to obtain a representative value of each material property. More will be discussed regarding the nature of these properties for the 36 in. DWB in Chapter 4.

Once the selection of E and kGA was complete, the remaining step was to use Weibull statistics to determine the A and B allowables for each value. For details on Weibull statistics refer to Chapter 1 and Appendix A.

3.4 Strength Testing Analysis

As described in Chapter 2, after stiffness testing was conducted on each beam for the four different spans, each 36 in. DWB was then loaded with progressively higher loads until failure occurred. This was done to obtain ultimate strength data, as well as to investigate the dependence of capacity upon span with the primary purpose being for specification in the structural design guide for the 36 in. DWB. And again, Weibull statistics were employed to the capacities of the beam to calculate A and B allowables for each span. In addition to the collection of strength data, moment to failure was calculated for each beam, maximum deflection ($\Delta_{m.s., max}$) and maximum bending strain ($\varepsilon_{b, max}$) were documented, and a physical analysis of the failure was conducted, all of which was done to explore the possibility of existing trends.

3.5 Figures

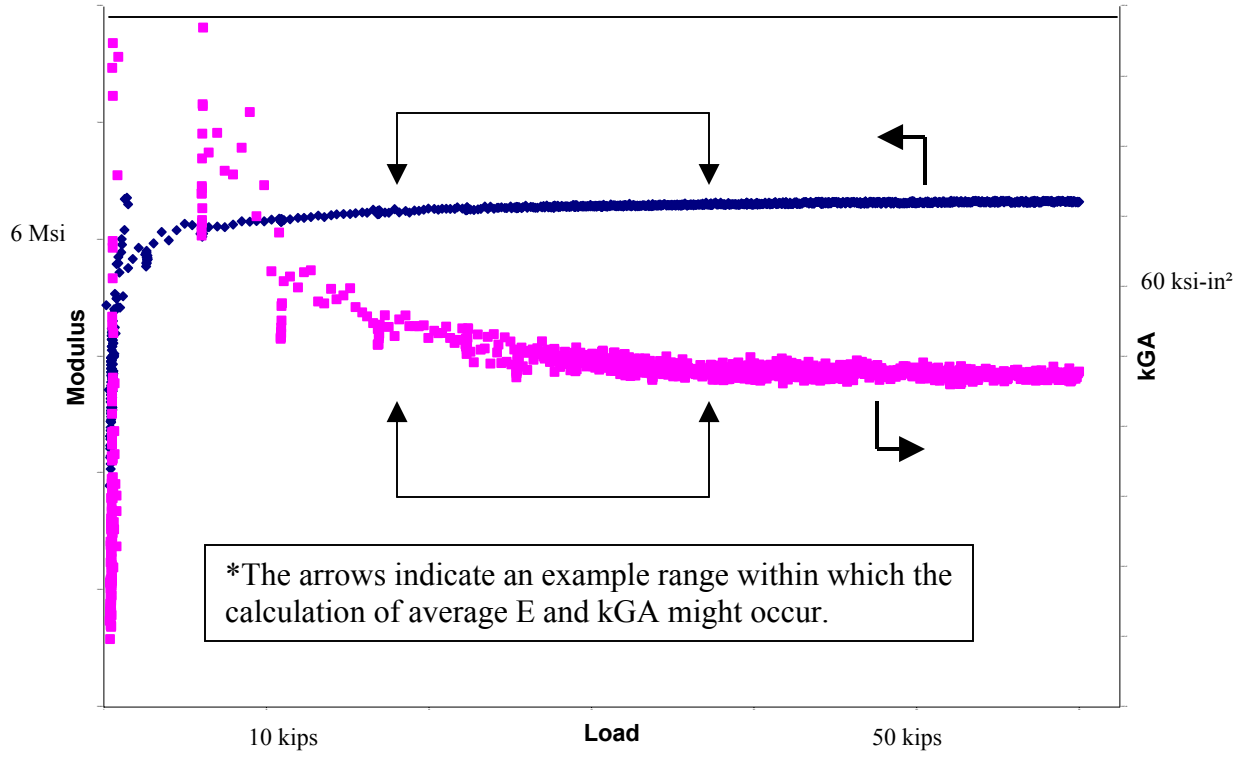

Figure 3-1. Example plot of Bending Modulus (E) and Shear Stiffness (kGA) versus Load to illustrate the selection of properties.

Chapter 4 Experimental Results and Discussion

As it has been discussed in the preceding chapters, the nineteen DWBs provided by Strongwell, Corp. were tested with the primary purpose of obtaining stiffness and strength data for the development of a structural design guide for the 36 in. (914 mm) DWB. The testing involved two main components: low-load stiffness testing for beam property characterization and failure testing to determine ultimate shear capacity and failure mode. In addition to the characterization of these traits, testing was also conducted to investigate a number of other beam attributes including, shear strain transfer characteristics in the web, shear lag effects in the flange, moment capacity, strain to failure, etc. The results of both portions of testing follow in the next few sections. In this chapter, *values in tables and figures are presented in U.S. Customary units as they will appear in the structural design manual.*

4.1 Stiffness Testing

The first portion of the design manual testing was low-load stiffness testing to determine the bending modulus (E) and shear stiffness (kGA). Following the procedures described in Chapter 2, each beam was loaded to approximately 20 to 100 kips (89 to 445 kN), depending on span, as was limited by the stroke of the deflection measuring equipment (i.e. the LVDT).

4.1.1 Beam Response

As in the testing previously conducted on the 36 in. DWB for the rehabilitation of the Route 601 Bridge, all girders demonstrated a linear-elastic response. Plots of load versus midspan deflection were generated for each test. A typical load versus deflection plot can be seen in Figure 4-1 and a typical plot of the end deflections due to the compressibility of the elastomeric bearing pad (measured at the four corners of the pad) can be seen in Figure 4-2. Also for each test, midspan bending strains on the top and bottom flange were recorded at three

evenly spaced points across the width of the beam and the average for each flange was computed. A plot of load versus the resulting average bending strains is presented in Figure 4-3.

As was previously mentioned, one point of interest in the testing of the 36 in. DWB was the investigation of shear strain transfer in the web of the beam. For one to two beams at each span, shear strain was measured in the web of the beam along the neutral axis in the proximity of both the load points and end supports. The original hypothesis based on the testing of the 8 in. (203 mm) DWB was that the lag in shear strain transfer (i.e. the distance required for the shear strain in the web to reach a constant value) was related to the width of the loading pad. For the short span testing of the 8 in. beam, a 6 in. (152 mm) load patch was used and the results appear to support the claim (Figure 2-3). However, according to Dufort [24], the transfer length may also be a function of the depth of the beam. For the 36 in. DWB, both cases can be argued (Figure 4-4). In the plot of shear strain versus position (Load = 80 kips (356 kN)), the shear strain appears to reach a constant value (or at least it appears to have stopped increasing) after a distance equivalent to one pad width extending out in the direction of the end supports. On the other hand, the strain between the load points appears to require approximately 18 in. (457 mm) before it reaches zero (recall that the constant moment region is theoretically absent of shear effects), which is a distance that could be related to the depth of the beam. And again in Figure 4-5 it can be seen that more than the distance of one pad width is required to reach a constant value, this time in the region around an end support. Essentially, a case can typically be made for both possibilities. For this reason, future testing is planned to further investigate shear strain transfer. Load versus far-field shear stress was also plotted to ensure its linearity (Figure 4-6).

In addition to examining shear strain in the web of the beam, there were a number of other beam responses that were examined using the various strain gauge configurations discussed briefly in Chapter 2. The distribution of bending strains across the width of the flange near one of the load points was measured and compared to those measured at midspan. A plot of these strains and their locations on the flange may be seen in Figure 4-7. From the plot it does not appear that there is any distinct effect of a concentrated load on the bending strains. Compressive strains in the web under the load patch were also recorded (Figure 4-8). As a means to gauge their magnitude, note that the bending strain at the same load (60 kips or 267 kN) during the test from which this data was taken was approximately 300 microstrain as well. One area where the compression of the web becomes significant is in the stress analysis of the

structure. The beam web is generally considered to be incompressible, but this data suggests that this may not be the case for this structure.

4.1.2 Bending Modulus (E) and Shear Stiffness (kGA)

The bending modulus (E) and shear stiffness (kGA) for each beam were calculated directly from midspan bending strain and deflection data, respectively, according to the methods described in Chapter 3. A typical plot of E and kGA versus load for a low load test can be seen in Figure 4-9. The flat nature of the curve for E and the non-constant nature of kGA were common to most every test. A summary of the values of E and kGA for each beam can be seen in Table 4-1. The reported values of both of these properties are obtained from taking the average for each for multiple tests. The calculated values for the majority of the individual load tests may be seen in Appendix B.

As it can be seen from the plot of kGA versus load (Figure 4-9), shear stiffness appears to decrease as the beam is loaded. This is the opposite case from what was measured during the testing of the beams for the Route 601 Bridge rehabilitation [23]. In that case kGA appears to increase as additional load was applied. Timoshenko beam theory (refer to Chapter 3) suggests that kGA, or G in particular, is a material property and should therefore be independent of load and remain constant, as the bending modulus appears to be. To date, this phenomenon is unexplained and is being studied further. There are a number of possible reasons for this and the variation in general that can be seen in the reported values of kGA, as well as the variation that can be seen in Figure 4-9. First of all, although Timoshenko, unlike Bernoulli/Euler beam theory, does account for shear deformation, it does so in a relatively simple manner. A more complex theory to capture the deformation may be needed.

One reason in particular that the accurate characterization of the shear deformation of the 36 in. DWB is important is that, especially at short spans, the contribution of shear deformation to the total deflection becomes a significant portion (Figure 4-10). In fact, in preparation for the rehabilitation of the Route 601 Bridge, it was calculated using the conservative values of E and kGA that were used for the bridge's design that shear deflection accounted for 16 percent of the

total deflection of the structure [23]. Using the average experimentally determined values of E and kGA reveals that this portion is smaller, but remains important nonetheless.

It has been found that shear stiffness is extremely sensitive to numerous factors, especially the midspan deflection from which it is directly calculated. For example, it has already been mentioned that kGA is calculated using deflections measured using LVDTs due to the increased accuracy they provide versus wire potentiometers. A plot comparing the property measured using each can be seen in Figure 4-11. In addition to the displacement transducer type, the resolution of the acquisition system is another key to measuring accurate deflections and thus reducing variation in kGA calculations. Mid-way through the testing of beams, the computer running the acquisition system crashed due to old age and was beyond repair. This acquisition system had been chosen due to its familiarity to users, but the computer crash required a change to a newer system with better resolution. The data collected using this system, as would be expected, proved to be more noise-free and more accurate. Figure 4-12 shows a plot of E and kGA from this system. This data was even calculated using the measurements from a wire-potentiometer, which with the old system, it would have been extremely difficult to obtain usable data. The importance of acquisition system resolution is demonstrated further in Chapter 5.

Another important point is illustrated by the plot of E and kGA versus load in Figure 4-12. The plot illustrates the problem in accurately reporting kGA when the data is taken from the low load ranges that were selected for consistency purposes in the design guide. The advantage of being able to accurately measure deflection up to failure loads or at least over a larger range is quite evident.

Along with the ability to accurately measure deflection, there are other factors contributing to the variation that can be seen in kGA. For instance, the span that is selected for analysis can contribute to the uncertainty in shear stiffness. The decision to select center-of-bearing to center-of-bearing as opposed to clear span impacts the value of kGA, not only because it goes directly into the calculation of E in the form of a moment arm, but also because it changes the coefficients in the Timoshenko shear deformable beam theory equations that are derived for the calculations (refer to Chapter 3).

This issue was of particular importance for the 18 ft (5.49m) span because the boundary conditions were different for each of the three beams tested for reasons that will be explained in the next section. For the short span, the center-of-bearing to center-of-bearing distance had to be

adjusted, which resulted in variations in both the bending moduli (especially relative to that of the other three spans) and also shear stiffnesses. And though two of the calculated values obtained for kGA are very close in magnitude, a close examination of the data shows that this may be only due to chance variation as well. These two beams had distinctly different boundary conditions (explained in the next section), different center-of-bearing to center-of-bearing spans, the largest difference between values of bending modulus of any of the combinations of beams within a span, and the largest difference between any two failure loads of any combination within a span, which suggests that the shear strains are most likely quite different although no shear gauges were present on either beam to confirm this speculation. Basically, it is the belief of the author that these two values are as good an indication of the variability of kGA as is the difference between the shear stiffness of these two beams and the third at this span, which it should be noted had the largest calculated value of kGA of any of the beams (note that due to the boundary conditions for this beam, it had end deflections due to the elastomeric bearing pads that were over three times that of any other beam).

There are other, more difficult to quantify factors that may contribute to the variations in kGA and the difficulties that are had in accurately characterizing this property. For instance, the load being applied through a load patch to the flange most likely has an effect (again, boundary conditions), the existence of significant compressive strains in the web (suggesting that the web may not be incompressible), material nonlinearities, and the shear lag that was discussed in the previous section (also discussed further in Chapter 5) is also most definitely contributing to the variation in and/or difficulty in measuring the shear stiffness of this structure.

4.2 Strength Testing

Once low load stiffness testing was complete for each beam, the straightforward process of strength testing was performed. The beams were simply loaded until they failed in some manner. The typical failure was accompanied by an explosive burst of sound, and was also defined by the sudden drop in load (though the shock wave was all that was necessary to signal failure). The beams provide little warning before failure in most cases, but although it is loud, it would not be considered catastrophic. In fact, post-failure testing of one beam showed the

ability to hold load and revealed that over 80% of the bending modulus (E) was retained (Figure 4-13).

As it was seen in the plot of shear capacity versus aspect ratio, there appears to be a linear relationship between shear capacity and span for the 8 in. DWB (Figure 2-4). Initial testing of the larger girder at the 39 and 58 ft (11.9 and 17.7 m) spans supported the hypothesis that the 36 in. DWB would behave in a similar fashion. Furthermore, the failure mechanism did not change at these two spans, just as it did not with the 8 in. girder. The 36 in. DWB appears to fail in a similar manner to the 8 in. DWB, which consistently fails by delamination in the top flange at a carbon-glass interface (an area of high interlaminar stress due to the differences in the modulus of the two materials), beginning in the vicinity of the loading patches and progressing outward in both directions along the primary beam axis. For the 36-inch DWB, delamination may also initiate at the internal ply drop-off underneath the flange (refer to Figure 1-3). This drop-off is the result of glass fabrics in the outer half of each web that fold over in the pultrusion die to form the inner half of each flange. Tests using crack detection gauges to capture the path of crack growth along the length of the beam were attempted. The results supported the idea that the delamination began at a load point, but due to the speed of the crack growth (and relatively slow acquisition speed of the system used), little else was able to be determined from the data. A picture of a typical delamination failure can be seen in Figure 4-14.

Testing for the 36 in. DWB began at the 58 ft span, progressed to the 39 ft girders, and then finally to the 18 ft (5.5 m) beams. As it was mentioned, testing of the two longer spans supported the original hypothesis that failure was controlled by shear capacity, that this shear capacity varied linearly with span, and that the failure mechanism remained was independent of span. Testing of the 18 ft DWBs revealed that this was not exactly the case. Three 18 ft, 36 in. DWBs were tested and all three failed by a different failure mechanism than the previously tested girders. It seems that shear capacity is not the only controlling factor as bearing failures occurred in all three of the 18 ft beams. The bearing failures occur at the end supports as a result of the elastomeric bearing pads creating additional stresses on the flanges, causing cracking at the web-flange junction. In the worst case, the crack propagated up the web of the beam, causing it to buckle as seen below in Figure 4-15.

Three different orientations of the elastomeric bearing pads were tried (one on each of the three girders tested), as it was thought that the original alignment created an upward stress on the

flange edge that was causing the cracking at the web-flange junction. The original pad orientation (used for the 39- and 58 ft spans) was such that the pads stuck out 5 in. (127 mm) on each side of the beam, relative to the 18 in.(457 mm) width of the beam (the pads were 9 in. (229 mm) along the length of the beam and 28 in. (711 mm) across the width). The second orientation turned the pads so that they went from flange edge to flange edge (14 in.(356 mm) along the beams length, 18 in. (457 mm) across the width). It was thought that this might alleviate some of the stress on the flange edges; testing revealed that it did not. On the third and final 18 ft girder tested, only one bearing pad was used, centered under the beam so that the pad edges lined up exactly with the webs of the beam (14 in. (356 mm) across the width) and was 9 in. (229 mm) along the length of the beam. The bearing failure seen in Figure 4-15occurred under this boundary condition. The orientation of the bearing pads for each girder can be seen in Figure 4-16.

After it was discovered that a bending-type failure (delamination of the top flange) could not be obtained at the short 18 ft span, an additional failure test of a DWB at a 30 ft (9.1 m) span was conducted. The bearing pads were oriented in the same manner as the second 18 ft test (18 in. (457 mm) wide, 14 in. (356 mm) along the length of the beam) and the beam did indeed fail by delamination in the top flange, the same mode as those of the two longest spans. Four additional beams provided by Strongwell Corp. were then tested at a span of 30 ft and all failed in the same manner as the first (i.e. top flange delamination). The testing of the 30 ft. span concluded the strength and stiffness portion of the design manual testing. The resulting plot of shear capacity versus aspect ratio may be seen for the 36 in. DWB in Figure 4-17. It must be noted that beams with an aspect ratio of 6 did not fail due to shear capacity and are therefore represented on the plot as individual data points. It also would not be representative to plot the average of those three tests, as the test geometries (boundary conditions) were quite different due to the dissimilar bearing pad orientations. A table showing a summary of the results of all the strength testing, as well as the stiffness testing, may be seen in Table 4-1.

In the summary table, the column headed “Batch” refers to which of the three pultrusion runs that particular girder belongs (Batch 1—Summer 2000, Batch 2—May 2001, Batch 3—July 2001). The ultimate capacity (broken down by batch in Figure 4-18) was the total load of the two actuators that the beam supported at failure and the shear capacity is the average of that resulting sum. Again, E is the bending modulus and kGA is the shear stiffness. The data that

was lost for maximum bending strain and deflection was a result of the aforementioned problems with the initial acquisition system. It should also be noted that the maximum deflections that are presented are net deflections (i.e. midspan deflection minus the average of the end deflections). It may also be of interest to note that for the first 18 ft girder listed, the relatively low net deflection of only 0.8 in. (20 mm) was a result of that particular bearing pad orientation (only one pad was used) causing an average end deflection of 0.5 in. (13 mm). A quick calculation of kGA using a deflection of midspan deflection minus only half of the average end deflection placed the value of kGA at approximately 35 to 40 Msi-in² (1560 to 1780 GPa-cm²). It is difficult to judge if this is a more or less accurate estimation of shear stiffness, but it may not be unreasonable to assume that the true value lays somewhere in between this estimation and the reported value.

4.3 A and B Allowables for the Structural Design Guide

As it has been mentioned previously, Weibull statistics will be employed to determine A and B allowables for E, kGA, ultimate shear strength, and moment to failure and the resulting values will be presented in the structural design guide for the 36 in. DWB. The purpose of reporting these values is that they are used to capture the variability in test data more thoroughly than does a normal mean and standard deviation and also to define with what certainty or confidence a given value may be used. A table summarizing the results of the Weibull calculations (refer to Appendix A for details) can be seen in Table 4-3. The Weibull mean along with the A and B allowables for bending modulus, shear stiffness, and shear capacity plotted versus span can also be seen in Figure 4-19, Figure 4-20, and Figure 4-21, respectively.

4.4 Tables and Figures

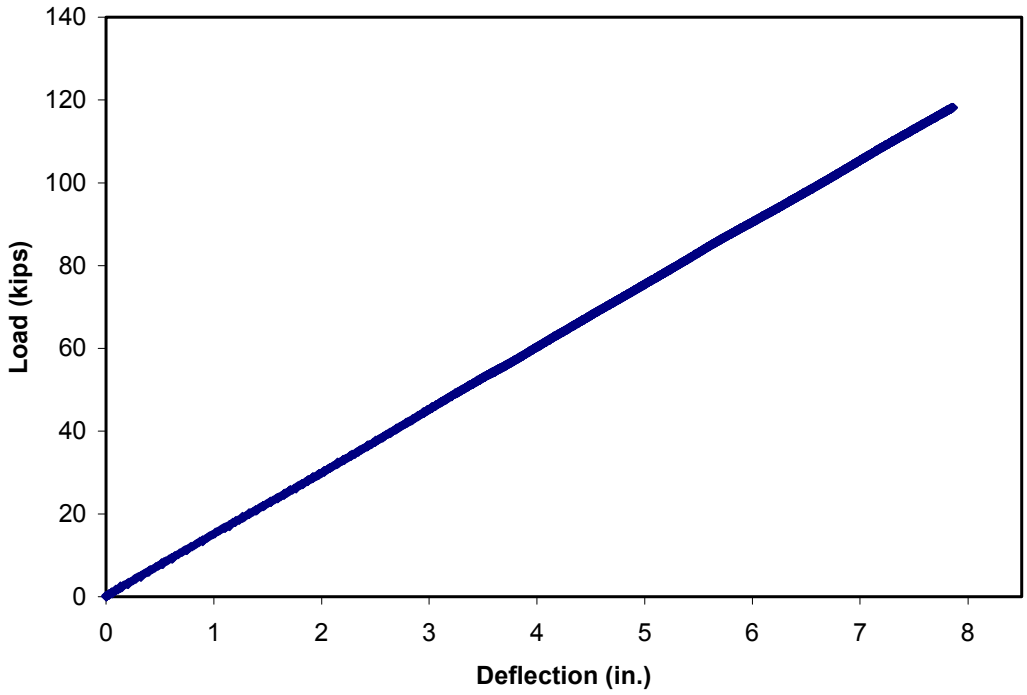

Figure 4-1. Typical load versus midspan deflection plot for 36 in. DWB (from a failure test)

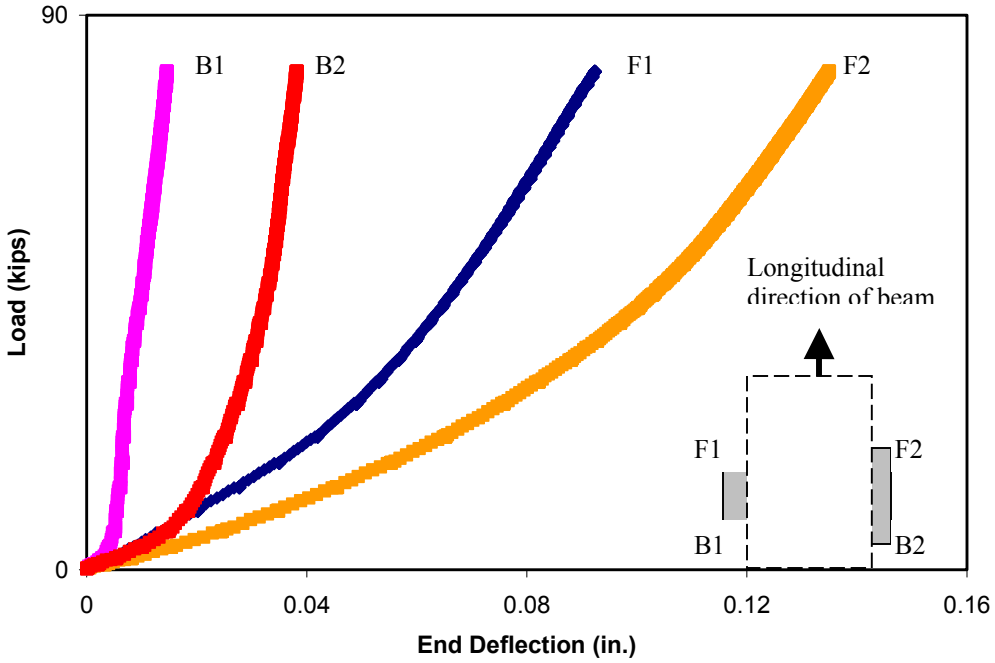

Figure 4-2. Typical load versus end deflections plot of elastomeric bearing pads, F and B denote that the displacement resulted at the front or back edge of the pad, respectively

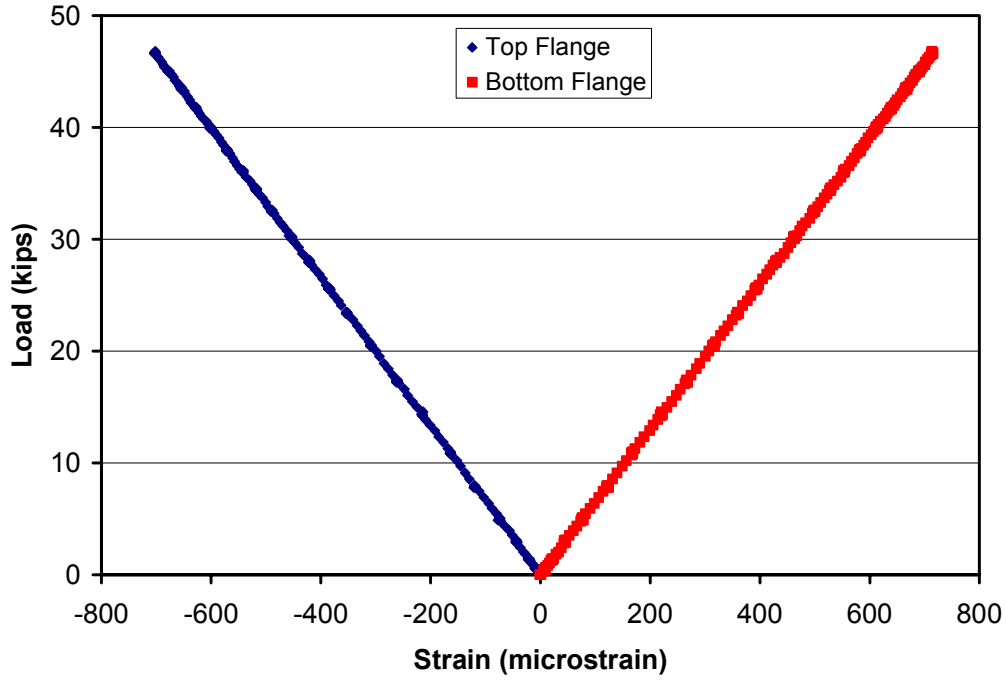

Figure 4-3. Typical load versus midspan bending strains plot (stiffness test)

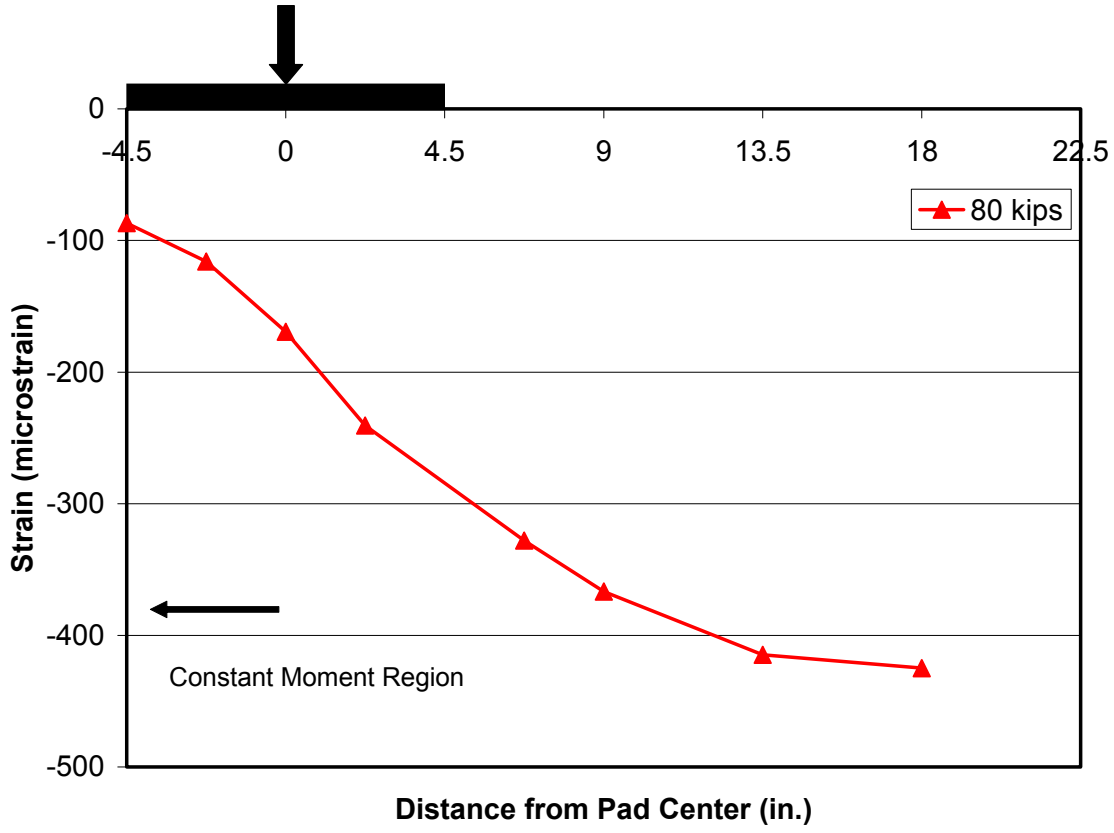

Figure 4-4. Shear strain distribution in web, along neutral axis (9 inch wide load patch)

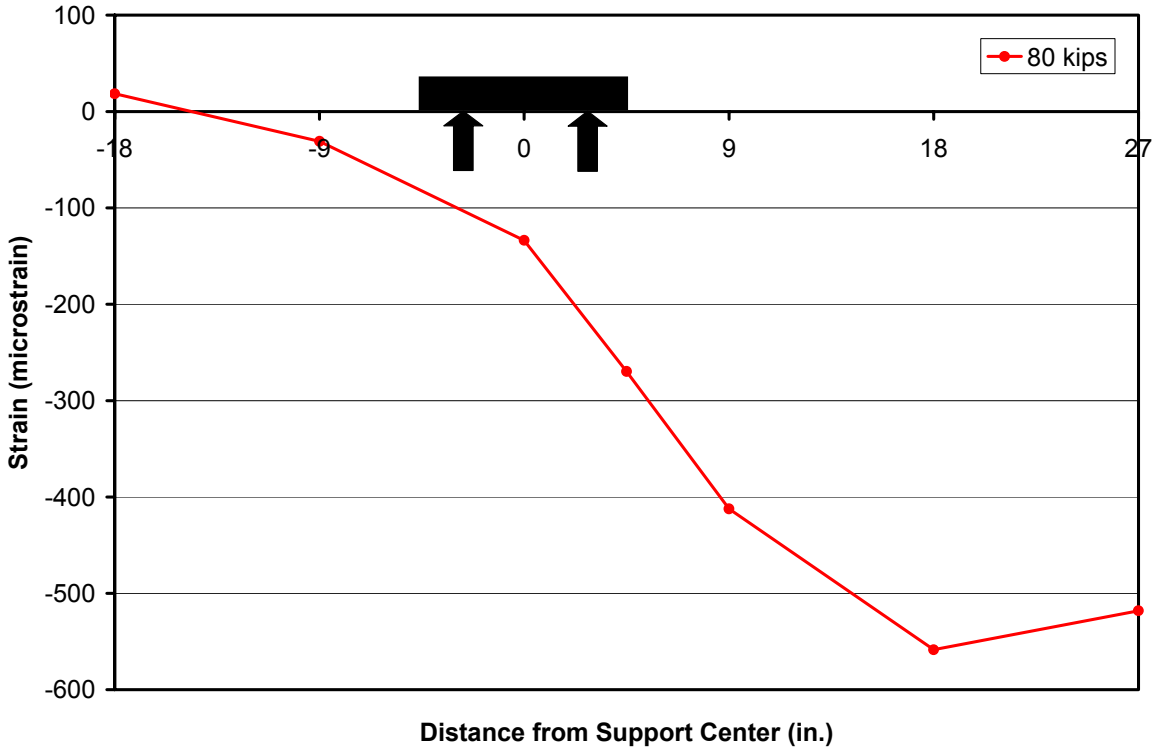

Figure 4-5. Shear strain distribution in beam web, along neutral axis at an end support

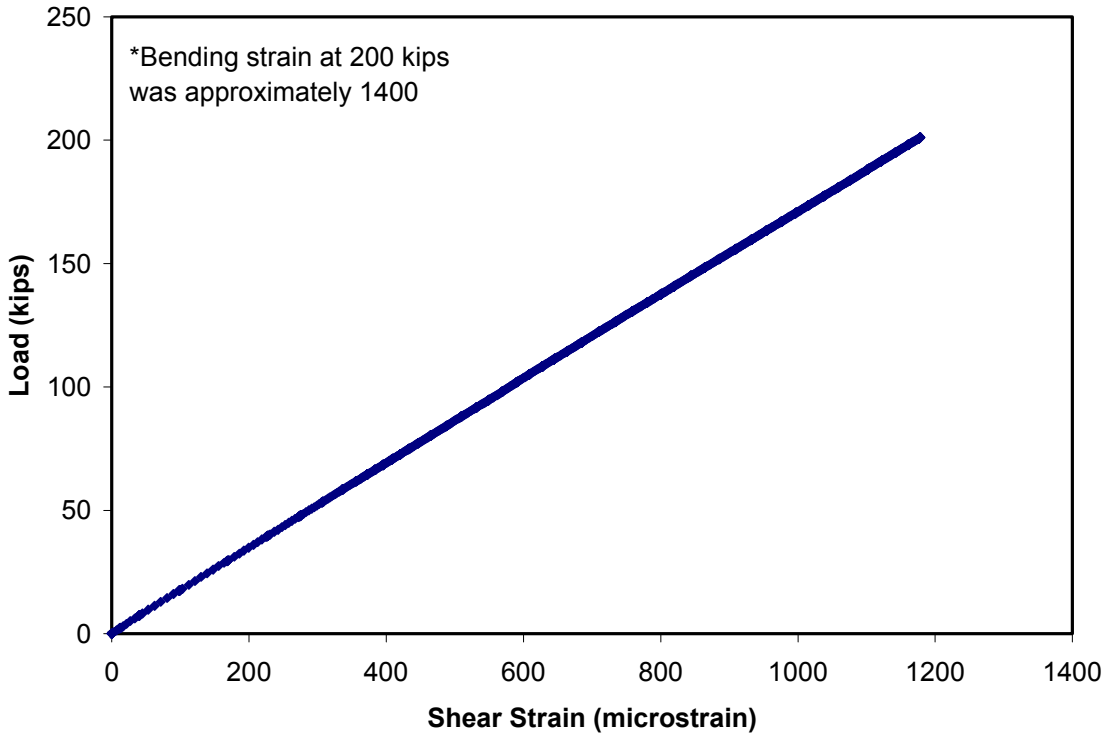

Figure 4-6. Typical plot of load versus far field shear strain in beam web

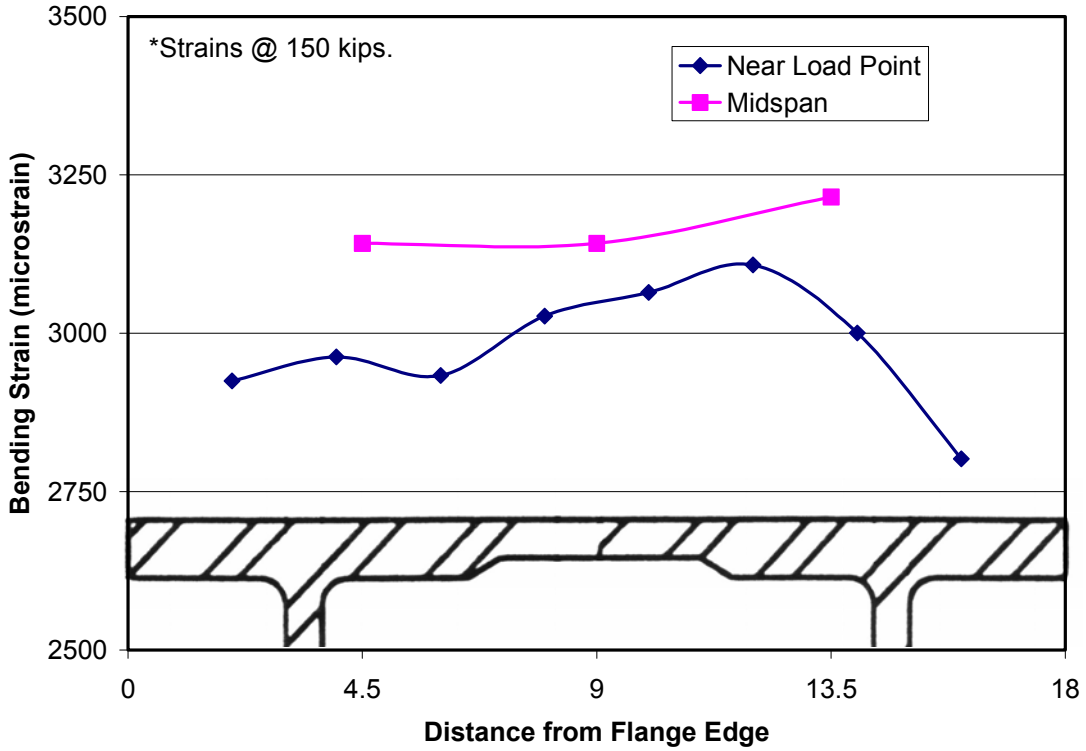

Figure 4-7. Top flange bending strain distribution across the width of the flange

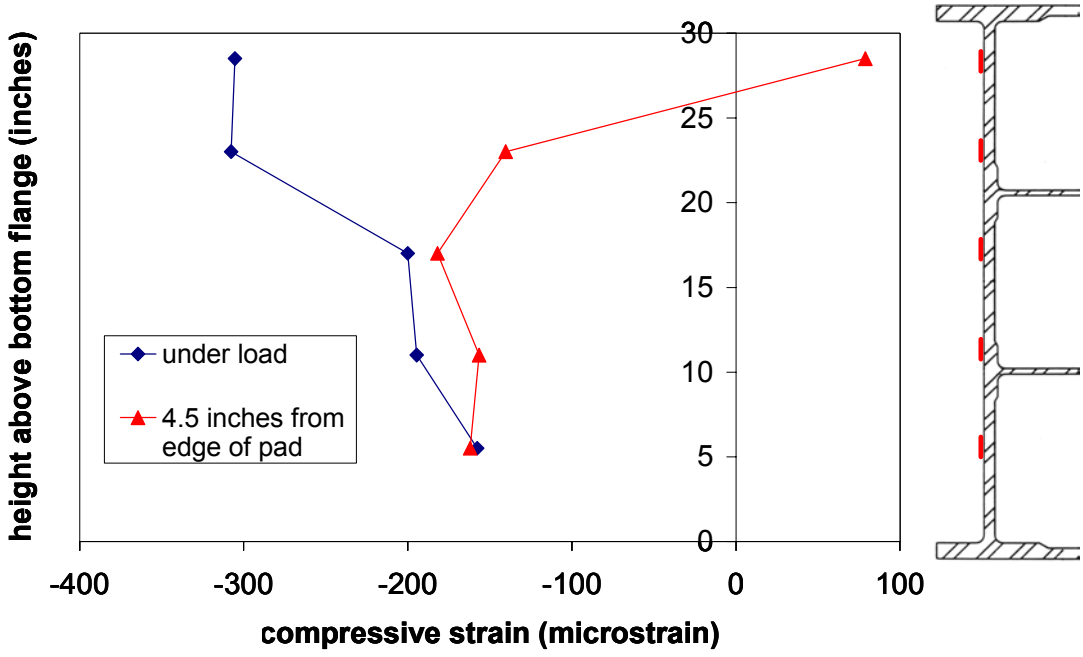

Figure 4-8. Compressive strain in beam web under a load point

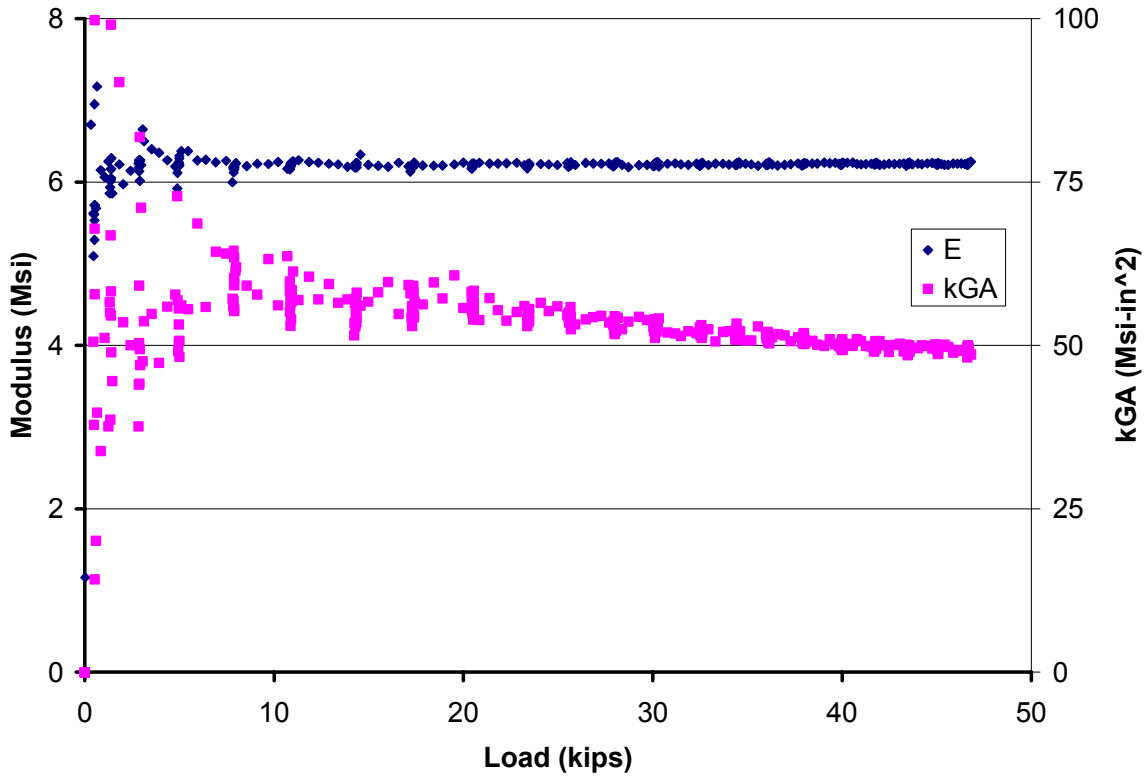

Figure 4-9. Typical plot of bending modulus (E) and shear stiffness (kGA) versus load

Table 4-1. Summary table of results of 36 in. DWB testing

L/d	Batch	Shear Capacity (kips)	Ultimate Capacity (kips)	$M_{failure}$ (kip-ft)	Max d_{ms} (in.)	Max ε_b ($\mu\varepsilon$)	E (Msi)	kGA (Msi-in^2)
6	3	156.0	312	994.5	0.80	2090	6.67	66.9
6	2	195.0	390	1283.8	1.31	2510	7.27	33.9
6	3	134.5	269	857.4	1.43	1850	6.52	33.6
10	1	121.5	243	1215.0	2.71	2540	6.70	47.3
10	3	129.0	258	1290.0	2.86	2830	6.44	43.4
10	3	143.0	286	1430.0	3.15	3205	6.38	49.1
10	3	143.5	287	1435.0	3.01	3090	6.63	50.3
10	3	138.0	276	1380.0	3.01	2985	6.52	62.4
13	3	113.5	227	1518.1	5.14	3440	6.27	44.5
13	3	72.0	144	963.0	3.27	2200	6.21	51.6
13	3	83.0	166	1110.1	lost data		6.02	58.5
13	3	106.5	213	1424.4	4.72	3150	6.49	47.2
13	1	117.0	234	1564.9	5.10	3570	6.61	39.5
13	1	81.5	163	1090.1	3.65	2570	6.28	46.2
19.33	2	82.5	165	1598.4	9.89	3660	6.40	53.5
19.33	2	73.5	147	1424.1	9.35	3170	6.66	52.3
19.33	2	59.0	118	1143.1	7.75	2620	6.45	38.0
19.33	3	60.5	121	1172.2	8.10	2620	6.37	42.1
19.33	3	66.5	133	1288.4	8.84	2930	6.39	43.9

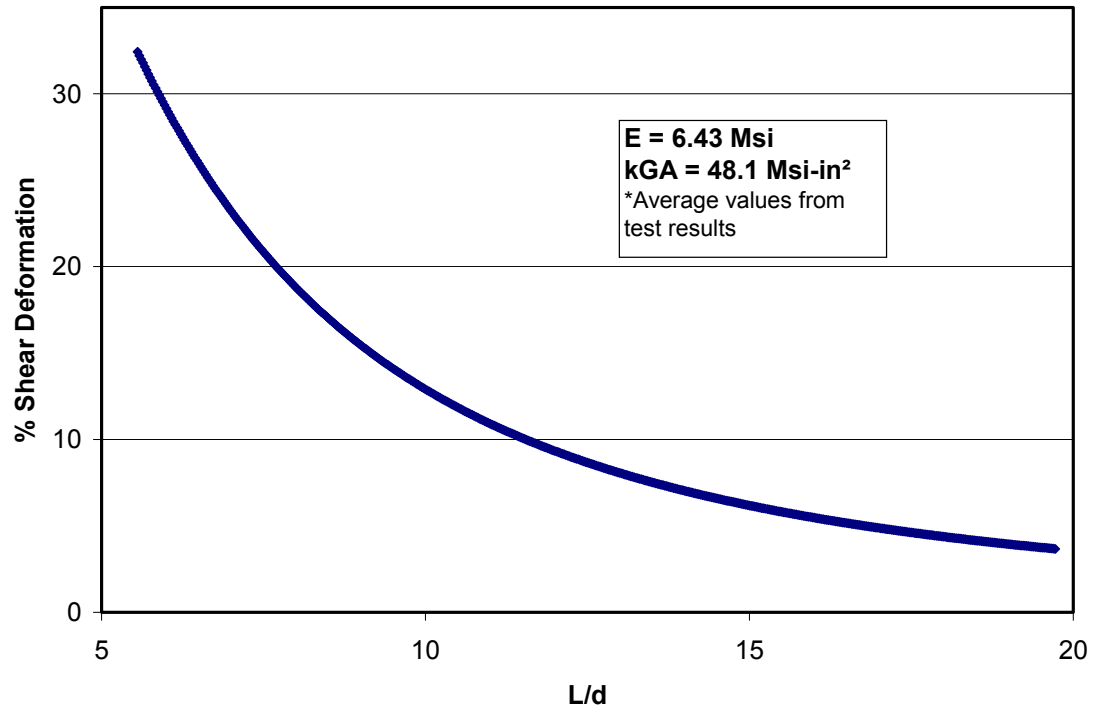

Figure 4-10. Contribution of shear deformation to total beam deflection versus span (average experimental E and kGA)

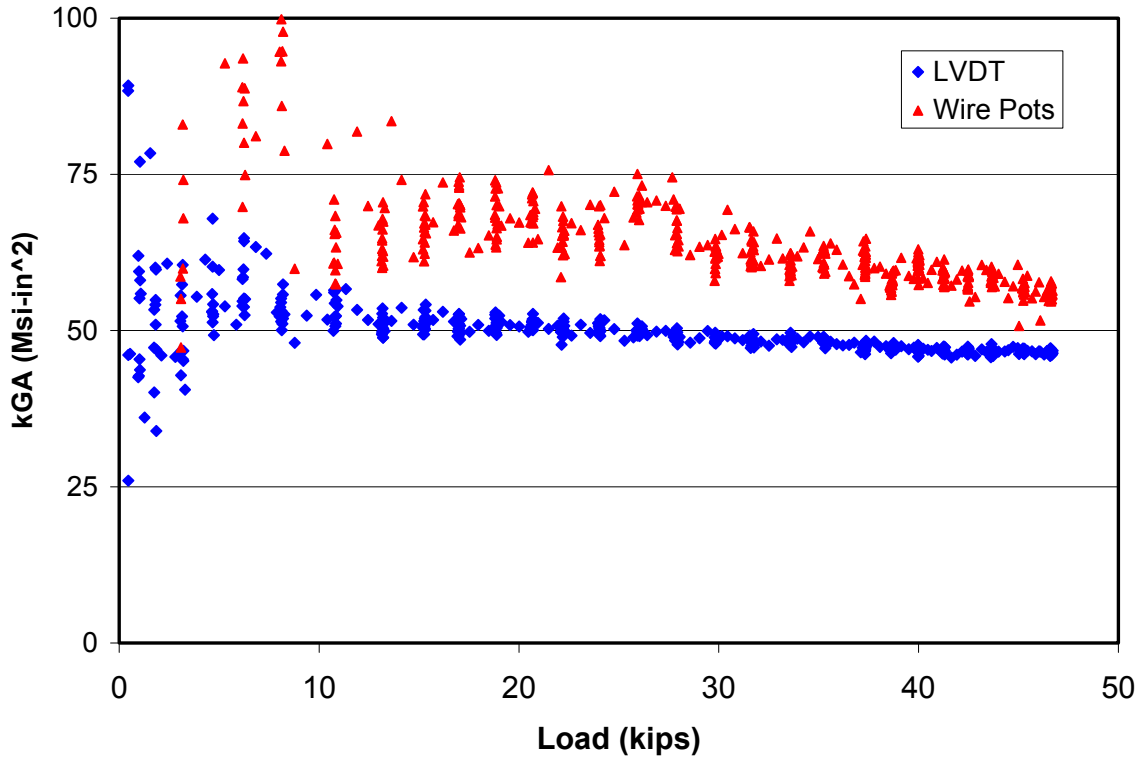

Figure 4-11. Plot of kGA versus load comparing data calculated from an LVDT and a wire pot

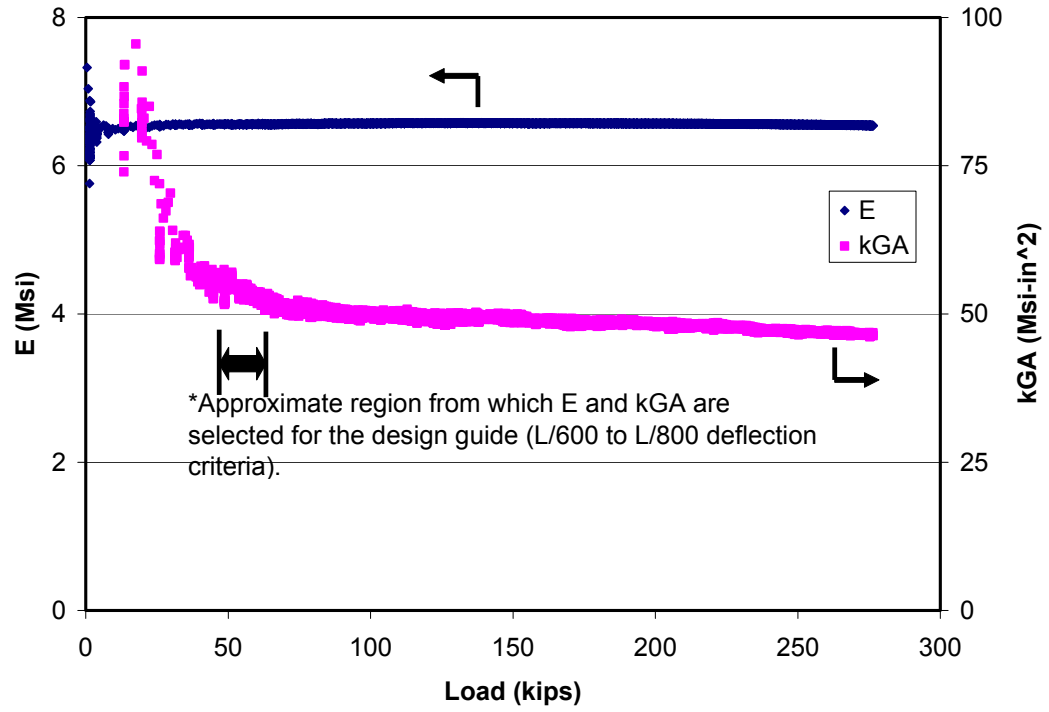

Figure 4-12. Modulus and kGA versus load calculated from wire pot data (System 6000)

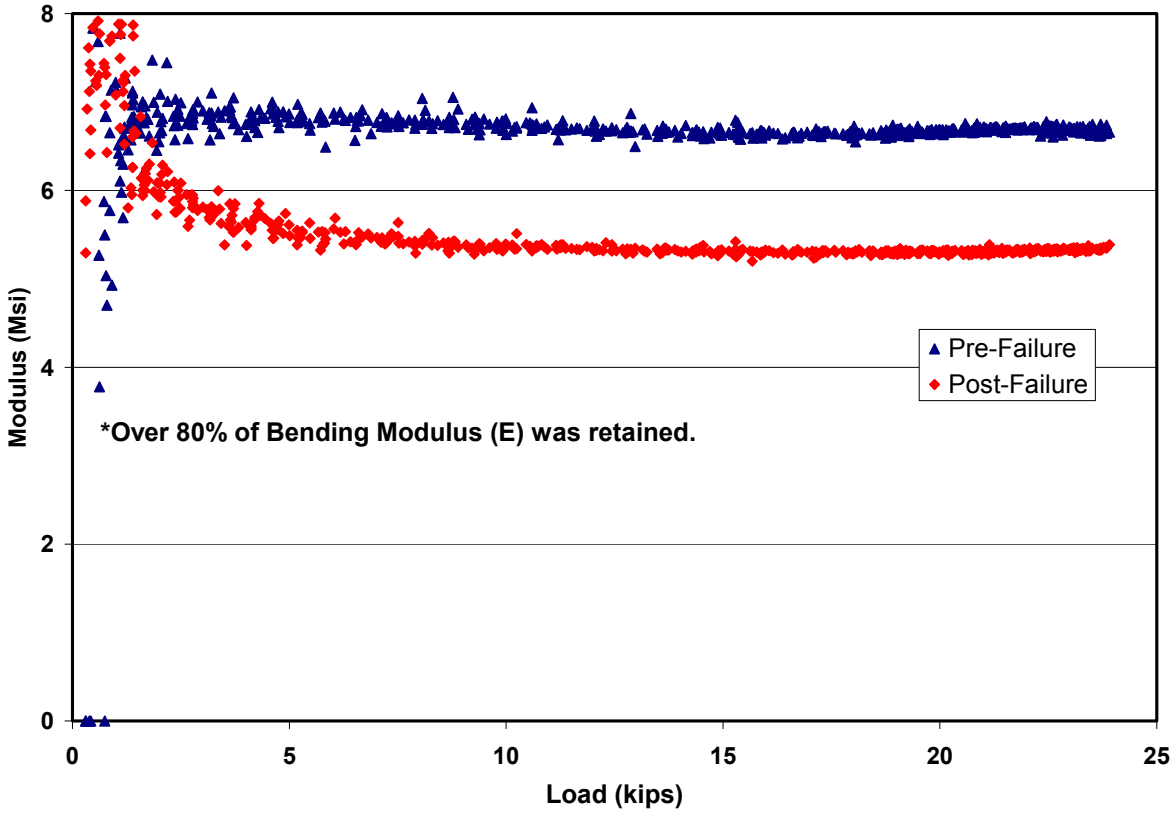

Figure 4-13. Post-failure bending modulus versus load (80% of modulus retained)

Figure 4-14. Typical delamination failure of 36 in. DWB

Figure 4-15. Bearing failure at supports for beam tested at L/d of 6

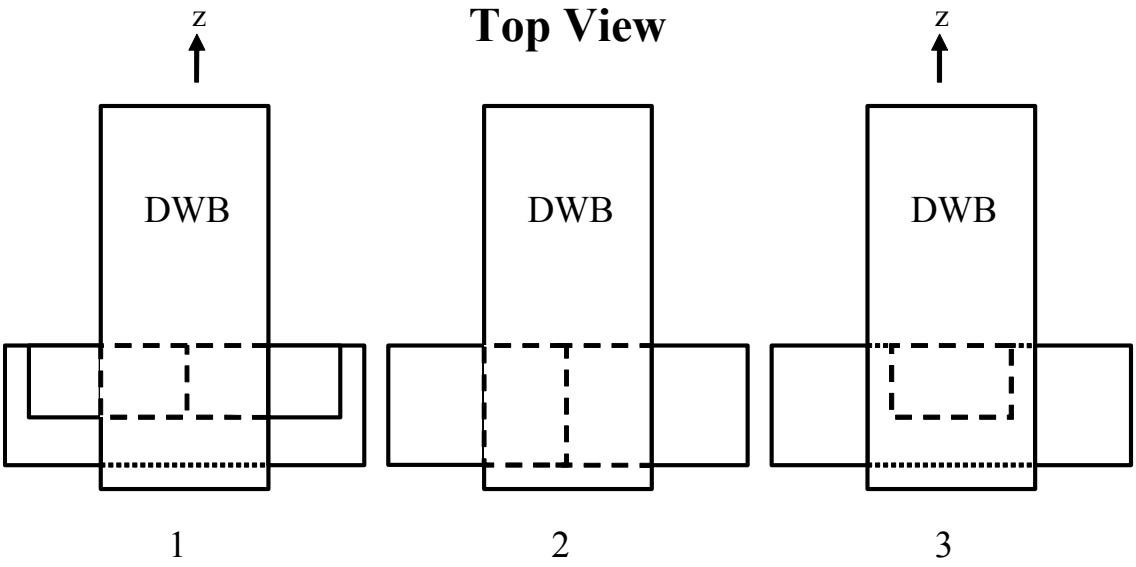

Figure 4-16. Schematic illustrating the three bearing pad orientations (BPO) used during testing

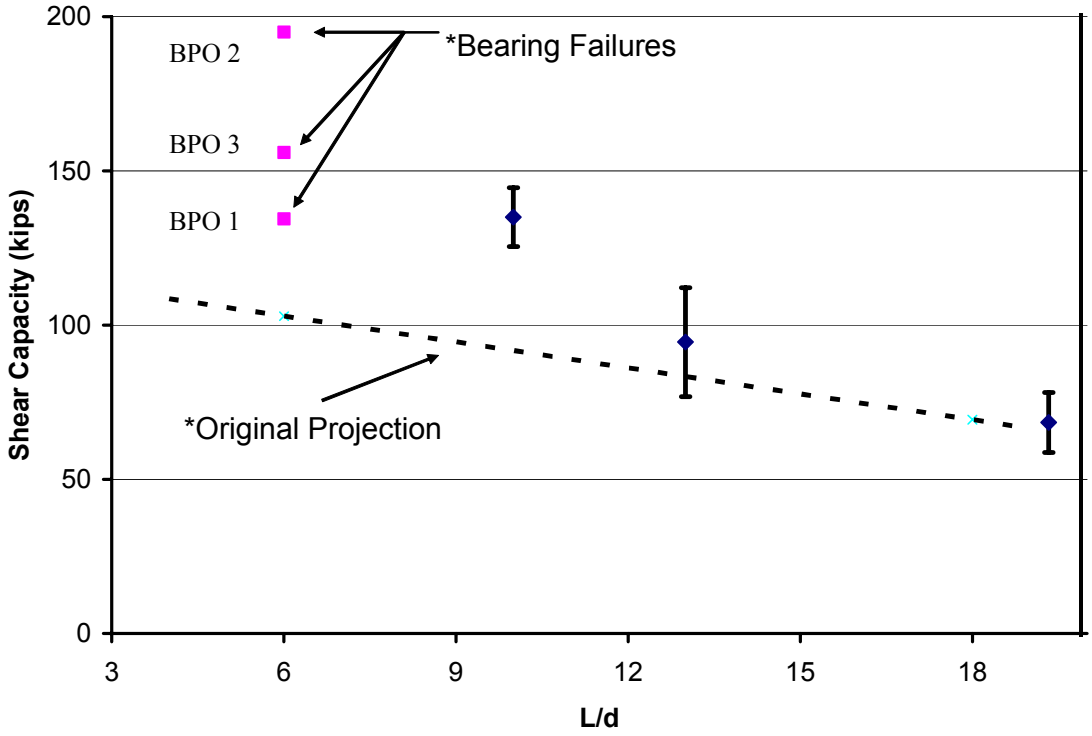

Figure 4-17. Shear Capacity versus span for the 36 in. DWB (note that beams with an L/d of 6 did not fail in shear), BPO – bearing pad orientation

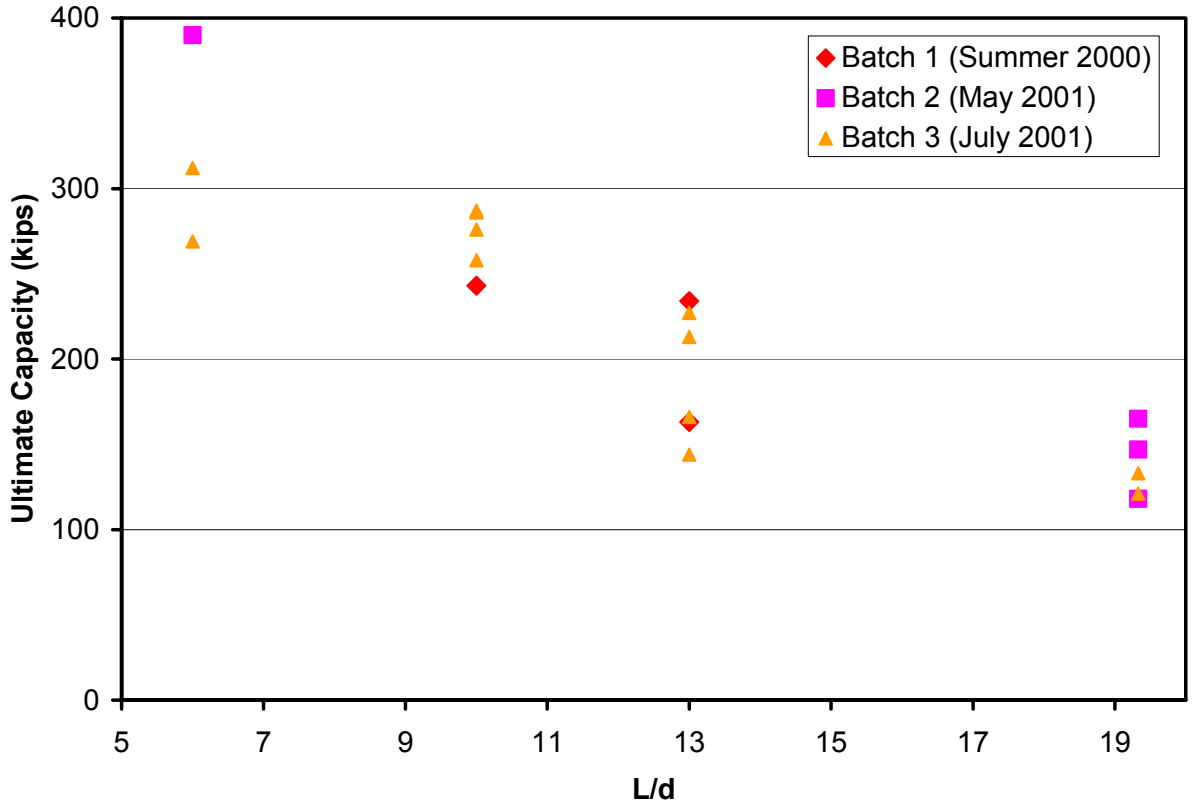

Figure 4-18. Ultimate capacity of 36 in. DWB broken down by manufacturing batch

Table 4-2. Summary of Weibull statistics data

L/d = 10	**E (Msi)**	**kGA (Msi-in²)**	**Shear Capacity (kips)**	**Moment Capacity (kip-ft)**
Mean	6.52	50.3	134.4	1344.4
Std. Dev.	0.16	8.5	11.7	116.8
A Allowable	5.95	25.5	96.4	964.0
B Allowable	6.23	35.7	113.9	1139.1
α	50.21	7.0	14.1	14.1
β	6.60	53.8	139.5	1395.0
L/d = 13	**E (Msi)**	**kGA (Msi-in²)**	**Shear Capacity (kips)**	**Moment Capacity (kip-ft)**
Mean	6.30	47.7	95.4	1275.8
Std. Dev.	0.26	7.4	21.9	293.5
A Allowable	5.43	25.9	36.8	492.8
B Allowable	5.86	35.2	59.1	790.1
α	30.98	7.7	5.0	5.0
β	6.41	50.8	103.9	1389.9
L/d = 19.33	**E (Msi)**	**kGA (Msi-in²)**	**Shear Capacity (kips)**	**Moment Capacity (kip-ft)**
Mean	6.44	45.6	68.1	1319.2
Std. Dev.	0.18	8.0	11.4	220.6
A Allowable	5.82	22.4	34.7	672.7
B Allowable	6.13	31.8	48.5	939.5
α	45.65	6.7	7.0	7.0
β	6.52	48.8	72.8	1409.9

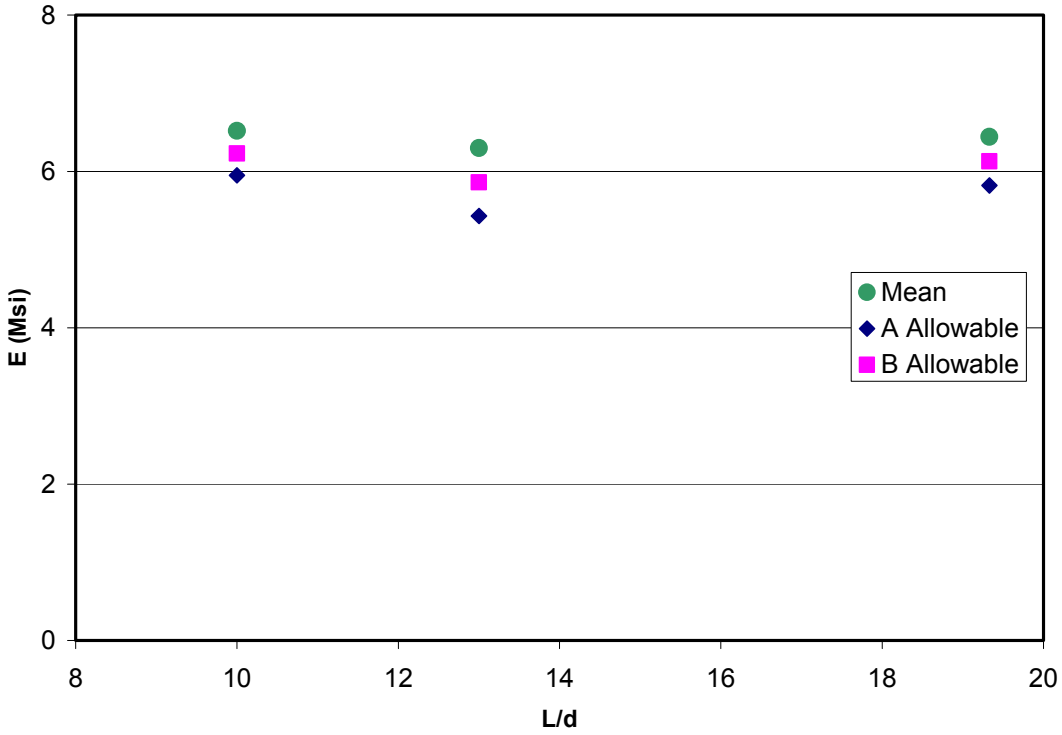

Figure 4-19. Weibull mean and A- and B-basis allowables for bending modulus

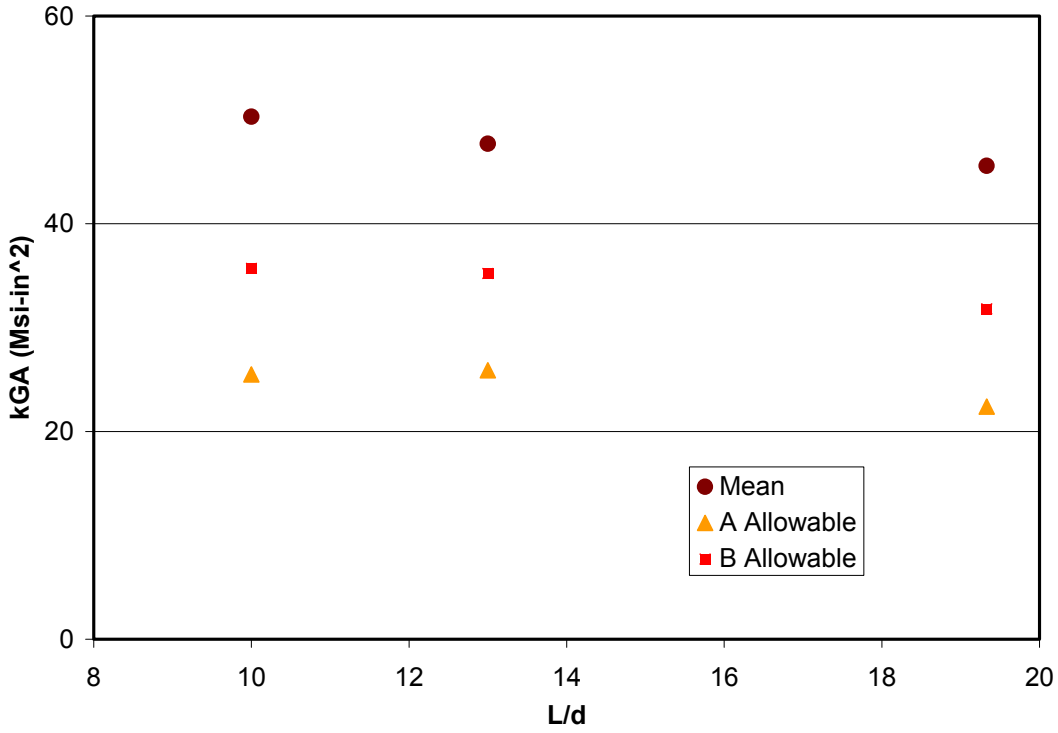

Figure 4-20. Weibull mean and A- and B-basis allowables for shear stiffness

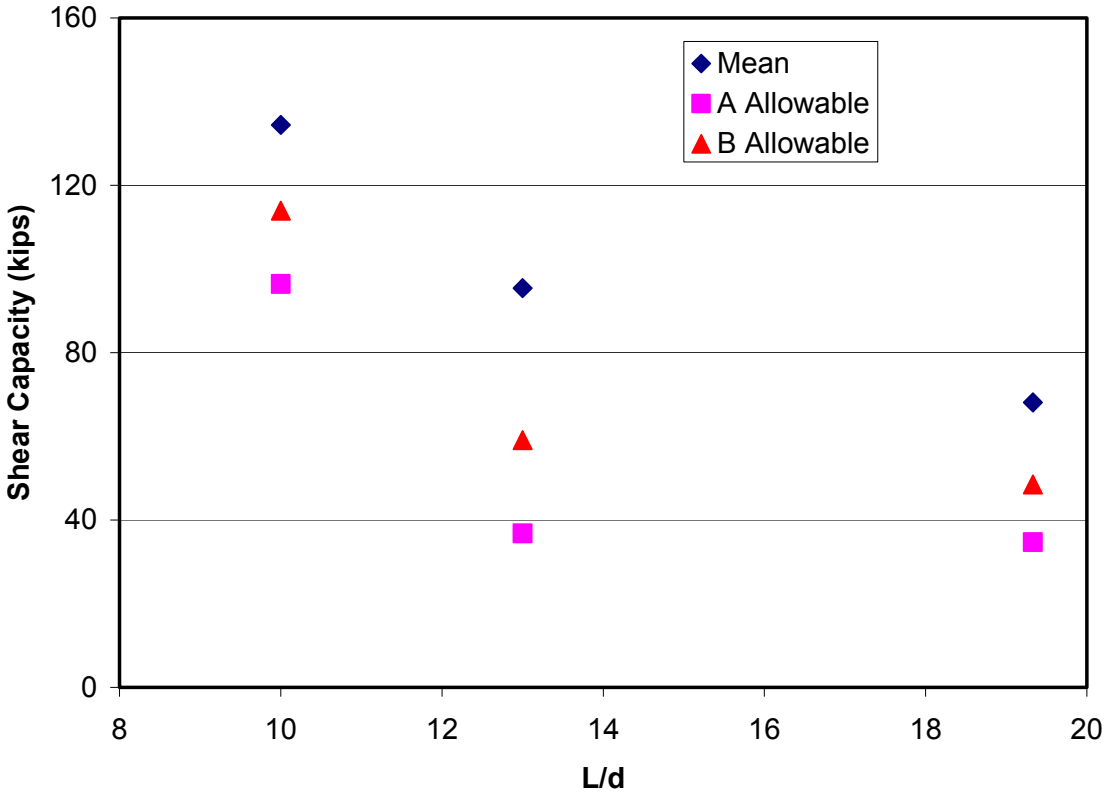

Figure 4-21. Weibull mean and A- and B-basis allowables for shear capacity

Chapter 5 Investigation of kGA in FRP Beams

5.1 Introduction and Purpose

As it was discussed in Chapter 4, the characterization of shear stiffness (kGA) in the 36 in.(914 mm) DWB can be less than straightforward. The wide range of factors that contribute to its variation have created a great deal of difficulty in accurately obtaining values from test data and have led to an increase in the uncertainty in these calculated values. Moreover, results from the testing of the 36 in. beam indicated that measured kGA values were in fact structural properties, dependent upon the test geometry and setup itself. For these reasons, it was decided to conduct a parametric investigation into the shear stiffness of FRP composite beams. It is believed and has been shown in many cases that some of the factors that significantly affect the value of and the ability to measure kGA include the method used for calculation (i.e. multi-span slope-intercept method versus calculation from deflection) deflection values and variation in deflection due to equipment sensitivities (i.e. displacement transducer and acquisition system resolution), location and delivery of load, span (e.g. selecting center-of-bearing to center-of-bearing versus clear span for the 36 in.(914 mm) DWB as discussed in Chapter 4), bearing pad orientation (boundary conditions), and material non-linearities. The purpose of this study was to determine if or how well kGA could be accurately and consistently characterized for FRP beams and attempt to examine some of the elements that lead to its variation. Additionally, this study's intent was to better describe for design engineers the effects of shear in composite structures and to better understand the test results provided in the structural design guide for the 36 in. (914 mm) DWB.

5.2 Experimental Methods

Unlike the previous chapter (36 in. (914 mm) DWB Testing Results), in this chapter all figures will be presented in SI units and tables will include both English and SI units as this data will not be published in the structural design guide.

5.2.1 Material Selection

For this study, a pultruded, 3 in. by 3 in. by ¼ in. (76 x 76 x 6 mm) wide flange (WF) composite beam was selected for testing and provided by Strongwell Corp from their family of Extren Fiberglass Structural Shapes [9]. This beam (Figure 5-1) is a more common single web structure comprised of glass fibers in a vinyl ester resin. It should be noted that two shipments of beams were received and the second batch consisted of glass fiber beams in a polyester resin. All testing was conducted before the mistake was identified. Analysis of the data revealed a less than two percent difference in both calculated E and kGA values for the two sets of beams. Reported values in the structural design guide for this beam reports the same value for both flexural and shear moduli (coupon tests). Coupon testing also determined the tensile moduli of the two materials to be only three percent different. Full section moduli of elasticity differences were found to be seven percent (determined from three-point bend tests). These reported values in the design guide are the minima obtained during testing. Due to the relatively small differences in reported values and even smaller differences in test results, the two sets of beams were treated identically for analysis purposes.

The glass fiber that reinforces the beam is a combination of glass roving and continuous strand mat (CSM). More on the actual fiber architecture is discussed in a later section. Beams in 20 ft (6.1 m) sections were provided (90 ft total (27.4 m)). The reported moment of inertia (I) is 3.17 in^4 (132 cm^4) and the weight per foot is listed as 1.69 lbs (7.5 N) [9].

In addition to the FRP beams, carbon fiber laminates were also selected for this study for reasons that are discussed in the next section. The laminates that were selected were unidirectional carbon fibers in an epoxy resin. One ply (0.007 in, 0.178 mm) and 3 ply (0.022 in, 0.559 mm) laminates were supplied in 36 in. (914 mm) wide by 72 in. (1.83 m) long sheets by

Aerospace Composite Products of San Leandro, California. The laminates were manufactured by hand lay-up and vacuum bagging of graphite/epoxy prepreg.

5.2.3 Beam Preparation

It was decided to test the WF beams at spans of similar aspect ratios to that of the 36 in. (914 mm) DWB testing described in the previous chapters. Also, in order to maximize the beams cut from the 20 ft (6.1 m) lengths provided and avoid wasting material, the beam lengths that were selected for cutting were 20 in. (51 cm), 40 in. (102 cm), and 60 in. (152 cm). The carbon laminates were then cut into 3 in. (76 mm) wide strips and cut again to the lengths of the beam segments (with the fibers running in the longitudinal direction). The laminates were then bonded to the FRP beams using epoxy adhesives (from three different manufacturers based on what was available: 1) 3M DP 420, 20 minute cure, 2) Devcon 2-Ton Epoxy, 30 minute cure, and 3) Fibre Glast System 2000 with 2060 hardener, 60 minute cure).

The surface of both the beam and laminate were sanded, roughed, and cleaned using acetone to promote good adhesion. Monofilament fishing line was used to maintain the bond thickness during application of pressure. Despite these preparations, bonding of the thin 1 ply laminates to the FRP beams was difficult. Whether it was due to the "flimsy" nature of the laminates or the lack of uniform pressure being applied, several of the 1 ply laminates were poorly bonded to the beams and the test data was unusable (they were also the first attempted so a learning curve may have played a role). Additionally, the last batch of Fibre Glast epoxy/hardener that was prepared was not mixed sufficiently and as a result did not cure sufficiently. Data for these beams was also discarded. In all, 27 beams were tested and the data for seven (six of the seven were 1 ply beams) revealed the abovementioned preparation flaws and was discarded from the final results.

5.2.4 Beam Testing

Despite the flaws present in some, 27 beams were tested in a four point bending setup to determine such characteristics as bending modulus (E) and shear stiffness (kGA), as well as to

investigate the many factors that contribute to the variability found in kGA. Nine beams at each span were tested, with three beams at each span having no carbon, three having 1 ply, and three bonded to the 3 ply laminates. The spans that were actually tested were 18, 39, and 57 in. (46, 99, 145 cm) in length, corresponding to length-to-depth ratios of 6, 13, and 19, respectively, which were equivalent to three of the four spans at which the 36 in. (914 mm) DWBs were tested. Pictures of the prepared beams can be seen in Figure 5-2 and Figure 5-3.

The load was applied at the third points by a screw-driven Instron 4206 test machine with a 30 kip (133 kN) load cell. The load was applied to the midspan of a steel spreader beam (¼ in. (6mm) thick, square steel tube), which delivered the load to 1 in. (25 mm) diameter, 4 in. (102 mm) long steel rollers located at the third points of the beam and at the end supports, resulting in boundary conditions considered to be pin-roller (the movement of one roller was always restricted). A steel I-beam was used as a base for this testing to provide the necessary test area to test the longest of the spans involved. Midspan bending strains were measured on the top and bottom flanges of the FRP beams. Midspan deflection was captured using two Linear Variable Displacement Transformers (LVDTs); one on each side of the beam. The location of the LVDTs was restricted by the Instron machine itself so an aluminum strip was clamped to the top of the bottom flange on each side of the beam (using the least amount of pressure possible so as to affect the strain profile as little as possible) in order to measure the deflection of the beam. A 16-bit acquisition system was used to record data providing clean, accurate deflection measurements calibrated beyond 1/1000 in. (0.00254 mm). Pictures of the test setup utilized can be seen in Figure 5-4, Figure 5-5, and Figure 5-6.

Similar test methods to those described in Chapter 2 for the 36 in. (914 mm) DWB were employed for the WF FRP beams in this study as well. Each beam was loaded to approximately L/180 in. (L/457 cm) of deflection and load, midspan deflection, and strain were recorded for each test. Load was applied at a rate of 0.125 in/min (3.18 mm/min) for the longer two spans and at 0.050 in/min (1.27 mm/min) for the short span. An additional plate was added to the load points and support locations to examine the effects of a load patch compared to the point-loads applied through the aforementioned rollers (Figure 5-7 and Figure 5-8). When testing with the additional plates at the load points and supports, span was again taken to be the distance between the centers-of-bearing. Additionally, a number of beams at the 60 in. (152 cm) length were tested at additional spans of 51, 45, and 39 in. (130, 114, and 99 cm) as well as the previously

mentioned 57 in. (145 cm) span for the purpose of using the multi-span slope-intercept method for determining E and kGA.

5.3 Analytical Methods

Twenty-seven WF beams were tested with the intention of determining E and kGA for each as well as exploring the factors that contribute to variations seen in the shear stiffness of the 36 in. (914 mm) DWB. Before testing began a model for the beam was generated in order to make predictions for E, kGA, and the ratio of EI to kGA. The carbon laminates that were selected were done so based on the initial predictions for EI/kGA. One of the primary objectives of this study and the basis upon which it was formed was to vary the bending stiffness of the FRP beams by bonding a stiffness enhancing material to the flanges, thus varying the aforementioned relationship between bending and shear stiffness, and examine what effect was had on the shear stiffness and shear lag. The shear lag being referred to in this case may not be the same as the traditional definition. Timoshenko shear deformable beam theory, as it was mentioned, may not be sufficient to accurately characterize kGA in FRP beams as it accounts for shear deformation in a relatively simple manner. As it was seen in the testing of the both the 8 in. (203 mm) and 36 in. (914 mm) DWBs, there is a certain distance that is required before the shear strain in the web, measured along the neutral axis, reaches a constant value. This phenomenon is what is being referred to as shear lag. The distribution of shear stress in the beam web that is assumed by Timoshenko along with an illustration similar to what testing has revealed to occur in the FRP beams may be seen in Figure 5-10.

5.3.1 Wide Flange Beam Model and Predictions

Before testing began, a model of the WF beams was developed. Using a schematic of the pultrusion thread-up provided by Strongwell Corp a lay up was devised. The specific lay-up (or thread-up) is proprietary, but the resulting model consisted of lamina comprised of various quantities of glass roving and CSM. Once a representative lay-up was generated for both the

web and flanges, the constituent material properties and lay-up were input to Classical Laminate Theory (CLT) and Mechanics of Laminated Beam (MLB) theory as formulated by Barbero, et al [22]. These theories were used to predict bending modulus (E), shear modulus (G), and moment of inertia (I) for the structure as well as the in-plane longitudinal and in-plane transverse moduli, in-plane shear modulus, and in-plane Poisson's (ν) ratios for both the web and flange panels. The model was first developed for the WF beam alone and then adjusted for the addition of the carbon laminates.

The resulting predictions for in-plane moduli and Poisson's ratios were then used to predict the shear correction factor (k) for each beam configuration (i.e. no carbon beams, 1 ply beams, and 3 ply beams) following the method developed by Cowper [14] and applied to thin-walled composite beams by Bank [15]. The equations resulting from the derivation of Timoshenko beam theory equations from three-dimensional elasticity [14] and then extended to thin walled composite beams for the shear coefficient [15] are given below. Refer to Figure 5-10 for an explanation of the geometry for the cross-section of the I-beam.

$$k^* = 20(\alpha + 3m)^2/[(E1/G1)(60m^2n^2 + 60\alpha mn^2) + (E1/G2)(180m^3 + 300\alpha m^2 + 144\alpha^2 m + 24\alpha^3) + \nu1(60m^2n^2 + 40\alpha mn^2) + \nu2(30m^2 + 6\alpha m + 4\alpha^2)] \quad (5\text{-}1)$$

where $n = b/h$, $m = 2bt_f / ht_w$, $\alpha = E1/E2$.

Additionally,

$$k = \frac{k^* E}{G} \quad (5\text{-}2)$$

In the above equations, k* refers to the modified shear coefficient, E1, E2, G1, G2, $\nu1$, and $\nu2$ are the aforementioned predicted panel properties. In Equation 5-2, E and G are the bending and shear moduli, respectively.

5.3.3 Beam Modulus and Stiffness Determination

Each of the 27 beams was tested with the primary intent of calculating bending modulus and shear stiffness. For the determination of E and kGA, the same procedure was used as for the 36 in. (914 mm) DWB (i.e. derivation of Timoshenko beam theory equations for four-point bending with loads applied at the third points to determine kGA, calculation directly from measured strain and deflection data). The derived Timoshenko beam theory equation used to determine kGA can be seen below.

$$kGA = -\frac{24EIP(a-L)}{24\Delta_{m.s.}EI + P(-4a^3 + 12a^2L - 9aL^2 + L^3)} \tag{5-3}$$

The above equation is valid for a general case of four-point loading, where "a" again is the distance from beam support to the load point (L/3 in this case) and L is the beam span.

Reported values of E and kGA were obtained in a similar manner to that explained for the 36 in. (914 mm) (refer to Chapter 3). The only exception being the actual deflection limits that made up the selection range. For the WF beam properties, E and kGA were computed from the average of ten evenly spaced points between and including the values at the L/180 in. (L/457 cm) and L/390 in. (L/991 cm) deflection criteria.

In addition to calculating E and kGA directly from strain and deflection data an additional technique was used to determine to the two properties. The second technique (attempted for six of the nine 60 in. (152 cm) girders) involved using a multi-span slope-intercept method. For this method, Equation (3-5) (or Equation (3-2) for a three-point bending case) is divided through by PL^3 and $\Delta_{m.s.}/PL^3$ is plotted versus $1/L^2$ for each span length (Equation (5-4)).

$$\frac{\Delta_{m.s.}}{PL^3} = \frac{23}{648EI} + \left(\frac{1}{3kGA}\right)\frac{1}{L^2} \tag{5-4}$$

The resulting line (of the form $y = mx + b$, with $y = \frac{\Delta_{m.s.}}{PL^3}$ and $x = \frac{1}{L^2}$) has a slope related to the shear stiffness ($m = \frac{1}{3kGA}$) and a y-intercept related to the bending stiffness ($b = \frac{23}{648EI}$). Solving for E and kGA gives the equations below:

$$E = \frac{23}{648Ib} \qquad kGA = \frac{1}{3m} \qquad (5\text{-}5)$$

The value of $\frac{\Delta_{m.s.}}{PL^3}$ was obtained from the slope of the load-deflection plot for each beam test and multiplying this value by $\frac{1}{L^3}$.

5.4 Experimental Results and Discussion

As it has been stated, mechanical properties for 27 WF composite beams with no plies, 1 ply, or 3 plies of unidirectional carbon fiber lamina bonded to the flanges were determined in an attempt to further investigate the characteristics of shear stiffness in FRP beams. The parameters that were purposely varied in this study to investigate their effect on kGA were the ratio of EI to kGA, span, boundary conditions, and test method. Also, somewhat unintentionally the resolution of the acquisition system was varied when the initial system proved to have too poor of resolution and the switch was made to a 16-bit system (the 16-bit system was only not used initially because it was not operational when testing began). This change turned out to be for the best as it was another significant parameter varied in the study.

5.4.1 Results of Modeling and Predictions

As it was discussed, CLT and MLB theory were used to develop predictions for the WF beams in this study. It was of interest to see how accurately predictions for bending and shear

moduli as well as for the shear correction factor could be made starting with a thread-up and then devising an effective lay-up. The predictions made for E, G, I, and k can be seen in Table 5-1, as well as the resulting prediction for EI/kGA. The moment of inertia predicted for the geometry containing no carbon plies appears to agree quite well with the reported value of 3.17 in^4 (132 cm^4) from the structural design guide. And both bending and shear moduli are considerably larger than the minimum reported values [9]. The shear correction factor reported in literature for an I-beam with a cross-sectional aspect ratio of one was 0.29 (note that the mechanical properties used to predict k are not known for this case) [15].

5.4.2 Test Results

The bending modulus and shear stiffness for the three beam types were determined using both a direct method and the multi-span slope-intercept method. A typical plot of load versus midspan deflection can be seen in Figure 5-11; a typical load versus average midspan bending strains in Figure 5-12; and a typical plot of E and kGA versus load for a 57 in. (1.45 m) span is shown in Figure 5-13. It is quite apparent from the plots the clean, noise-free, almost contrived appearance of the data relative to that seen previously for the testing of the 36 in. (914 mm) DWB. This is a direct result of the use of the 16-bit data acquisition system. To further illustrate this factor, plots of E and kGA versus load can be seen for a beam tested by both systems in Figure 5-14 and Figure 5-15. The data obtained for the 12-bit system (Figure 5-15) had a lower sampling rate in an attempt to eliminate some noise, but even so the comparison between the two systems shows the benefits of the higher resolution system (Figure 5-14 versus Figure 5-15).

Bending modulus and shear stiffness were calculated for each test for each beam. The values for both properties were selected for each test between two set deflection points, as described above. The results for each test were then averaged over the course of two tests and confirmed visually by a third (i.e. the data for a third test was scanned to confirm the values of E and kGA, but not used to calculate the averages). The results of the calculated values of E and kGA from the direct method are summarized in Table 5-2. The calculated values for E and kGA for each beam can be seen in Table 5-3. A plot of the ratio of EI/kGA versus span can be seen in Figure 5-16 and the relationship between the average kGA and span is illustrated in Figure 5-17.

A table showing the average, minimum, maximum, and standard deviation for the selection of E and kGA within the set deflection range for each individual test used to calculate both properties can be seen in Appendix C. The average difference between individual test values for both E and kGA was less than 1%, for most cases considerable less.

In an attempt to separate the shear modulus from kGA, the predictions for the shear correction factor were used to back out G from the experimentally determined values of kGA. The results of these calculations are presented in Table 5-4. The area (A_v) used to separate G from the measured shear stiffness is the shear area of the beam, considered to be the area of the web along with the area of the flange directly above the web, including the additional thickness created by the addition of the carbon plies. A number of things can be seen from the table. First of all, the values are significantly higher than the predicted value of G (40 to 180% higher). Also, the value definitely varies with span and somewhat with the addition of the unidirectional carbon plies. If in fact what was being calculated was a material property, as shear modulus should be, span should not affect the value, but a definite variation with span can be seen. The addition of the carbon plies should also have little effect on G since it is primarily a function of the web.

5.4.3 Parameter Variation Effects on kGA

To summarize, the bending stiffness of the beams was varied by adhering the carbon fiber laminates to the flanges. The multi-span slope-intercept method for determining E and kGA was attempted and compared to the method of direct calculation from strain and deflection data. Boundary conditions were changed from the elastomeric bearing pads used for the DWB testing to the elimination of those pads and by testing beams with both rollers and additional plates at all four reaction points. The quality and accuracy of deflection data was varied by use of two different acquisition systems. And finally, the effect of span was examined not only by testing beams at three different spans, but also by testing each of the 60 in. (152 cm) beams at multiple spans.

The first parameter that was varied was the ratio of EI/kGA with the addition of the carbon laminates. An examination of the data (refer to Table 5-2, Table 5-3, and Figure 5-16)

shows that this parameter does appear to have a significant effect on the measured shear stiffness, which was not expected since shear stiffness is thought to be a web dominated property. There was a 7 to 26% increase in the shear stiffness, depending on the span, with the application of the 3-ply laminates (refer to Table 5-2). Just taking the long span, approximately 20 of the 26% (i.e. 80% of the actual difference) difference may be accounted for by the differences in k and A_v. The remaining difference can not be completely accounted for at this time (some may of course be due to experimental error). The distribution of shear strain in the webs along the neutral axis (Figure 5-18) shows a similar distribution for both cases, but does not contain enough data points to be completely certain (i.e. additional shear strain measurements are needed in the spaces between those already measured to ensure the distributions are in fact the same) . In Figure 5-19, the percentage of total deflection due to shear deformation versus span can be seen. It is difficult to see in the figure, but the curves for the 1-ply and 3-ply beams are virtually identical. The curves were generated using the Timoshenko beam theory equation for deflection, the average calculated E for each beam, and the kGA that was used was calculated using the same shear modulus (the average of the values that were calculated despite the variation, refer to Table 5-4) for each, the calculated A_v, and the predicted values for k. The reason for the nearly indistinguishable curves for the 1 ply and 3 ply beams can be seen in the ratios of EI/kGA being virtually identical. As the figure illustrates, there is a slight difference between the percent of total deflection due to the shear contribution that may also contribute to the aforementioned variation in kGA between the two beam types.

The use of the multi-span slope-intercept method (Figure 5-21) to determine E and kGA proved to be completely ineffective, assuming that values obtained from the previous method are accurate. The results (Table 5-5) completely disagreed with what was obtained calculating E and kGA directly from strain and deflection data as can be seen from Table 5-6 showing the percent difference between results of the two methods. The huge discrepancies are currently unexplained.

The effect of altering boundary conditions was examined by changing from point loading to a distributed load plate in six different cases. The results of the variation of this parameter are somewhat inconclusive. Both E and kGA did change in every case (the largest change was a 13% change in kGA, all other variations were less than 10%), but this is most likely also a factor of changing the span somewhat and the introduction of additional experimental error (due to the

use of two plates, instead of simply rotating a single plate/roller combination 180° so that the plate contacted the beam, creating *considerable* alignment difficulties). The center-of-bearing to center-of-bearing span remained the same, but the clear span did change. The basis for the belief that the variation was due more to span issues than kGA was also supported by the fact that the ratio of EI/kGA in each case varied by only about 1.5 to 5%, with the exception of the one test involving the largest change in kGA, which had an 11% difference in the ratio of EI/kGA. Again, insufficient data is available to draw firm conclusions. It may be interesting to note that although once again there may not be enough data points to conclude with complete certainty, it appears that the addition of the plates did not change the distribution of shear strain in the web (Figure 5-20).

The ability to calibrate deflection accurately beyond $1/1000^{th}$ of an inch ($1/4^{th}$ of a millimeter) proved to be a definite advantage. The clean, noise-free nature of the deflection data provided smooth curves for kGA versus load leading to far less difficulty in accurately selecting a representative value. Additionally, the testing of the 36 in. (914 mm) DWB required that the deflection of the bearing pads be subtracted from the midspan deflection of the beam to provide a net deflection for the structure. This introduced an additional source of error since the noise and variation of two devices were then involved in the deflection data. This allowed the variation associated with the two devices to propagate into the calculations for kGA. This testing had no such problem due to the use of the steel rollers. The higher resolution data measured in this study also allowed for the investigation of the other varied parameters without the fear that any and all variation in kGA was due to erroneous measured deflections.

The final parameter that was purposely altered was the test span. Due to the possibility of shear lag effects, it was hypothesized that the span at which each beam was tested may have an affect on the measured value of shear stiffness. At shorter spans, the shear lag effect becomes amplified due to the larger portion of total beam deformation being attributed to shear. Referring to Figure 5-19, it can be seen that for these WF beams (according to Timoshenko beam theory) shear deformation contributes over half of the total beam deflection for beams with small L/d ratios. Testing six of the 60 in. (152 cm) FRP beams at multiple spans (length-to-depth ratios of 13, 15, 17, and 19), confirmed that span does in fact play a large role in the calculation of kGA, as can be seen in Figure 5-22 for no carbon beams and summarized in Table 5-7. An increase of 50% was typical moving from the longest to the shortest span where the contribution of shear

deformation ranges from only 13 to 25%, respectively. Moving to shorter spans the contribution of shear will continue to increase and amplify this shear lag effect. This may also be seen in the overall test data (Table 5-3), as kGA as much as doubles moving from the longest to the shortest span.

A brief summary of the variation of the aforementioned parameters and the results in each case can be seen in Table 5-8. It seems that this study has generated as many new questions as it has provided answers for previous ones. Firm conclusions are difficult to draw in many cases since many factors are still unclear. One point that this testing does seem to indicate is that the shear stiffness being measured in this type of testing of FRP beams is a structural property, not a material property. Beam theory assumes that shear stiffness is a material property, but a material property would not vary significantly with span or test setup as kGA does in this case. A structural property, on the other hand, is a function of the test setup (i.e. span, loading, boundary conditions, etc.). The shear stiffness values obtained were shown to be characteristic of the test setup. This must be considered for the proper design and use of structural composite beams, as the values determined for kGA are only representative under the same loading conditions and test geometries from which they were obtained.

5.5 Tables and Figures

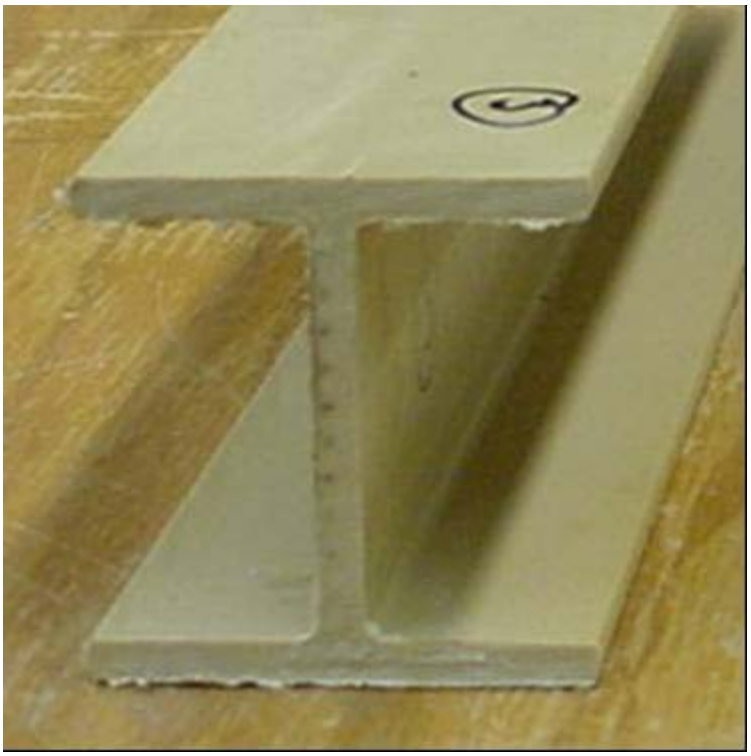

Figure 5-1. Wide flange glass FRP beam

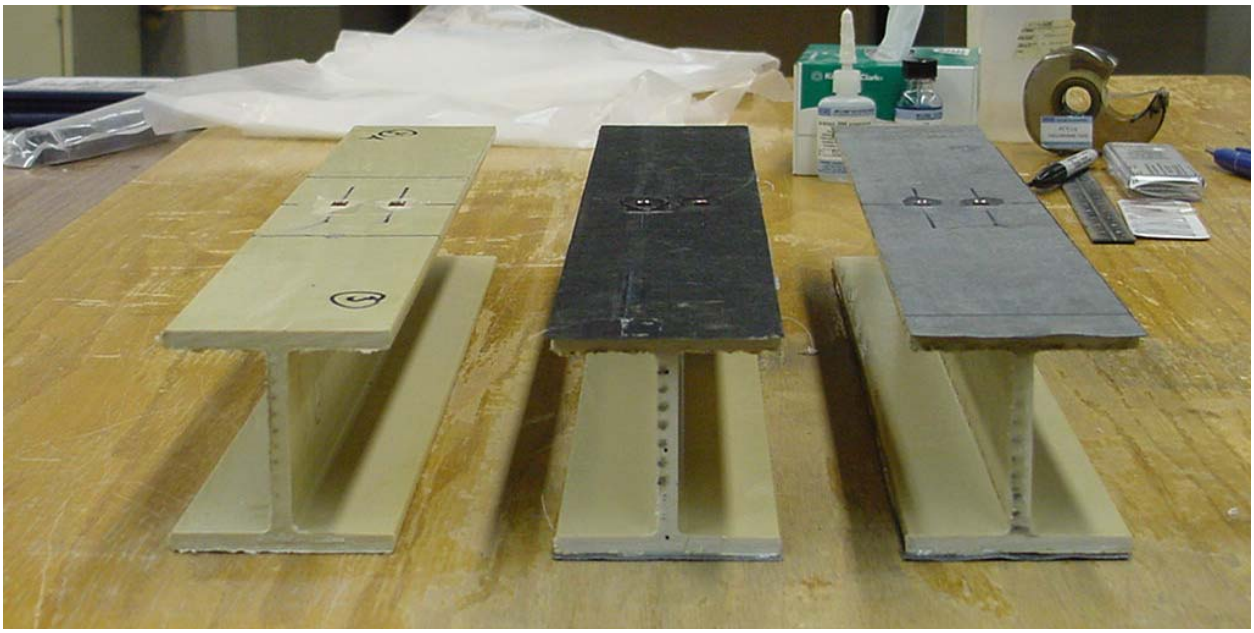

Figure 5-2. WF beams with 0-, 1-, and 3-plies of unidirectional carbon bonded to flanges

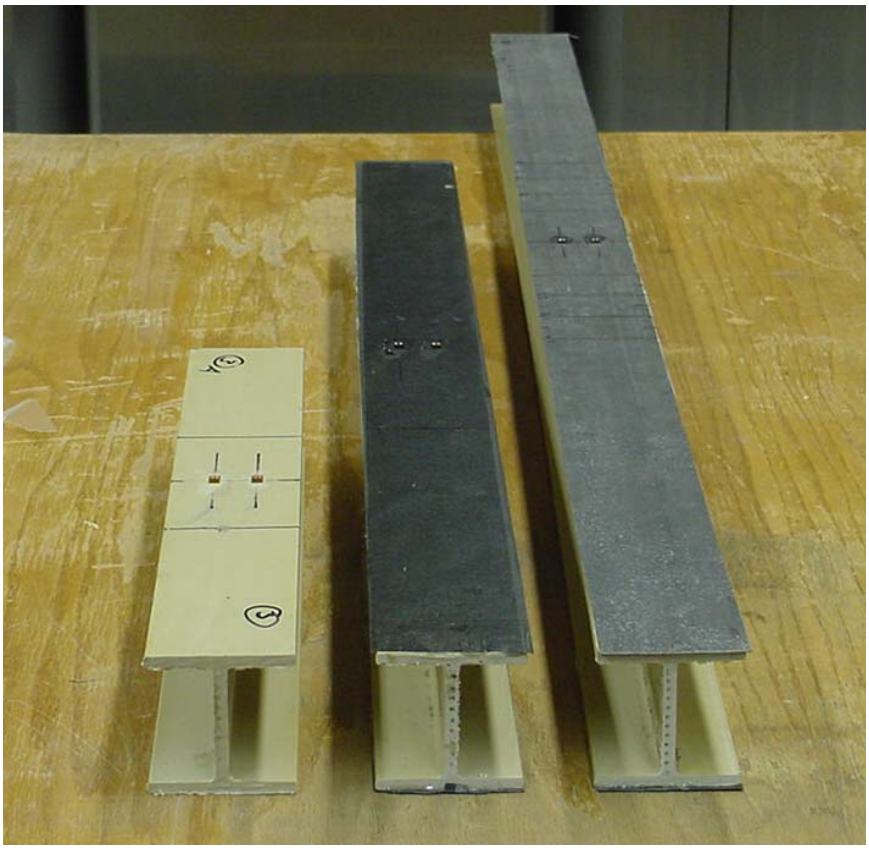

Figure 5-3. WF beams shown in three spans tested (L/d of 6, 13, and 19)

Figure 5-4. Four-point bending test setup for WF beams

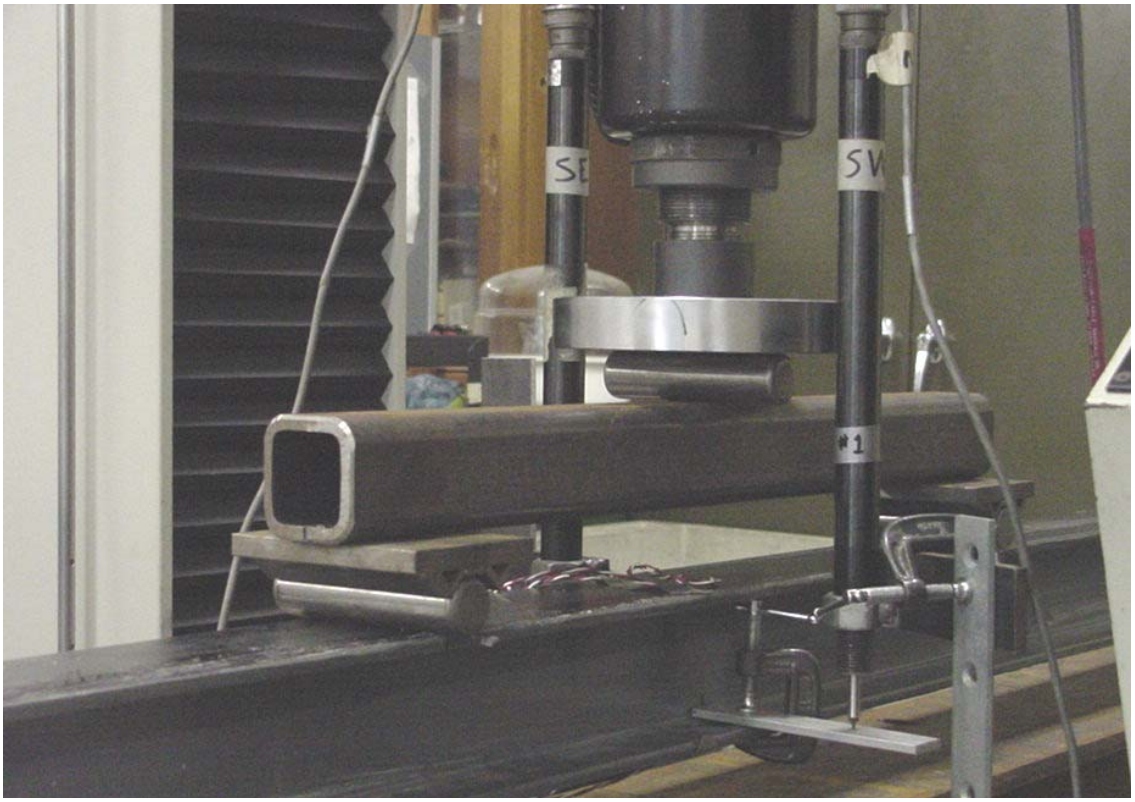

Figure 5-5. Close-up of four-point bend test setup

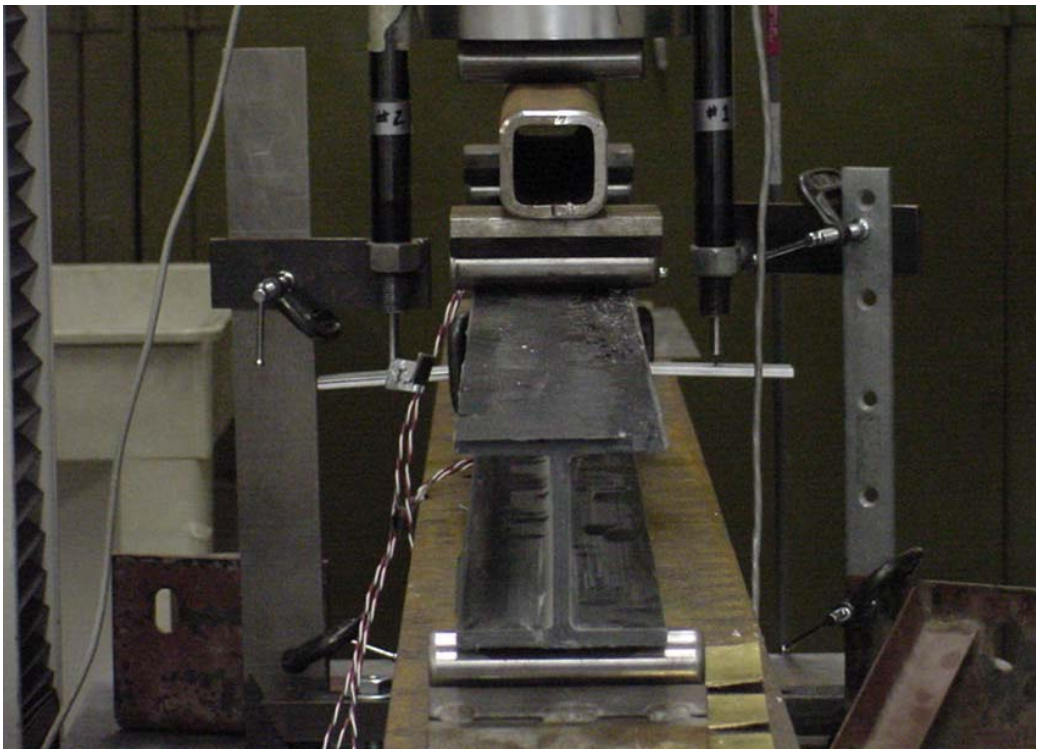

Figure 5-6. End view of four-point bend test setup

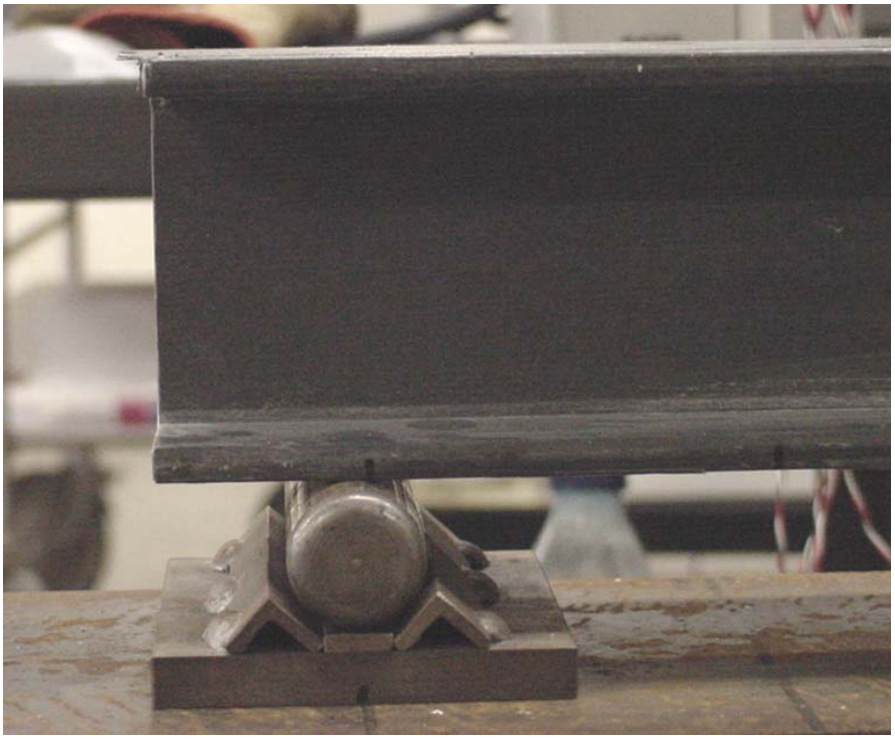

Figure 5-7. Steel end support roller utilized for four-point bend setup

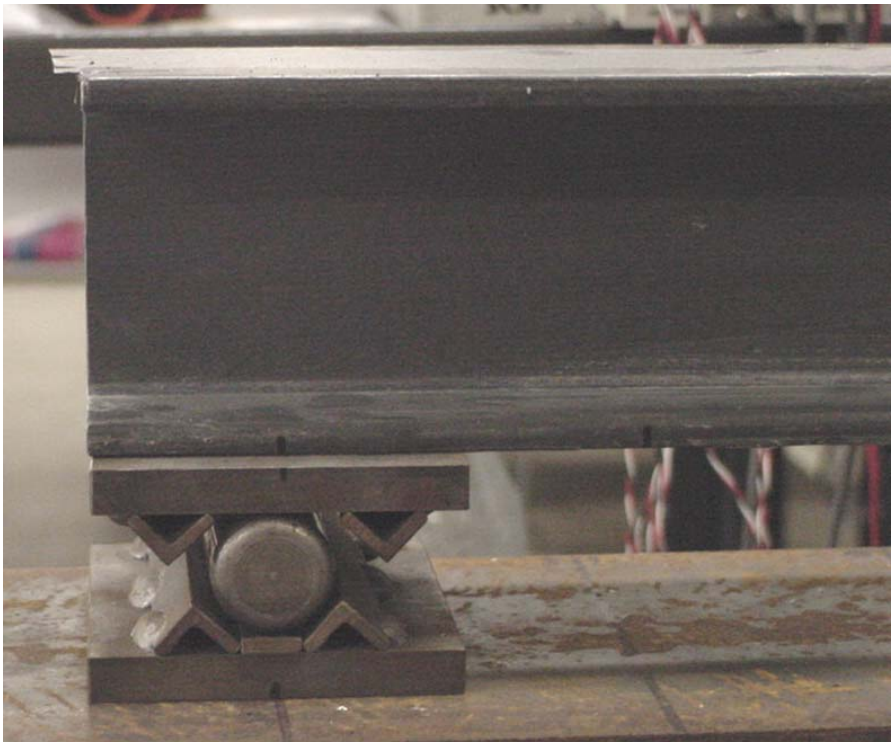

Figure 5-8. Steel end support roller with top plate utilized for four-point bend setup

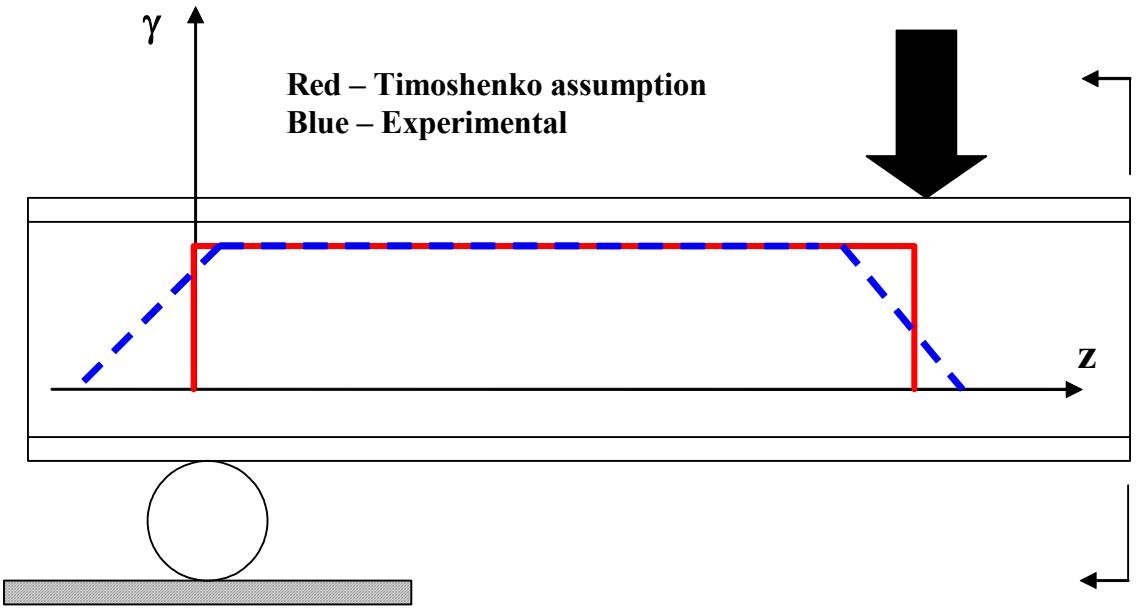

Figure 5-9. Illustration of the differences between the theoretical and experimental shear distributions in the web of an FRP beam

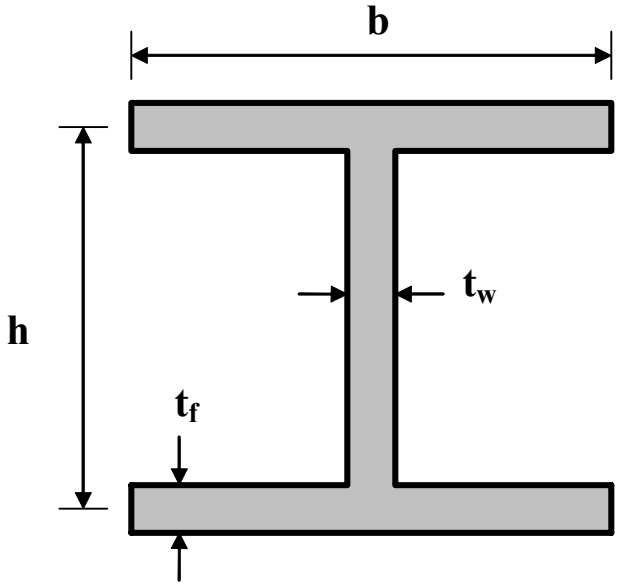

Figure 5-10. Cross-sectional geometry of a WF beam used to determine shear correction factor

Table 5-1. Summary of predicted values for E, G, I, and k of WF section

	E		G		I		k	EI/kGA
	Msi	GPa	ksi	GPa	in^4	cm^4		
0 Plies	3.32	22.9	605	4175	3.169	131.9	0.273	102.0
1-Ply	3.76	25.9	605	4175	3.249	135.2	0.278	115.4
3-Plies	4.62	31.9	605	4175	3.421	142.4	0.287	119.7

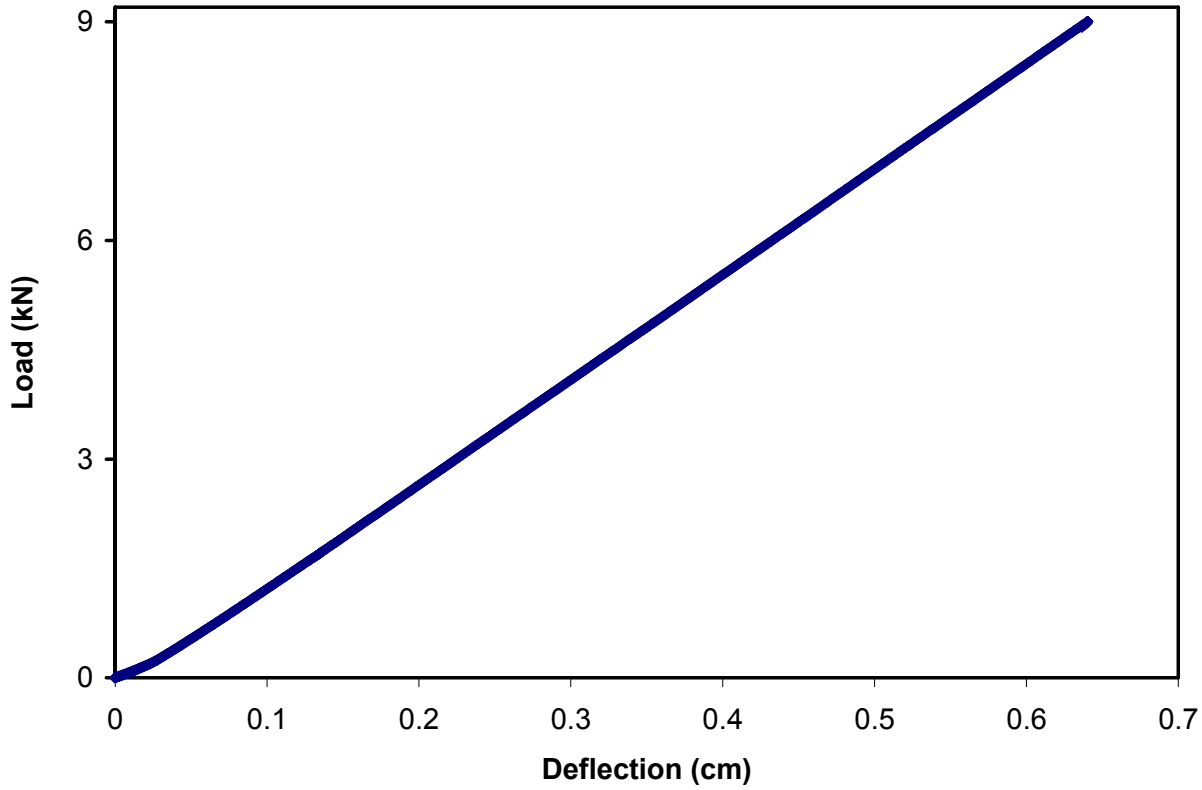

Figure 5-11. Typical load versus deflection plot for four-point testing of WF section

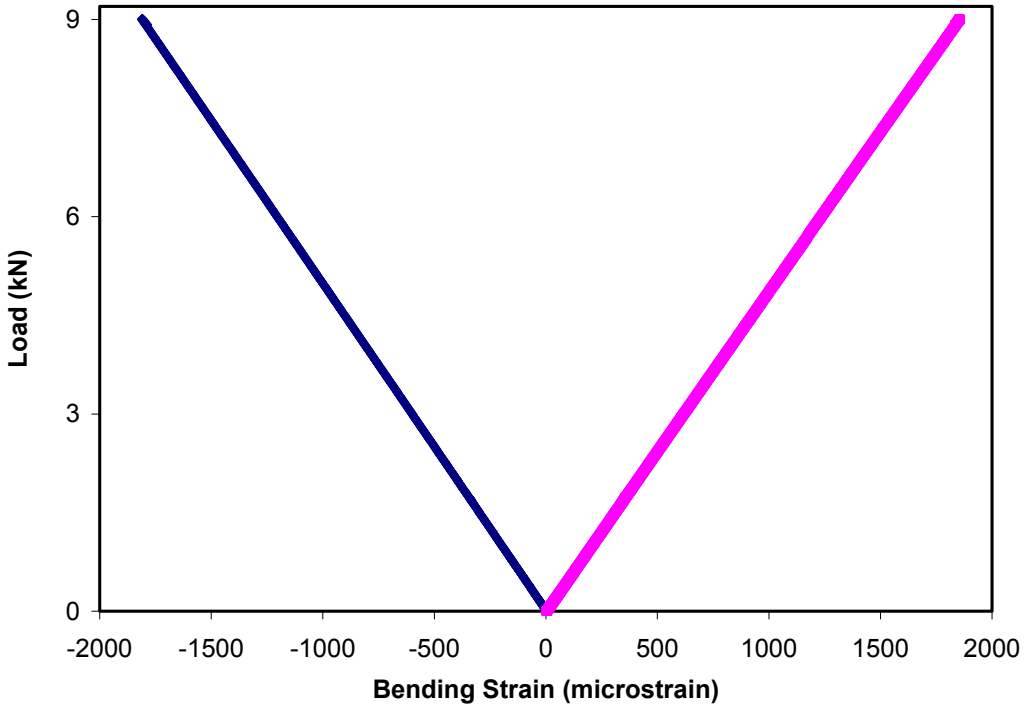

Figure 5-12. Typical load versus top and bottom flange midspan bending strains

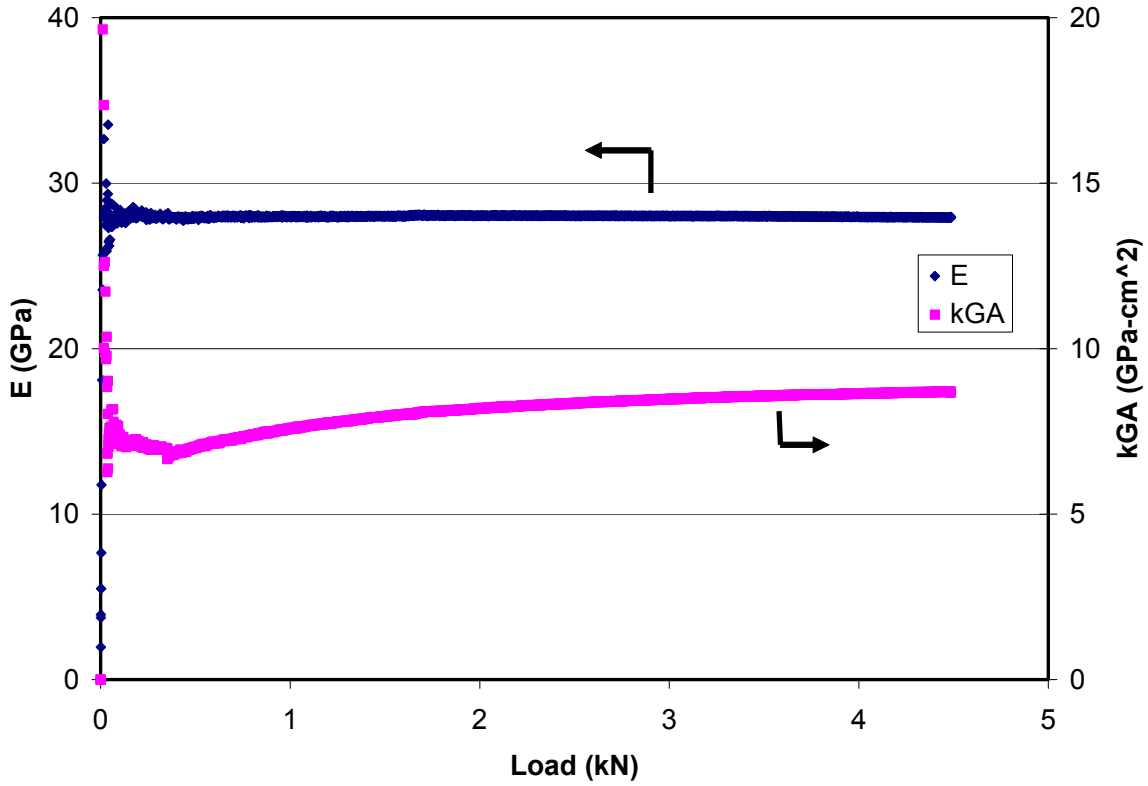

Figure 5-13. Typical plot of bending modulus and shear stiffness versus load

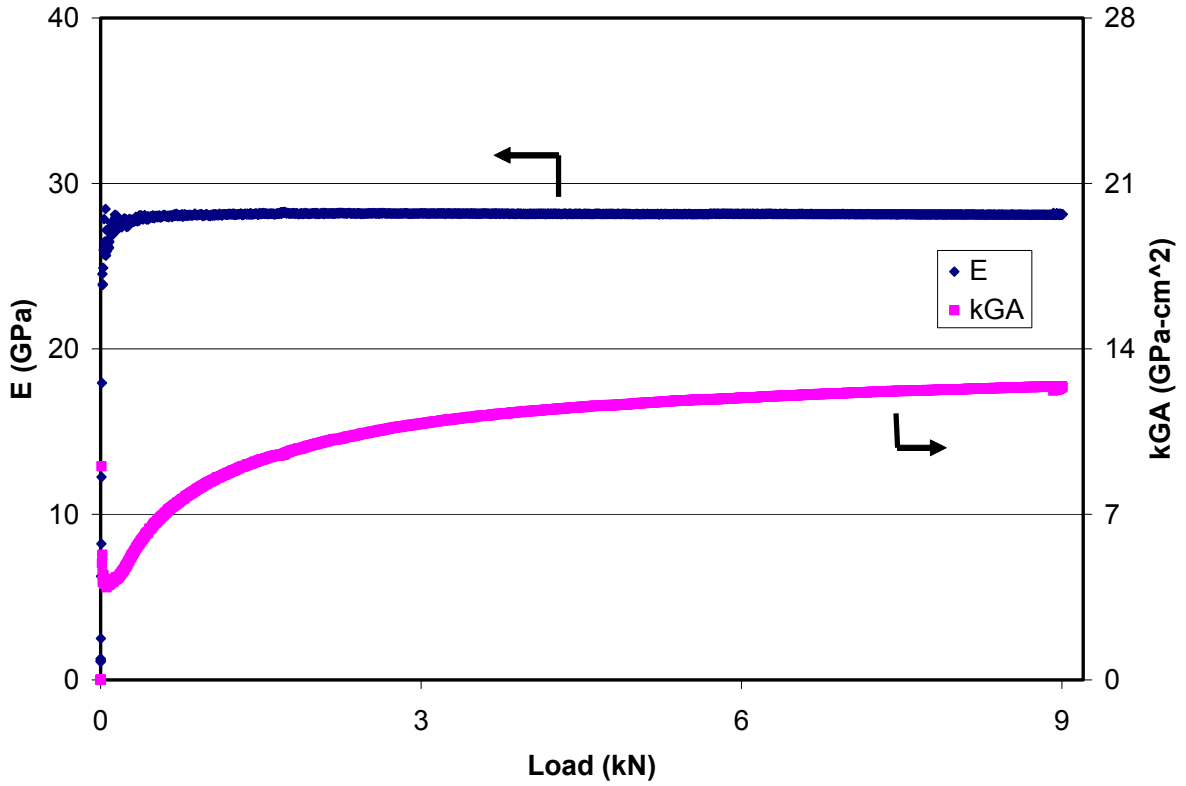

Figure 5-14. Plot of bending modulus and shear stiffness from 16-bit acquisition system data

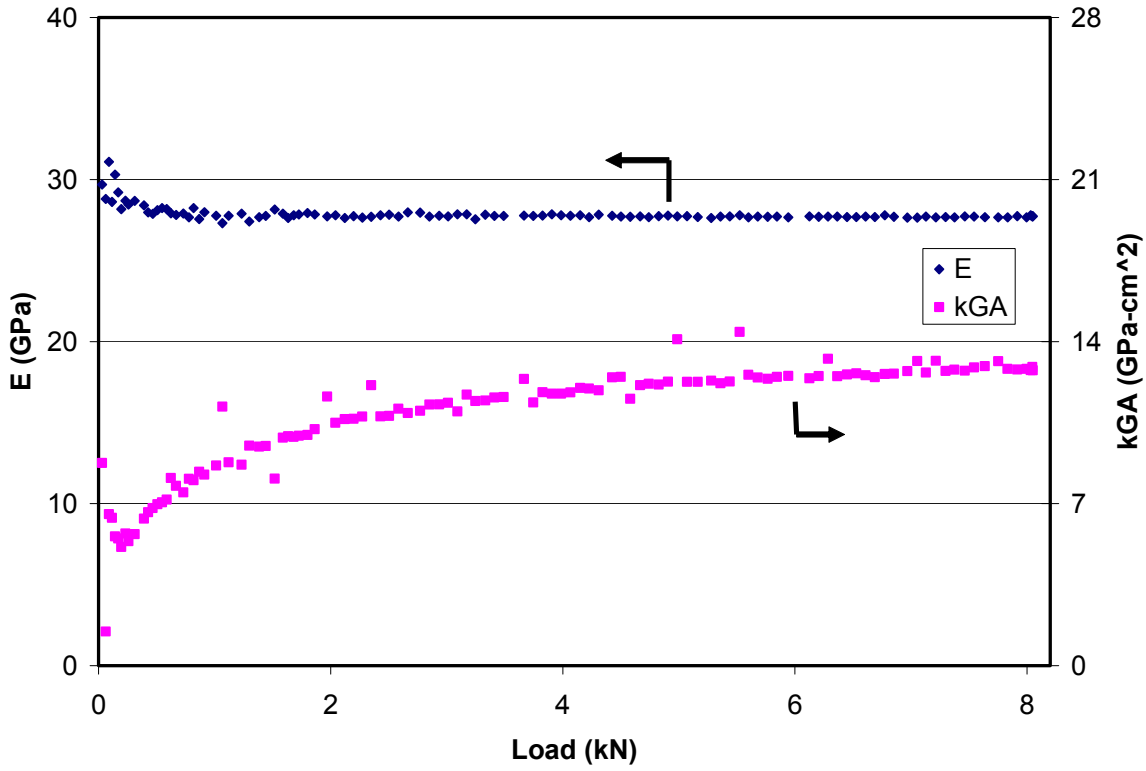

Figure 5-15. Same beam as shown in Figure 5-14 tested using 12-bit acquisition system

Table 5-2. Summary of average E and kGA for each span for WF beam testing. Note that the case where the Coefficient of Variation is zero occurred when the two beams tested had identical calculated values for kGA.

L/d	C-Plies	E_{avg}		C.O.V.	kGA_{avg}		C.O.V.	EI/kGA
		Msi	GPa	%	ksi-in²	GPa-cm²	%	
6	0	4.13	28.48	3.31	346	15.4	1.26	37.81
13	0	4.07	28.06	0.51	260	11.6	1.02	49.65
19	0	4.09	28.20	1.22	176	7.8	4.26	73.62
13	1	4.45	30.68	3.02	308	13.7	0	46.89
19	1	4.36	30.06	-	232	10.3	-	61.07
6	3	5.18	35.72	1.58	371	16.5	11.99	42.96
13	3	4.99	34.41	1.50	350	15.6	2.33	48.80
19	3	5.06	34.89	1.82	239	10.6	3.55	72.43

Table 5-3. Individual beam results for E and kGA

C Plies	L/d	E (Msi)	E (GPa)	kGA (ksi-in^2)	kGA (GPa-cm²)	EI/kGA
0	6	4.22	29.1	341	15.2	39.22
0	6	4.19	28.9	349	15.5	38.05
0	6	3.97	27.4	348	15.5	36.16
3	6	5.16	35.6	421	18.7	38.84
3	6	5.27	36.3	358	15.9	46.65
3	6	5.11	35.2	335	14.9	48.34
0	13	4.09	28.2	263	11.7	49.29
0	13	4.08	28.1	258	11.5	50.12
0	13	4.05	27.9	259	11.5	49.56
1	13	4.54	31.3	308	13.7	46.72
1	13	4.35	30.0	308	13.7	44.76
3	13	5.06	34.9	359	16.0	44.67
3	13	4.91	33.9	344	15.3	45.24
3	13	4.99	34.4	346	15.4	45.71
0	19	4.04	27.9	184	8.2	69.59
0	19	4.09	28.2	176	7.8	73.65
0	19	4.14	28.5	169	7.5	77.64
1	19	4.36	30.1	232	10.3	59.56
3	19	5.12	35.3	233	10.4	69.64
3	19	4.99	34.4	245	10.9	64.55

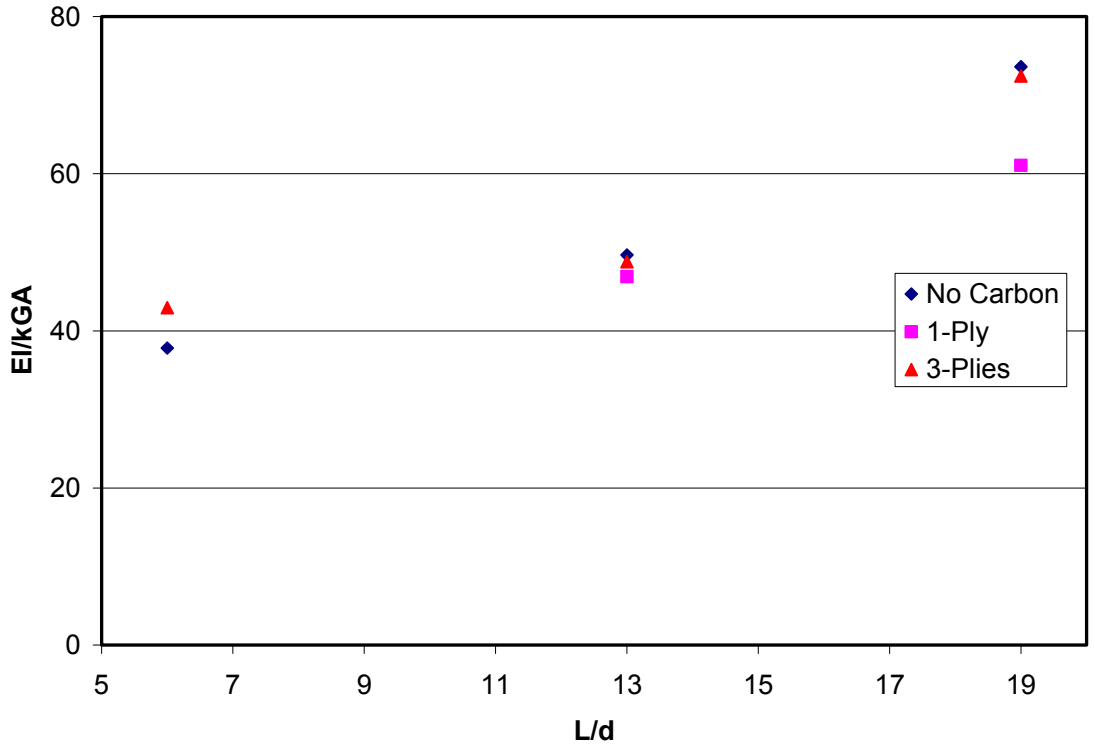

Figure 5-16. Ratio of EI/kGA versus span for all three beam types

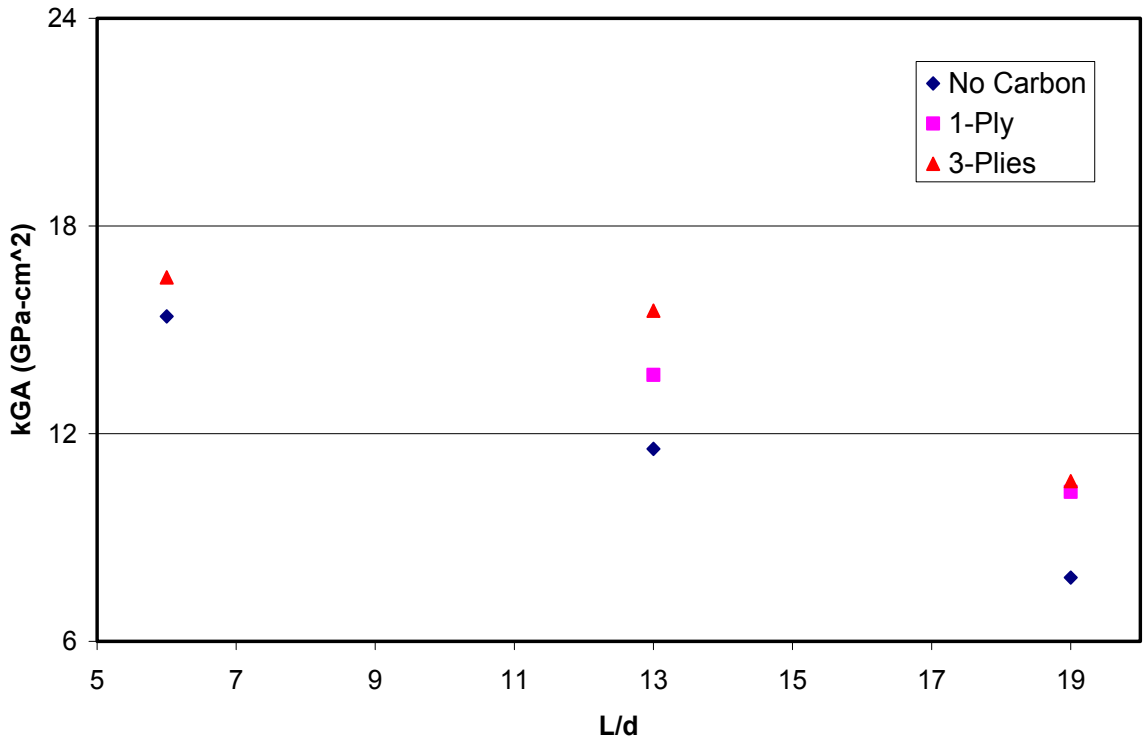

Figure 5-17. Average kGA for each beam type versus span

Table 5-4. Summary of results for shear modulus determined by back calculating G from kGA

L/d	C-Plies	kGA		k	A_V		G	
		ksi-in²	GPa-cm²		in²	cm²	ksi	GPa
6	0	346	15.4	0.27284	0.750	4.84	1691	11.66
13	0	260	11.6	0.27284	0.750	4.84	1271	8.76
19	0	176	7.8	0.27284	0.750	4.84	862	5.94
13	1	308	13.7	0.2781	0.754	4.86	1470	10.13
19	1	232	10.3	0.2781	0.754	4.86	1107	7.63
6	3	371	16.5	0.28678	0.886	5.72	1461	10.08
13	3	350	15.6	0.28678	0.886	5.72	1376	9.49
19	3	239	10.6	0.28678	0.886	5.72	941	6.49

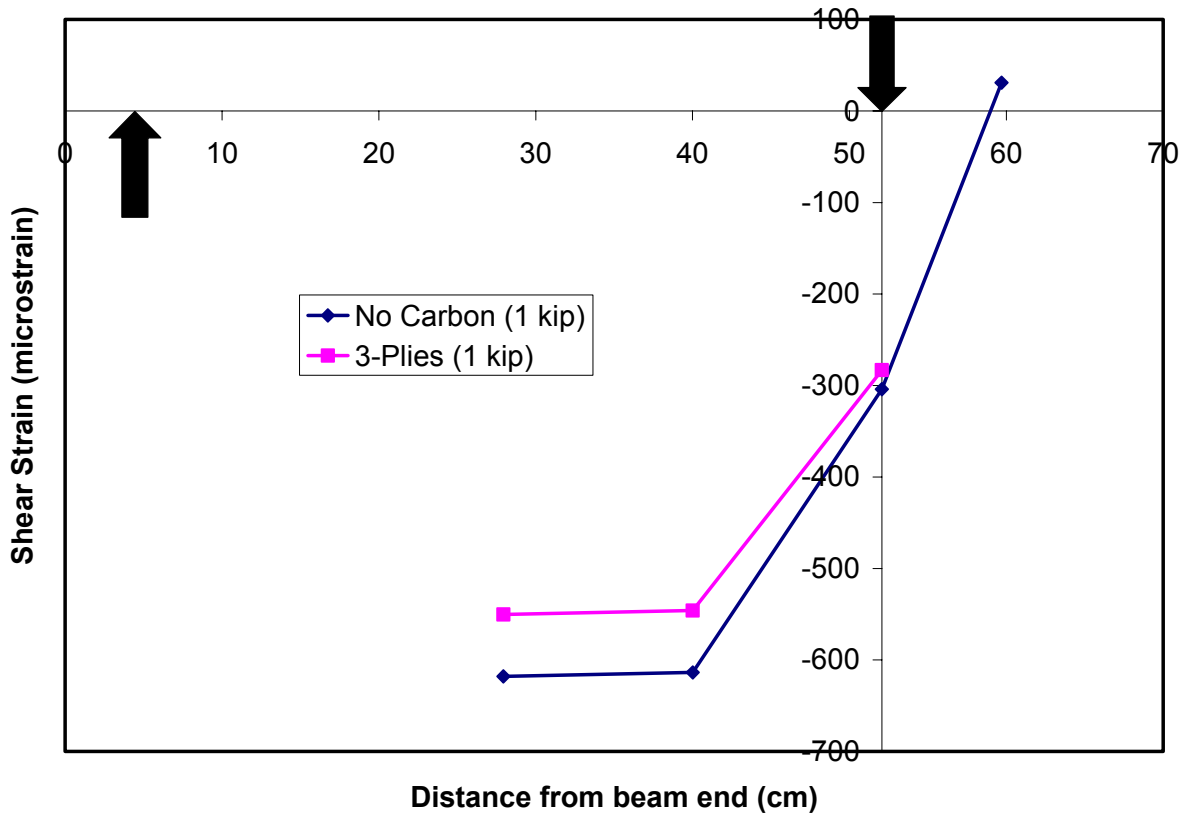

Figure 5-18. Distribution of shear strain in beam web for no plies and 3-plies of carbon lamina

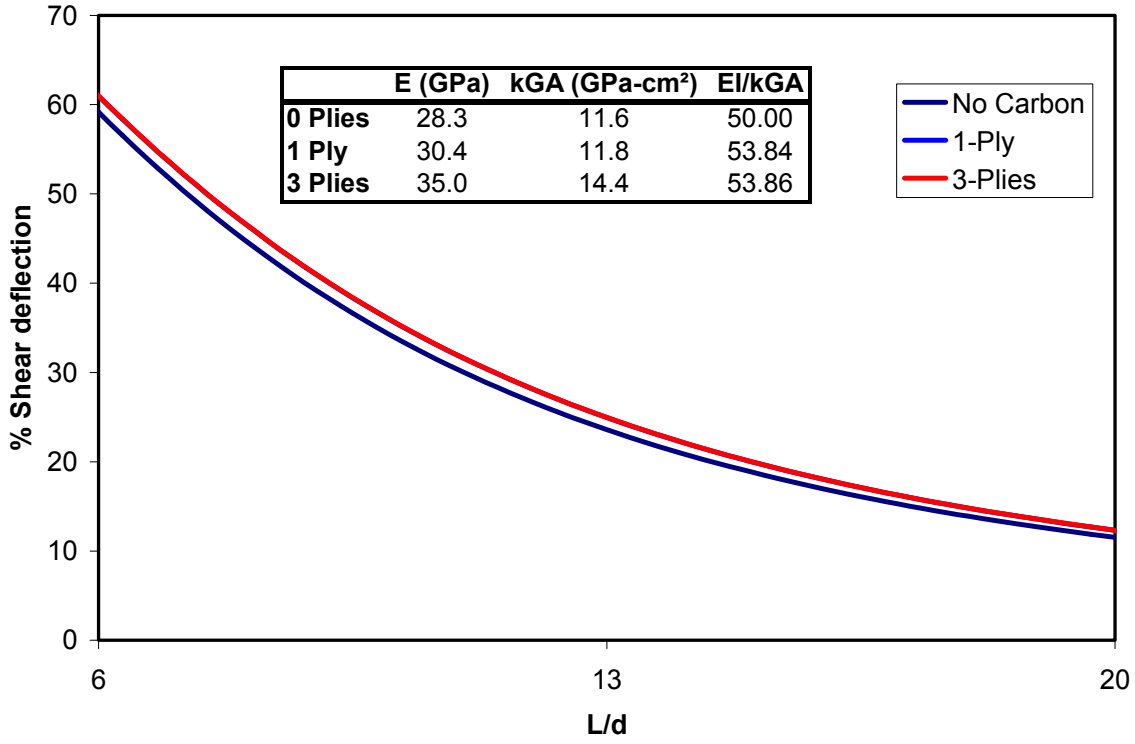

Figure 5-19. Contribution of shear deformation to the total beam deflection at test spans, calculated using the average bending modulus and shear stiffness for each beam

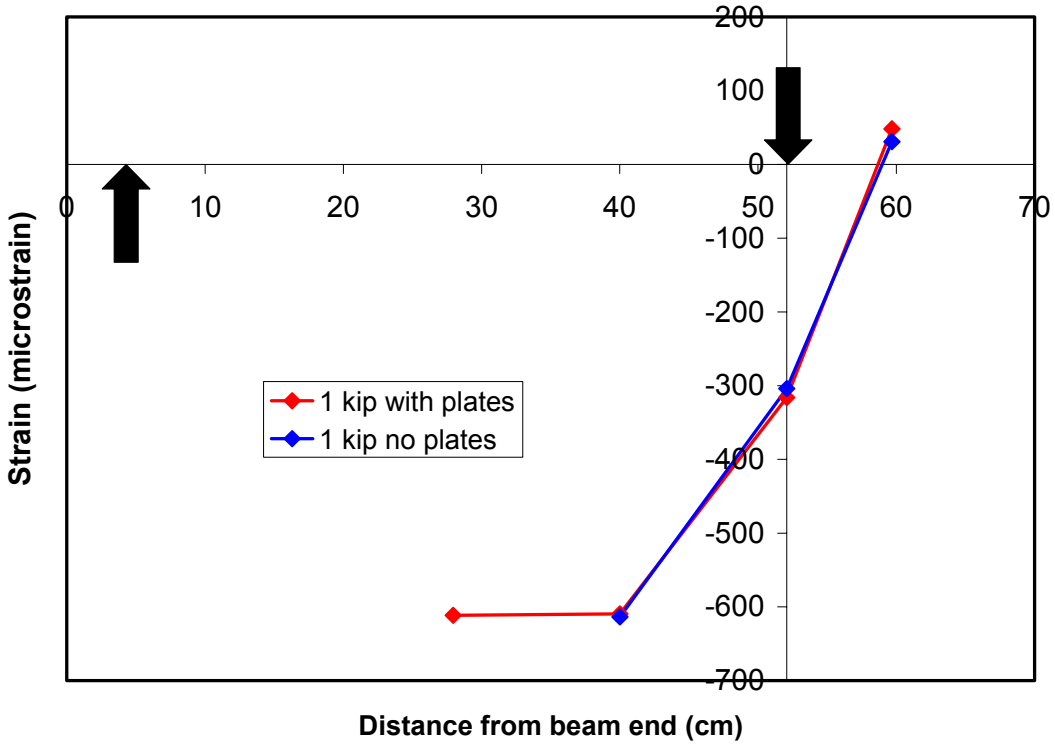

Figure 5-20. Distribution of shear strain in beam web for point load and load patch cases

Table 5-5. Summary of results from slope-intercept method of determining E and kGA

C Plies	E		kGA	
	Msi	GPa	ksi-in²	GPa-cm²
0	6.52	44.9	692.9	30.8
0	6.52	44.9	666.1	29.6
0	6.60	45.5	495.9	22.1
1	7.57	52.2	536.1	23.8
3	8.36	57.6	680.9	30.3
3	8.46	58.3	620.6	27.6

Table 5-6. Summary of % differences between slope-intercept method and the direct method

C Plies	E_{avg}		% Diff from Direct Method	kGA_{avg}		% Diff from Direct Method
	Msi	GPa		ksi-in²	GPa-cm²	
0	6.54	45.12	60	618.29	27.50	251
1	7.57	52.20	74	536.10	23.80	131
3	8.41	57.97	66	650.76	28.95	172

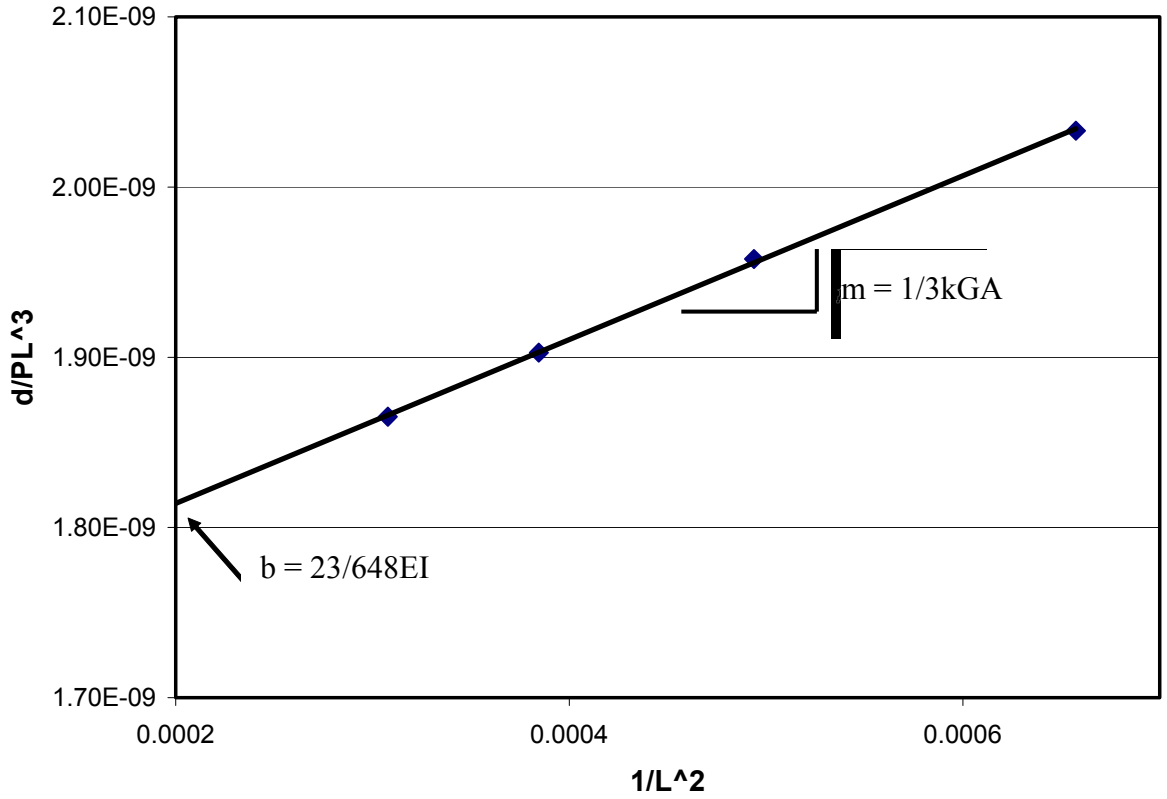

Figure 5-21. Typical plot for determination of E and kGA from slope-intercept method

Table 5-7. Summary of results from testing 57 in. (145 cm) beams at multiple spans

L/d	C-plies	E		kGA	
		Msi	GPa	ksi-in²	GPa-cm²
19	3	5.12	35.3	233	10.4
17		5.14	35.4	285	12.7
15		5.12	35.3	317	14.1
13		5.09	35.1	353	15.7
19	3	4.99	34.4	245	10.9
17		5.02	34.6	277	12.3
15		5.02	34.6	314	14.0
13		4.97	34.3	345	15.3
19	1	4.36	30.1	232	10.3
17		4.34	29.9	259	11.5
15		4.33	29.9	307	13.7
13		4.33	29.9	314	14.0
19	0	4.14	28.5	169	7.5
17		-	-	-	-
15		4.13	28.5	226	10.1
13		4.11	28.3	260	11.6
19	0	4.04	27.9	184	8.2
17		4.03	27.8	213	9.5
15		4.03	27.8	244	10.9
13		4.05	27.9	284	12.6
19	0	4.09	28.2	176	7.8
17		4.08	28.1	202	9.0
15		4.09	28.2	232	10.3
13		4.09	28.2	270	12.0

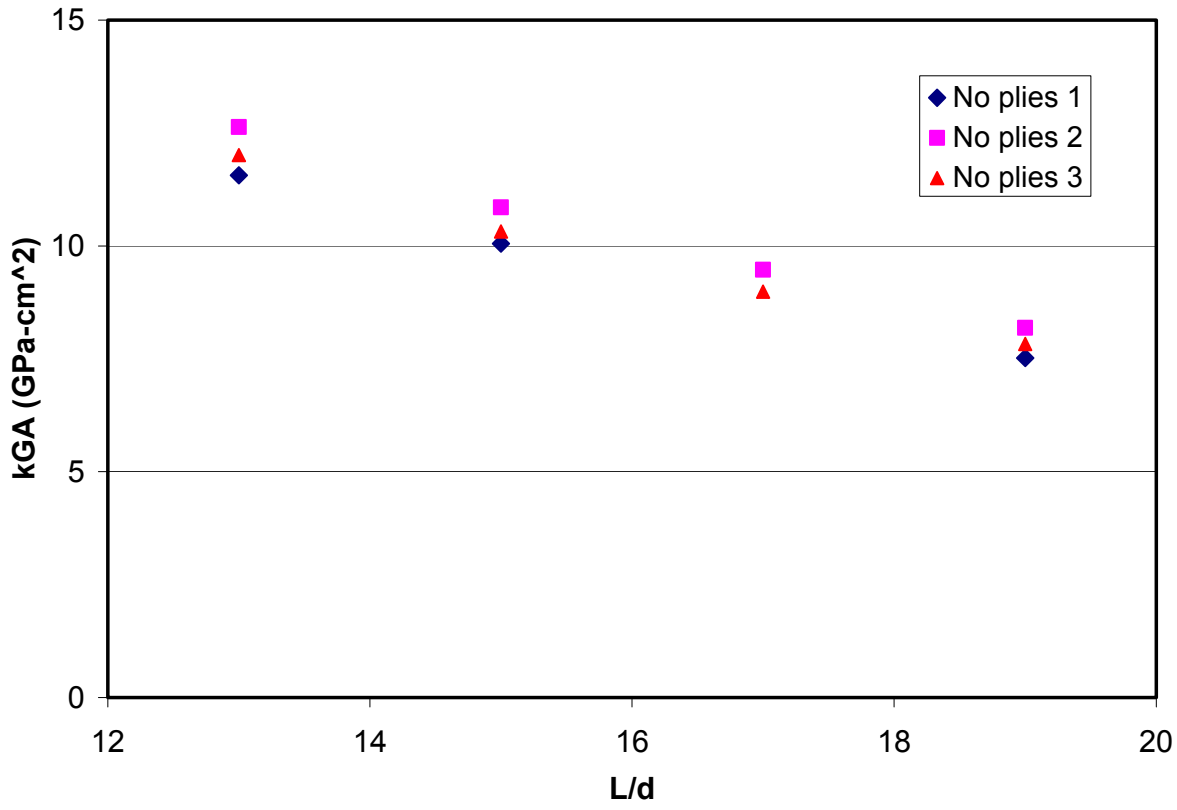

Figure 5-22. Span dependence of shear stiffness for beams with no carbon plies

Table 5-8. Summary of parameters varied, the method of variation, and results from testing of WF FRP sections

Varied Parameter	Method of Variation	Results and Comments
EI/kGA	Addition of carbon plies.	7 to 26% increase in kGA, but k and A contribute 80% of that.
Boundary Conditions	Steel plates at load/supports	Typically less than 10% change in kGA. EI/kGA changed very little (1.5 to 5%, one 11% change). No significant affect on distribution of shear strain in web (limited test data).
Test Method	Multi-Span Method was used.	Multi-span results were drastically different, attributed to test method, not kGA.
Deflection	16-bit acquisition system and LVDT used for measurements	Test to test variation in kGA was typically well below 1%. Data was clean and noise-free leading to confidence in kGA calcualtions.
Test Span	60 in. (152 cm) beams were tested at multiple spans. And three spans were used overall.	Significant affect on kGA. 50% increases for L/d changes of 6. 100% or more increases were not uncommon going from longest to shortest span.

Chapter 6 Conclusions and Recommendations

Based upon the investigations performed during the research and writing of this thesis, the following conclusions and recommendations are made:

- By means of the low load stiffness testing of nineteen 36 in. DWBs, the values for bending modulus (E) and shear stiffness (kGA) were determined that will be included in the structural design guide for this girder.

- Through the failure testing of the same nineteen 36 in. DWBs, the ultimate load limits were determined for the structural design guide. In addition to this, the failure modes of the structure were determined. It was found that there is more than one factor controlling design utilizing this structure, i.e. the shear capacity of the structure seems to dominate the failure mode until a span limit is reach (somewhere between an L/d of 6 and 10), at which bearing failures occur due to the concentration of stresses created by the elastomeric bearing pads.

- The A and B allowables for E, kGA, shear capacity, and moment capacity were determined in order to provide future users of the design guide with material properties that will lead to safely and efficiently designed structures.

- A great deal of variation can be seen in the experimentally determined value of shear stiffness (kGA) for the 36 in. DWB. Inaccurate and high-noise deflection data is believed to be one of the primary sources of the variation as it has been seen that kGA is extremely sensitive to measured deflections. It was determined that it was essential to use deflection data measured using a highly sensitive device, such as the LVDT used in this research. The use of higher resolution acquisition systems proved to be an important aspect of testing as well. The use of an acquisition system with 16-bit resolution combined with a deflection measuring device with a longer stroke would be ideal as it appears that kGA tends to level off as load increases

- In order to further examine shear effects in FRP beams, the small WF beam testing described in Chapter 5 was conducted. This study revealed that it is possible to consistently obtain values for shear stiffness as test to test variation was minimal and beam to beam variations were reasonable. It also revealed that all the factors thought to affect kGA or the ability to measure it do indeed have affects. Structure stiffness, boundary conditions, span, and deflection data all proved to have considerable affects on the measurement of kGA. The slope-intercept method for determining kGA proved to be ineffective for unexplained reasons.

- Predictions made during the WF beam study proved to be on the conservative side. This may in part be due to the difficulty had in turning a thread-up into an accurate and representative lay-up to be used in CLT and MLB theory.

- The study conducted on the WF beams also seemed to raise as many, if not more, questions regarding the characterization of shear effects in FRP structures as it answered. What is the true length required before shear strain in the web levels off to a constant value around the load points? What are the effects of shear lag in FRP structures? Exactly how much does span and the increased contribution of shear deformation at short spans play a role in the value of kGA? How necessary is a more complex beam theory to better account for the shear deformation in FRP structures? What measured kGA is the true property? Etc.

- Although the WF beam study introduced a number of questions, it seems to have at least suggested a path and pointed researchers in the direction of better understanding shear effects. It is a foundation upon which to build.

- And finally, the kGA being measured in these experiments was shown to be a structural property, characteristic of the test setup from which it was obtained. That said, care must be taken to ensure proper use of kGA in design using these structures. The values presented for shear stiffness, kGA, are specific to the test setups/conditions described herein.

References

1. Hayes, M.D., Lesko, J.J, Weyers, R.E., Cousins, T.E., Haramis, J., Gomez, J. and Masarelli, P. 2000. "Laboratory and Field Characterization of the Tom's Creek Bridge Superstructure," *Journal for Composites in Construction*, 4(3): 120-128.
2. Strongwell. 2000. "EXTREN DWB™ Design Guide"
3. AASHTO (1998), LRFD Bridge Design Specification, 2nd edition, American Association of State Highway and Transportation Officials, Washington, D.C.
4. GangaRao, H.V.S., H.K. Thippeswamy, V. Shekar, C. Craigo, "Development of Glass Fiber Reinforced Polymer Composite Bridge Deck," *SAMPE Journal*, Vol. 35, No. 4, July/August 1999.
5. Brailsford, B., S.M. Milkovich, D.W. Prine, J.M. Fildes, "Definition of Infrastructure Specific Markets for Composite Materials: Topical Report," Northwestern University BIRL Project P93-121/A573, July 11, 1995.
6. Hayes, M.D., "Characterization and Modeling of a Fiber-Reinforced Polymeric Composite Structural Beam and Bridge Structure for Use in the Tom's Creek Bridge Rehabilitation Project," Master's Thesis, Virginia Polytechnic Institute and State University, 1998.
7. Hargrave, M.W., E. Munley, and T.J. Pasko, "FHWA's applied highway infrastructure research program on composite materials," *Public Roads*, v60 n4 (Spring 1997), 23 (9).
8. Lesko, J.J., S.W. Case, T.E. Cousins, "Design Manual Development for FRP Structural Shapes: Practical and Durability Considerations," International SAMPE Symposium and Exhibition, v.46 II 2001:1576-1586.
9. Strongwell. 1989. "EXTREN™ Design Guide"
10. Hardcore Composites Website: www.hardcorecomposites.com
11. Creative Pultrusions Website: www.creativepultrusions.com
12. Machida, A. ed., "Recommendation for Design and Construction of Concrete Structures Using Continuous Fiber Reinforcing Materials," Japan Society of Civil Engineers, 1997.
13. American Concrete Institute, "Guide for the Design and Construction of Concrete Reinforced with FRP Bars," ACI Committee 440, Revised January 17, 2000.
14. Zenkurt, D., An Introduction to Sandwich Construction, Engineering Materials Advisory Services LTD., 1995: 50-61.
15. Omidvar, B., "Shear Coefficient in Orthotropic Thin-Walled Composite Beams," *Journal of Composites for Construction*, February 1998.
16. Cowper, G.R., "The shear Coefficient in Timoshenko's Beam Theory", *Journal of Applied Mechanics*, June 1966: 335-340.
17. Bank, L.C., "Shear Coefficients for Thin-Walled Composite Beams," *Composite Structures*, 1987.
18. Whitney, J.M., "Shear Correction Factors for Orthotropic Laminates Under Static Load," *Journal of Applied Mechanics*, 1973, 40(3), 302-304.
19. Madabhusi-Raman, P., J. Davalos, "Static shear Correction Factor for Laminated Rectangular Beams," *Composites*. Part B, 27(3-4), 285-293.
20. Bank, L.C., "Flexural and Shear Moduli of Full-Section Fiber Reinforced Plastic Beams," ASTM, 1989.
21. Pai, P.F., M.J. Schulz, "Shear Correction Factors and an Energy-Consistent Beam Theory," *Intl. J. of Solids and Structures*, 36, 1999: 1523-1540.

22. Barbero, E.J., R. Lopez-Anido, J.F. Davalos, "On the Mechanics of Thin-Walled Laminated Composite Beams," *J. of Composite Materials*, Vol. 27, No. 8, 1993.
23. Waldron, C.J., "Determination of the Design Parameters for the Route 601 Bridge," Master's Thesis, Virginia Polytechnic Institute and State University, 2001.
24. Dufort, L., M. Grediac, Y. Surrel, "Experimental Evidence of the Cross-Section Warping in Short Composite Beams Under Three Point Bending," *Composite Structures*, 51, 2001: 37-47.
25. Weibull, Waloddi (1951), "A Statistical Distribution Function of Wide Applicability," *J. of Applied Mechanics*, 293-297.
26. Weibull, Waloddi (1949), "A Statistical Representation of Fatigue Failures in Solids, Transitions of the Royal Institute of Technology", No. 27, Stockholm.
27. Mil-17 Organization, "The Composite Materials Handbook", www.mil17.org.

Appendices

Appendix A

The basis for the calculations in the design guide comes from Weibull statistics, where the cumulative probability distribution function that describes the distribution of experimental values is derived from,

$$F(x) = 1 - \mathrm{Exp}[-(x/\beta)^{\alpha}] \qquad (A-1)$$

where α and β are parameters used to fit the data. Alpha is the shape parameter, which describes the breadth of the distribution. Beta is the location parameter, which defines the value nearest the center of the distribution. The probability of failure, F(x), is related to the reliability, R(x), by,

$$R(x) = 1 - F(x) \qquad (A-2)$$

This relationship can then be arranged to obtain expressions for A and B basis allowables, as seen below in Equations (A-5) and (A-6). Further details on Weibull statistics and the equations seen below can be found in the EXTREN DWB Design Guide [2], Weibull [25, 26], and from the Mil-17 Specification "The Composite Materials Handbook" [27].

- Mean:

$$\mu = \beta \cdot \Gamma\left(\frac{\alpha+1}{\alpha}\right) \qquad (A-3)$$

  where Γ is the gamma function.

- Standard deviation:

$$\sigma = \beta^2 \cdot \left[\Gamma\left(\frac{\alpha+2}{\alpha}\right) - \Gamma^2\left(\frac{\alpha+1}{\alpha}\right)\right]^{1/2} \qquad (A-4)$$

- A allowable:

$$\tilde{\beta}_{lower}\left[\ln\left(\frac{1}{0.99}\right)\right]^{1/\alpha} \qquad (A-5)$$

- B allowable:

$$\widetilde{\beta}_{upper}\left[\ln\left(\frac{1}{0.90}\right)\right]^{1/\alpha} \qquad \text{(A-6)}$$

where $$\widetilde{\beta}_{lower} = \beta\left[\frac{2n}{X^2_{0.05}}\right]^{1/\alpha}, \ \widetilde{\beta}_{upper} = \beta\left[\frac{2n}{X^2_{0.95}}\right]^{1/\alpha} \qquad \text{(A-7)}$$

- Weibull density function: $f(x) = \frac{\alpha}{\beta}\left(\frac{x}{\beta}\right)^{\alpha-1}\exp\left[-\left(\frac{x}{\beta}\right)^{\alpha}\right]$ (A-8)
- Weibull cumulative distribution: $F(x) = \int_0^{\infty} f(x)dx = 1 - \exp\left[-\left(\frac{x}{\beta}\right)\right]^{\alpha}$ (A-9)
- reliability: $R = \exp\left[1-\left(\frac{x}{\widetilde{\beta}}\right)^{\alpha}\right]$

where x is the allowable design value (A-10)

Appendix B

*All values are in English units (E—Msi, kGa—Msi-in²)

Beam	Span	test	Load	E (600-800)	kGA (600-800)	E (min-600)	kGA (min-600)
30 footer	30	failure test	250	6.70	47.3	6.76	44.6
7/12-2a	30	test 11	250	6.44	43.2	6.45	42.3
		8	150	6.41	41.5	6.42	41.7
		7	80	6.37	40.5	6.39	40.7
		6	80	6.47	46.2	6.47	44.9
		5	60	6.49	45.4		
7/12-2b	30	failure test	260	6.28	50.8	6.32	48.1
		7	100	6.41	51.6	6.41	49.5
		6	80	6.41	46.5	6.41	46.4
		5	80	6.41	47.4	6.41	47.3
7/10-#5	30	8	100	6.63	49.7	6.65	47.7
		7	100	6.62	50.4	6.64	48.1
		6	80	6.63	50.4	6.64	48.7
		5	80	6.63	50.8	6.64	48.7
7/12-#3	30	8	100	6.52	64.3	6.53	58.4
		7	80	6.53	60.7	6.53	56.3
		6	80	6.52	62.1	6.53	57.8
7/11-#1	39	4	40	6.27	44.5		
		5	40	6.26	44.4	6.28	43.2
7/12-#1	39	3	40	6.18	49.0	6.20	47.1
		4	40	6.22	52.3	6.22	50.3
		5	40	6.24	53.5	6.24	50.7
7/9-#2	39	8	40	6.01	53.9	6.03	53.7
		9	40	6.04	60.6	6.04	58.1
		10	40	6.00	61.1	6.00	58.5
7/9-#1	39	3 (LVDT)	40	6.50	39.2	6.50	38.0
		4 (LVDT)	40	6.46	41.6	6.46	39.8
		5 (LVDT)	40	6.51	39.4	6.50	38.1
		3 (WP)	40	6.50	60.4	6.50	52.8
		9 (WP)	100	6.48	46.8	6.48	45.8
#14	39	3	40	6.62	39.9	6.62	38.8
		5	40	6.61	40.4	6.62	39.2
		failure (WP)	230	6.61	38.3	6.60	38.1
#24	39	3	40	6.28	46.6	6.28	44.6
		4	40	6.28	45.8	6.28	44.2
5/31-#1	58	15	20	6.40	53.5		
5/31-#3	58	2	20	6.67	52.0	6.66	42.5
		3	20	6.64	52.5	6.71	43.6
5/29-#1	58	3	20	6.44	36.6		
		4	20	6.46	39.4		
7/11-#1	58	3	20	6.37	41.2		
7/11-#2	58	3	20	6.37	41.3		
		5	20	6.40	46.5		

Appendix C

All values are in English units (E—psi, kGA—psi-in²)

beam	test	E (avg)	Emin	Emax	St Dev	kGA (avg)	kGA min	kGA max	St Dev
20(0)-2A	test 2	4.24E+06	4.22E+06	4.26E+06	1.21E+04	3.32E+05	3.04E+05	3.60E+05	1.93E+04
	test 3	4.19E+06	4.18E+06	4.21E+06	1.16E+04	3.51E+05	3.23E+05	3.79E+05	1.93E+04
20(0)-3A	test 3	4.19E+06	4.18E+06	4.21E+06	1.16E+04	3.51E+05	3.23E+05	3.79E+05	1.93E+04
	test 4	4.19E+06	4.17E+06	4.20E+06	1.17E+04	3.47E+05	3.18E+05	3.76E+05	1.98E+04
20(0)-G	test 1	3.95E+06	3.95E+06	3.96E+06	3.43E+03	3.51E+05	3.41E+05	3.59E+05	6.17E+03
	test 3	3.98E+06	3.97E+06	3.98E+06	1.74E+03	3.45E+05	3.35E+05	3.55E+05	6.90E+03
20(3)-1A	test 2	5.16E+06	5.15E+06	5.17E+06	9.04E+03	4.22E+05	4.05E+05	4.39E+05	1.20E+04
	test 3	5.15E+06	5.14E+06	5.16E+06	8.15E+03	4.20E+05	4.04E+05	4.36E+05	1.14E+04
20(3)-2A	test 1	5.28E+06	5.27E+06	5.28E+06	1.99E+03	3.58E+05	3.32E+05	3.84E+05	1.78E+04
	test 2	5.27E+06	5.27E+06	5.27E+06	1.73E+03	3.58E+05	3.31E+05	3.86E+05	1.94E+04
20(3)-G	test 2	5.05E+06	5.03E+06	5.06E+06	1.23E+04	3.42E+05	3.23E+05	3.61E+05	1.28E+04
	test 1	5.17E+06	5.12E+06	5.18E+06	2.23E+04	3.29E+05	3.12E+05	3.45E+05	1.11E+04
40(0)-1A	test 1	4.08E+06	4.08E+06	4.09E+06	2.41E+03	2.62E+05	2.49E+05	2.75E+05	8.56E+03
	test 2	4.09E+06	4.08E+06	4.10E+06	4.55E+03	2.65E+05	2.53E+05	2.79E+05	8.87E+03
40(0)-2A	test 1	4.08E+06	4.06E+06	4.10E+06	1.69E+04	2.58E+05	2.48E+05	2.68E+05	6.44E+03
40(0)-G	test 2	4.04E+06	4.03E+06	4.05E+06	4.65E+03	2.58E+05	2.56E+05	2.59E+05	9.48E+02
	test 3	4.05E+06	4.04E+06	4.06E+06	6.57E+03	2.61E+05	2.60E+05	2.62E+05	5.77E+02
40(1)-2A	test 1	4.53E+06	4.50E+06	4.57E+06	2.39E+04	3.10E+05	3.09E+05	3.11E+05	5.75E+02
	test 2	4.55E+06	4.52E+06	4.58E+06	2.03E+04	3.07E+05	3.05E+05	3.08E+05	8.80E+02
40(1)-3A	test 1	4.34E+06	4.34E+06	4.35E+06	4.02E+03	3.09E+05	3.00E+05	3.19E+05	6.02E+03
	test 2	4.35E+06	4.34E+06	4.36E+06	4.51E+03	3.08E+05	2.97E+05	3.18E+05	7.11E+03
40(3)-1A	test 1	5.06E+06	5.04E+06	5.07E+06	8.08E+03	3.53E+05	3.43E+05	3.64E+05	7.02E+03
	test 2	5.07E+06	5.05E+06	5.08E+06	7.57E+03	3.65E+05	3.57E+05	3.73E+05	5.19E+03
40(3)-3A	test 1	4.92E+06	4.91E+06	4.94E+06	9.28E+03	3.30E+05	3.07E+05	3.56E+05	1.64E+04
	test 2	4.90E+06	4.90E+06	4.91E+06	2.12E+03	3.58E+05	3.41E+05	3.78E+05	1.26E+04
40(3)-G	test 4	4.98E+06	4.96E+06	4.99E+06	1.04E+04	3.44E+05	3.39E+05	3.51E+05	3.85E+03
	test 5	5.01E+06	4.98E+06	5.02E+06	1.32E+04	3.47E+05	3.39E+05	3.56E+05	5.50E+03
60(0)-2A	test 1	4.03E+06	4.03E+06	4.04E+06	3.96E+03	1.84E+05	1.79E+05	1.89E+05	3.26E+03
	test 2	4.04E+06	4.03E+06	4.05E+06	5.95E+03	1.84E+05	1.79E+05	1.89E+05	3.32E+03
60(0)-3A	test 1	4.09E+06	4.08E+06	4.10E+06	7.09E+03	1.75E+05	1.70E+05	1.80E+05	3.28E+03
	test 2	4.10E+06	4.08E+06	4.11E+06	9.89E+03	1.76E+05	1.72E+05	1.81E+05	3.09E+03
60(0)-G	test 1	4.13E+06	4.11E+06	4.14E+06	7.47E+03	1.68E+05	1.67E+05	1.68E+05	4.47E+02
	test 2	4.15E+06	4.13E+06	4.17E+06	1.21E+04	1.71E+05	1.70E+05	1.72E+05	4.08E+02
60(1)-3A	test 1	4.37E+06	4.35E+06	4.38E+06	8.63E+03	2.31E+05	2.27E+05	2.34E+05	2.30E+03
	test 2	4.35E+06	4.34E+06	4.37E+06	1.06E+04	2.34E+05	2.33E+05	2.36E+05	9.48E+02
60(3)-1A	test 1	5.12E+06	5.11E+06	5.12E+06	7.02E+03	2.31E+05	2.22E+05	2.41E+05	6.17E+03
	test 2	5.13E+06	5.11E+06	5.14E+06	9.86E+03	2.36E+05	2.26E+05	2.45E+05	6.52E+03
60(3)-2A	test 1	4.99E+06	4.99E+06	5.00E+06	1.61E+03	2.44E+05	2.38E+05	2.50E+05	3.98E+03
	test 2	4.99E+06	4.98E+06	4.99E+06	3.74E+03	2.46E+05	2.39E+05	2.52E+05	3.84E+03

Appendix D – Typical Failure Pictures for the 36 in. DWB

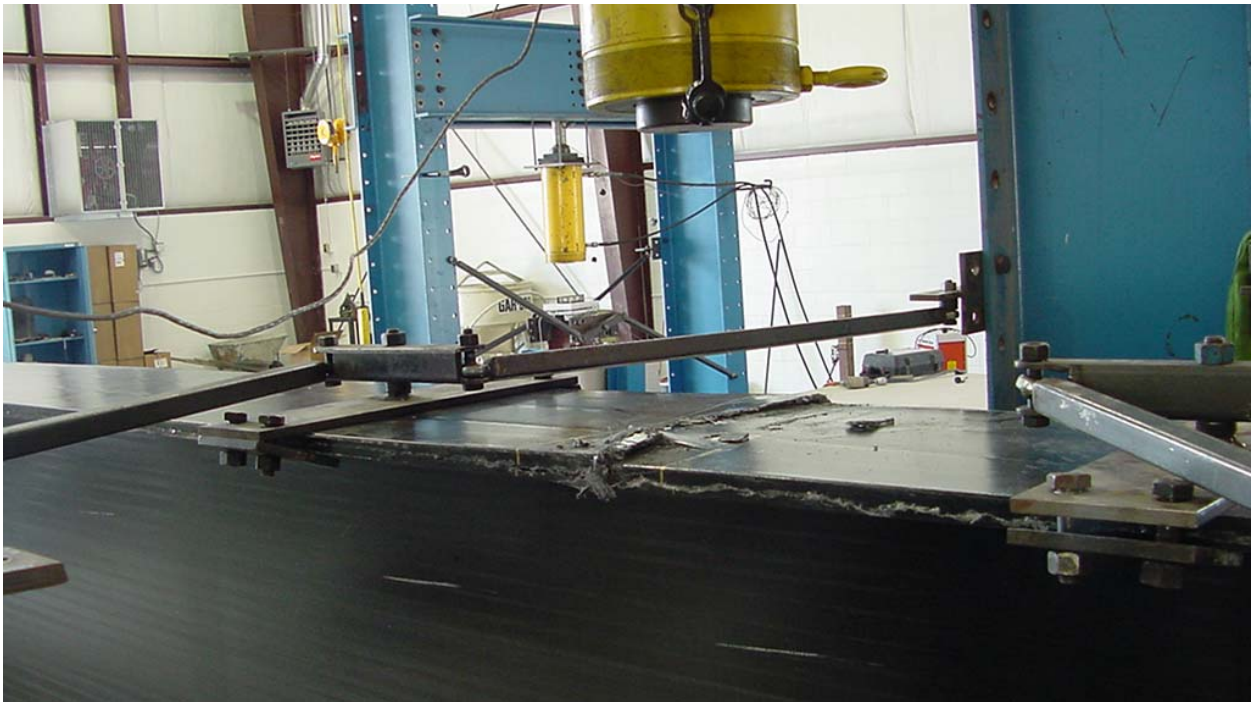

Vita

Timothy J. Schniepp was born in Rochester, Minnesota on January 17, 1978 to Becky and Brian Schniepp. He grew up in the town of Elgin, Minnesota in Southeastern Minnesota. Tim graduated from Elgin-Millville High School as valedictorian in 1996 and then proceeded to attend Winona State University in Winona, MN. Tim graduated from WSU in May 2000 with a B.S. in Composite Materials Engineering and then made the decision to continue his education at Virginia Tech. While working to fulfill the requirements for his M.S. in Engineering Science and Mechanics at VT, Tim studied various aspects of fiber-reinforced composite materials and their use in civil infrastructure applications. Upon completion of his M.S. in August 2002, Tim has accepted a position working for Lockheed Martin Aeronautics Company in Marietta, Georgia where he will be a member of the Composites and Adhesives division of the Materials, Processes, and Producibility department.